Optical properties of ion-implanted impurities in gallium nitride.

Metcalfe, R. D.

Award date:
1976

Awarding institution:
University of Bath

OPTICAL PROPERTIES OF ION-IMPLANTED IMPURITIES IN GALLIUM NITRIDE

Submitted by Richard Duncan Metcalfe for the degree of Ph.D. of the University of Bath.

1976

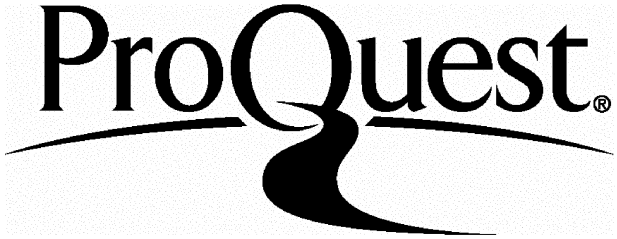

Abstract

The III-V semiconductor GaN is of technological interest because of its high band gap (3.44 eV at 300 K). The impurities K, Ca, Zn, B, Al, C, Si, P, As, S, F, and Cl have been implanted into GaN. After annealing, the optical spectra of the implanted material were investigated. Studies were also made of neutron irradiated GaN and some $Ga_{1-x}Al_xN$ alloys.

Broad emission bands at 2.9, 2.85, and 2.58 eV were identified with the impurities Zn, P, and As respectively. Sharper emissions near 3.5 and 3.3 eV were seen in the Al implant. Peaks near 3.27 eV, associated with DA pair transitions in purer GaN, were seen in the B, Al, F and Cl implants.

The intrinsic luminescence of most samples is reduced by an amount dependent on the damage introduced during implantation. A broad band near 2.2 eV is associated with defects introduced by implantation and by the dissociation of GaN during high temperature annealing. A reduction in efficiency of implanted luminescence centres is also associated with high temperature annealing.

CONTENTS

			Page
Chapter 1.		INTRODUCTION	1
Chapter 2.		GALLIUM NITRIDE PROPERTIES I GENERAL	
	2.1	STRUCTURE	5
	2.2	CRYSTAL GROWTH METHODS	5
	2.3	CHEMISTRY OF CRYSTAL GROWTH	10
Chapter 3.		GALLIUM NITRIDE PROPERTIES II OPTICAL	
	3.1	INTRODUCTION	14
	3.2	OPTICAL TRANSITIONS IN PURE SEMI-CONDUCTORS	14
	3.3	OPTICAL TRANSITIONS IN HIGHLY IMPURE SEMICONDUCTORS	19
	3.4	GALLIUM NITRIDE - ABSORPTION	23
	3.5	GALLIUM NITRIDE - LUMINESCENCE	26
Chapter 4.		DOPING OF GALLIUM NITRIDE	
	4.1	SELF COMPENSATION	37
	4.2	CHOICE OF DOPANT	38
	4.3	METHODS OF DOPING	42
	4.4	INVESTIGATION OF IMPLANTED LAYERS IN GALLIUM NITRIDE	44
Chapter 5.		ION IMPLANTATION	
	5.1	DISTRIBUTION OF IMPLANTED ATOMS	49
	5.3	ION IMPLANTATION - EXPERIMENTAL DETAILS	55
	5.4	HEAT TREATMENT	59

5.5	DISCUSSION OF IMPLANTATION AND ANNEALING	62
Chapter 6.	OPTICAL INVESTIGATION OF IMPLANTED LAYERS EXPERIMENTAL DETAILS	
6.1	INTRODUCTION	71
6.2	CATHODOLUMINESCENCE	72
6.3	PHOTOLUMINESCENCE	82
6.4	ABSORPTION SPECTRA	82
6.5	EXCITATION SPECTRA	84
Chapter 7.	OPTICAL INVESTIGATION OF IMPLANTED LAYERS RESULTS	
7.1	INTRODUCTION	86
7.2	GENERAL FEATURES OF THE LUMINESCENCE	86
7.3	SPECIFIC IMPLANTED IMPURITIES	99
7.4	LUMINESCENCE OF NEUTRON IRRADIATED GAN	137
7.5	EXCITATION SPECTRA	141
7.6	ABSORPTION SPECTRA	145
7.7	$Ga_{1-x}Al_xN$ ALLOYS	152
Chapter 8.	DISCUSSION AND CONCLUSIONS	
8.1	SPECIFIC IMPURITIES	158
8.2	GENERAL FEATURES	170
8.3	CONCLUSIONS	178
	REFERENCES	182

DIAGRAMS

Figure		page
2.1	Band structure of GaN (25)	6
2.2	Schematic diagram of furnace systems used to produce GaN epitaxial layers	7
2.3	Slip bands in (11.0) GaN deposited on (21.1) α-Al_2O_3 substrate (after annealing at 850°C)	9
3.1	Recombination mechanisms in semiconductors	16
3.2	a) Variation of energy gap with position in the presence of charged impurities - Tunneling assisted transitions may occur. b) The resulting density of states diagram (41)	21
3.3	Optical absorption in GaN	25
3.4	Near-gap luminescence in GaN	
3.5	As-grown GaN Cathodoluminescence 77 K 15 kV	30
3.6	Variation of photoluminescence intensity with temperature GaN : Zn 910°C annealed (from ref 74)	31
3.7	Deep impurity luminescence in GaN	
3.8	Model for the photoluminescence process and distribution of states in Zn-doped GaN (59)	35
4.1	Wurtzite structure (11.0) plane	40
4.2	Covalent and ionic radii of the elements	41

5.1	The behaviour of the nuclear and electronic contributions to the rate of energy loss dE/dx of implanted ions, as a function of ion energy E (69)	50
5.2	Range distribution for 85 Kr ions of various energies implanted in amorphous Al_2O_3 (76)	52
5.3	Integral range distribution of 45 keV ^{85} Kr ions implanted into single crystal aluminium and amorphous Al_2O_3 (77)	53
5.4	Possible damage events produced during ion implantation (80)	56
5.5	Penetration of implanted species in GaN calculated from tables in ref 69	61
5.6	Annealing furnace for GaN wafers	63
5.7	Critical dose to produce amorphous layers in GaN	65
5.8	Surface damage in GaN after annealing at 930°C	69
6.1	Electron gun and vacuum chamber	74
6.2	Electron gun and cryostat assembly	74
6.3	Cathodoluminescence apparatus	76
6.4	Penetration of electrons into GaN	79
7.1	Temperature dependence of photoluminescent intensity GaN unannealed, unimplanted	88
7.2	Photoluminescence 8 K GaN : Al unannealed	89
7.3	Photoluminescence 9 K GaN : F 10^{18} cm^{-3}	91

7.4	Effect of implantation on LNT A-band intensity of GaN after 900°C anneal	92
7.5	Cathodoluminescence 73 K GaN 900°C annealed	94
7.6	Effect of annealing on luminescence intensity	95
7.7	Temperature dependence of emission energies in GaN	97
7.8	Cathodoluminescence 77 K GaN : K 900°C annealed 8 kV	101
7.9	Cathodoluminescence 77 K GaN : Zn 900°C annealed 9 kV	104
7.10	Cathodoluminescence 77 K GaN : Ca 900°C annealed 9 kV	107
7.11	Photoluminescence 73 K GaN : B 850°C annealed	110
7.12	Cathodoluminescence 76 K GaN : B 900°C annealed 9 kV	110
7.13	Photoluminescence 77 K GaN : Al 750°C annealed	114
7.14	Photoluminescence 77 K GaN : Al 800°C annealed	114
7.15	Photoluminescence 77 K GaN : Al 850°C annealed	114
7.16	Cathodoluminescence 77 K GaN : Al 900°C annealed 10 kV	114
7.17	Cathodoluminescence 77 K GaN : Al 930°C annealed 10 kV	115

7.18 Cathodoluminescence 2959 C GaN : Al 930°C annealed 15 kV 115

7.19 Cathodoluminescence 77 K GaN : C 900°C annealed 8 kV 118

7.20 Cathodoluminescence 77 K GaN : C 900°C annealed 10^{18} cm^{-3} 8 kV and 15 kV 118

7.21 Cathodoluminescence 77 K GaN : Si 900°C annealed 8 kV 121

7.22 Cathodoluminescence 77 K GaN : Si 900°C annealed 10^{18} cm^{-3} 121

7.23 Cathodoluminescence 294 K GaN : P 900°C annealed 8 kV 124

7.24 Cathodoluminescence 77 K GaN : P 900°C annealed 8 kV 124

7.25 Cathodoluminescence 77 K GaN _ P 900°C annealed 10^{18} cm^{-3} 124

7.26 Cathodoluminescence 294 K GaN : As 900°C annealed 8 kV 127

7.27 Cathodoluminescence 76 K GaN : As 900°C annealed 8 kV 127

7.28 Cathodoluminescence 73 K GaN : As 900°C annealed 10^{18} cm^{-3} 127

7.29 Cathodoluminescence 74 K GaN : S 900°C annealed 9 kV 130

7.30 Photoluminescence 9 K GaN : F 700°C annealed 133

7.31 Cathodoluminescence 75K GaN : F 900°C annealed 8 kV 133

7.32	Cathodoluminescence 75 K GaN : F 900°C annealed 10^{18} cm^{-3}	133
7.33	Photoluminescence 73 K GaN : Cl 850°C annealed	136
7.34	Cathodoluminescence 75 K GaN : Cl 900°C annealed 10 kV	136
7.35	Cathodoluminescence 75 K GaN : Zn neutron irradiated and reannealed to 900°C 8 kV	139
736	Cathodoluminescence 293 K GaN : Zn neutron irradiated and re-annealed to 920°C 9 and 15 kV	139
7.37	Cathodoluminescence 76 K GaN : Si neutron irradiated and re-annealed to 900°C 9 kV	139
7.38	Emission and 2.90 eV excitation spectra LNT GaN Zn doped	143
7.39	GaN excitation spectra LNT	144
7.40	GaN excitation spectra RT	144
7.41	Absorption RT GaN unimplanted unannealed	149
7.42	Free carrier absorption RT GaN unimplanted unannealed	149
7.43	Absorption RT GaN : Cl unannealed	149
7.44	Absorption RT GaN : As unannealed	150
7.45	Edge absorption RT GaN : As unannealed	150
7.46	Edge absorption RT GaN : Cl unannealed	151
7.47	Relative absorption RT GaN : Cl unannealed	151
7.48	Absorption RT GaN : Cl	151
7.49	Absorption RT GaN : Cl 930°C annealed	151
7.50	Optical spectra of $Ga_{1-x}Al_xN$ (low x)	157

7.51	Optical spectra of $Ga_{1-x}Al_xN$ (high x)	157
8.1	Luminescence of Zn-doped GaN	160
8.2	Principal luminescence features of some $Ga_{1-x}Al_xN$ alloys	167

Chapter 1.

INTRODUCTION

Increasing interest is being shown in semiconducting light sources (1). Their small size and compatibility with the voltage and power requirements of transistor electronics give them considerable advantages over conventional filament and discharge tube lamps in some applications. The greatest potential is in information display, for instance in pocket computers, but semiconducting lasers are also a field of growing interest for optical logic and communication systems.

The light emitting diode (LED) producing recombination radiation in semiconducting junctions is the most common type of source. External quantum efficiencies from p - n junction diodes as high as 27% in the direct gap material GaAs, and 7.2% in the indirect gap material GaP have been reported (2). These efficiencies are in the far red where the sensitivity of the eye is lowest. GaP diodes with 0.6% efficiency emitting in the green, near the peak sensitivity of the eye, appear nearly as bright as the higher quantum efficiency red diodes (2).

A good material for LEDs should have a direct energy gap for high internal quantum efficiency, an emission peaking near the peak response of the human eye, and an energy gap well above this photon energy to minimise internal losses due to absorption and reflection. It should also be dopable to both p- and n-type conductivity to permit the fabrication of junction diodes.

Gallium nitride is a semiconductor whose optical properties (3 - 5) make it a possible material for LEDs. It has a direct energy gap (6 - 11) at a width near 3.50 eV at 1.6 K, and 3.44 eV at 300 K (9). It emits strongly in the near ultra-violet and with suitable doping giving deep impurity levels, or with down-converting phosphors it could give light anywhere in the visible spectrum.

However all GaN material grown to date has been of n-type conductivity. Nominally pure GaN has carrier concentrations ranging from 10^{17} cm^{-3} to 10^{20} cm^{-3} depending on the growth conditions (12). A residual donor thought to be the nitrogen vacancy (13, 14) is responsible for the high carrier concentrations. Attempts to compensate this donor by doping with impurities such as Zn, Mg, Be, and Li which are usually acceptors in III - V compounds give semi-insulating material (3 - 5) but do not change the conductivity type. Although p - n junctions have not been made, electroluminescence has been demonstrated at photon energies from 1.7 eV to 3.4 eV (15 - 20) using metal-insulator-semiconductor (MIS) diodes. A prototype seven segment alphanumeric display has been produced, emitting in the yellow (21) and stimulated emission has been observed in externally pumped crystals (22).

One research field of current interest is the doping of GaN with acceptor and other impurities in attempts to reduce the carrier concentration and to produce deep levels which will emit visible light in luminescence.

Indications are that the solubility of many dopants in GaN is low (11,17). A method of doping which can give impurity concentrations much higher than are obtainable by orthodox methods is ion implantation, and the effect of a range of implanted impurities on the properties of GaN is described in the thesis.

The GaN material was grown by Wickenden at the Hirst Research Centre of GEC. It was in the form of epitaxial layers about 10 μm thick and 1cm square, deposited on α-Al_2O_3 substrates. Ion implantation was carried out by Todkill also at HRC. The implanted layers were annealed to reduce the damage introduced during implantation and the resulting changes in semiconducting properties were measured by luminescent methods at Bath University. The earlier measurements used an He - Cd laser on loan from HRC to excite photoluminescence and the later ones a cathodoluminescence rig built at Bath. Absorption spectra were also measured at Bath and some excitation spectra were recorded at HRC. It was also possible to study the optical properties of neutron-irradiated GaN and of a range of $Ga_{1-x}Al_xN$ alloys grown by Wickenden at HRC.

In the second chapter of this thesis a survey is made of the structure and growth chemistry of GaN. The third chapter describes the luminescent and other optical properties. This is followed by a chapter discussing the reasons for choosing ion implantation as a method for doping GaN and optical methods for investigating the

implanted layers. Chapter five deals with the theory of ion implantation, the experimental details of the impurities introduced and the heat treatment necessary to restore crystal order. In chapter six the experimental procedures and the apparatus used for photoluminescence, cathodoluminescence, absorption and excitation spectra are described. Chapter seven records the results of the luminescent investigations of each of the samples studied, of the absorption spectra, and of the excitation spectra; and in chapter eight the conclusions drawn from these results are discussed.

Chapter 2.

GALLIUM NITRIDE PROPERTIES I

GENERAL

2.1 STRUCTURE

GaN crystallises normally in the hexagonal wurtzite structure (space group 6_3mc) in which each atom is co-ordinated by four unlike nearest neighbours. It has lattice parameters a = 3.18Å, c = 5.18Å, and a density of 6.1g cm^{-3} (23,24). The concentration of Ga or of N atoms is therefore 4.4 x 10^{22} cm^{-3}.

When pure, GaN is transparent throughout the visible. Band structure calculations (25-27) indicate a direct energy gap of about 3.5 eV. All optical transitions other than the E_o transition at the Γ point in k-space are above 6 eV (Fig 2.1).

2.2 CRYSTAL GROWTH METHODS

The material used in this work was grown at the GEC Hirst Research Centre by Wickenden using the chemical vapour deposition technique first developed by Maruska and Tietjen (28,29). Gallium is transported to the reaction zone of the furnace as the subchloride GaCl by passing HCl and N_2 carrier gas over a boat of molten Ga, there it meets a countercurrent of NH_3 (Fig 2.2) and at growth temperatures between 1000°C and 1200°C GaN is formed. Single crystal material is formed as an epitaxial layer on a suitable substrate.

Ideally, substrate and deposited material should have identical lattice parameters and expansion coefficients,

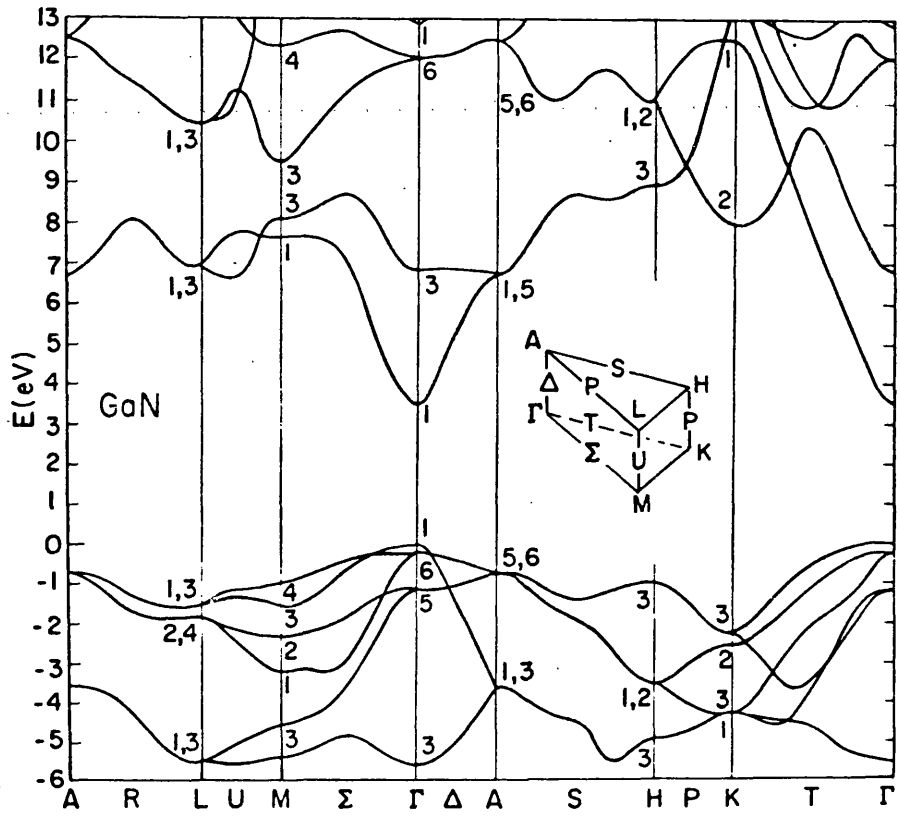

Figure 2.1 Band structure of GaN (25)

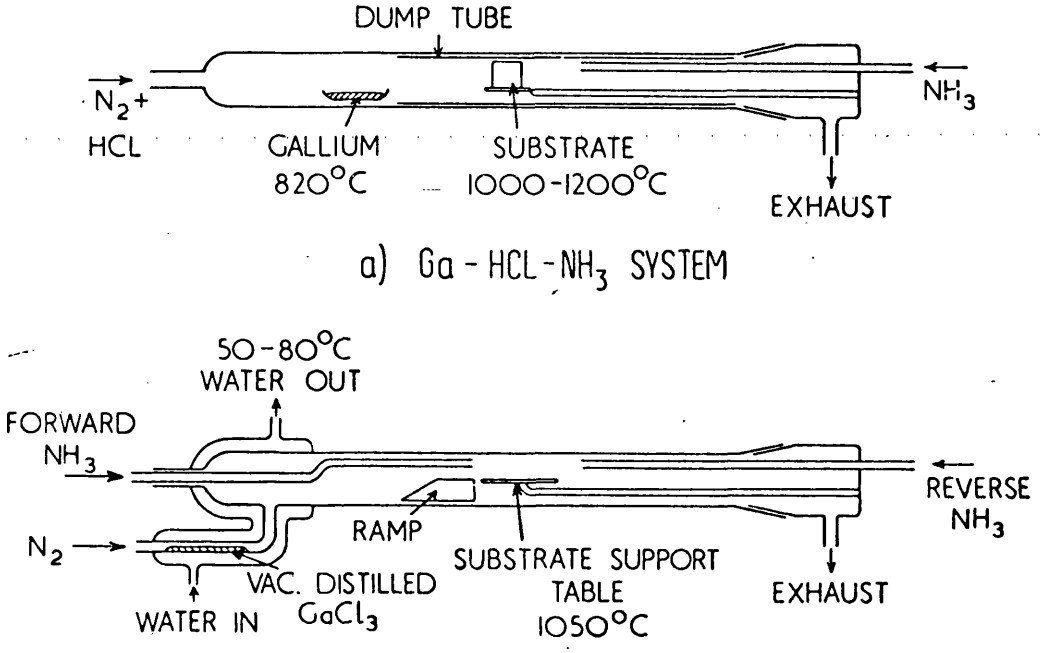

Figure 2.2 Schematic diagram of furnace systems used to produce GaN epitaxial layers (29)

and strong chemical bonding between their constituents. A number of substrate materials have been investigated for GaN growth (29,30). The most satisfactory is corundum (α-Al_2O_3), despite the wide disparity between the lattice constants and a considerable thermal mis-match. Presumably strong bonding is the dominant factor. The first GaN grown at GEC was on (00.1) α-Al_2O_3 substrates (29) but after a detailed study of the epitaxial relationship between GaN and α-Al_2O_3 (31) maximum growth was found to occur when (11.0) GaN is deposited on (21.1) α-Al_2O_3. In this orientation layers of about $1cm^2$ area and a uniform thickness of about 10μm are formed. Thermal shock due to the differing rates of contraction on cooling does however cause a variable density of well-defined slip bands to form parallel to (00.1) (Fig 2.3). A considerable degree of residual strain is also to be expected. Away from the slip bands the surface is of much better optical quality than in other growth orientations. To facilitate absorption measurements both surfaces of the α-Al_2O_3 substrates used were polished optically flat.

A review of growth methods is found in Rabenau (32). More recently work has been concentrated on the epitaxial growth of extended single crystal material for semiconductor investigations. Ammonolysis of a number of volatile Ga compounds has been used, the growth from GaCl described above being most satisfactory (33). GaN is unstable at the usual growth temperatures (12,14) and some low temperature methods have been utilised. Chemical methods involve the dissociation of volatile complexes such

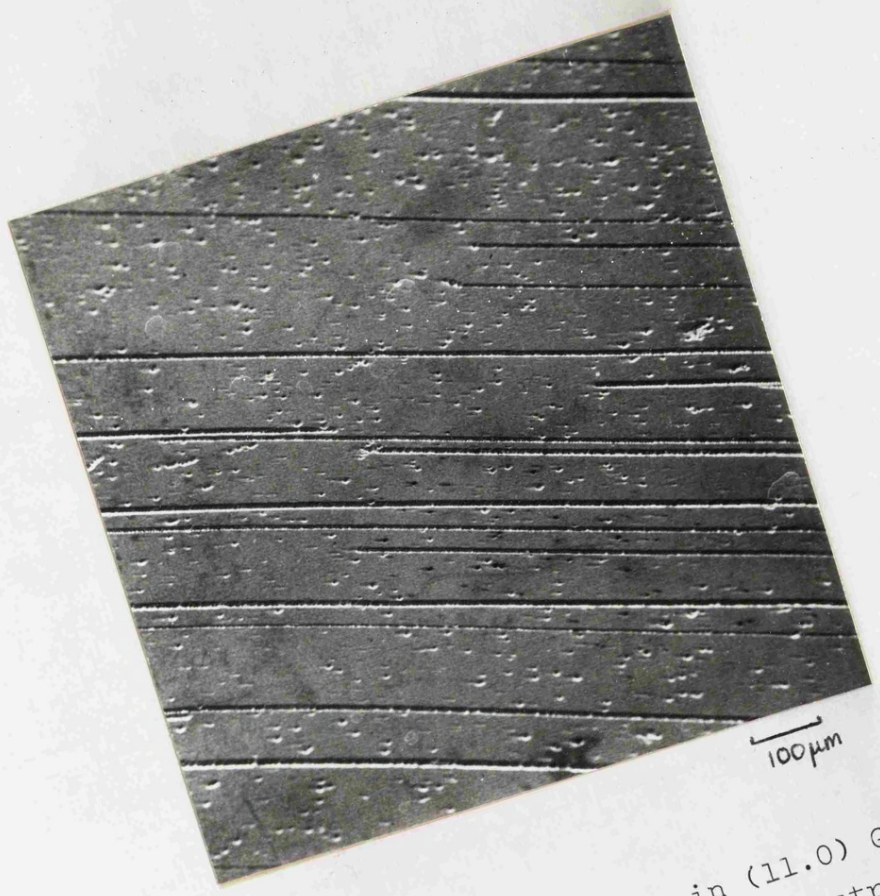

Figure 2.3 Slip bands in (11.0) GaN deposited on (21.1) α-Al_2O_3 substrates (after annealing at 850°C)

as $GaBr.NH_3$ (34). Physical methods have included radio frequency sputtering (35) and the reaction of Ga or GaCl with active nitrogen generated from a microwave discharge in N_2 rather than by dissociation of NH_3 (36). Growth from Ga solution has been reported (37) and sufficiently large GaN crystals have been produced by one group (33) to permit homo-epitaxial growth of GaN on GaN. This should result in strain-free crystals. None of these methods have produced insulating undoped GaN as yet, however, and the material is always n-type. The native defect seems to be a dominant feature in GaN grown by all methods.

2.3 CHEMISTRY OF CRYSTAL GROWTH

Some understanding of the properties of GaN may be gleaned from the growth chemistry. Lorenz and Binkowski (13) discovered that their polycrystalline GaN began to lose N_2 slowly above 600°C and suggested that as-grown GaN was deficient in nitrogen. Improved growth techniques may give better crystal quality and more stable GaN but indications are that GaN is unstable at the normal growth temperatures (38). Loss of N led to the suggestion that Ga interstitials or, more probably, N vacancies were the residual donor species (12).

Ban (14) in a detailed mass-spectrographic study of the chemical species present during the vapour deposition of GaN by the method of Maruska and Tietjen (28) identifies the controlling reaction:-

$$GaCl(g) + NH_3(g) \overset{K_1}{=} GaN(s) + GaCl_3(g) + H_2(g) \qquad 2\text{-}1$$

Free energies of formation ΔF^{o}_{f} of the species involved in the reaction have been calculated (14), showing that at 900°C GaN is unstable with respect to:-

$$GaN(s) = Ga(l) + \tfrac{1}{2}N_2(g) \qquad 2\text{-}2$$

with a free energy of reaction $\Delta F^{o}_{r} = -26\ kJmol^{-1}$

Ammonia is also unstable with respect to the reaction:-

$$NH_3(g) = \tfrac{1}{2}N_2(g) + \tfrac{3}{2}H_2(g) \qquad 2\text{-}3$$

with a free energy of reaction $\Delta F^{o}_{r} = -79\ kJmol^{-1}$

The only reason that GaN can be formed by the reaction 2-1 ($\Delta F^{o}_{r} = -40\ kJmol^{-1}$) which involves two unstable species is that the rates of reactions 2-2 and 2-3 are much slower than that of 2-1.

i.e. since $K_1 >> K_2, K_3$; GaN is formed as a metastable state only because it is deposited much faster than it decomposes.

It would not be surprising however if native defects in sufficient numbers to affect semiconductor properties are formed in this reaction. If the residual defect is a N vacancy acting as a single donor the carrier concentration about $10^{19}\ cm^{-3}$ corresponds to a departure from stoichiometry of only 0.015%.

Investigations of impurity concentrations in GaN by spark emission spectroscopy and ion probe mass spectrometry (12) show no correlation between impurity concentration and carrier concentration suggesting that the high electron concentration is due to a lattice defect rather than residual impurities.

Low carrier concentrations are, however, associated with high growth rates so a slow dissociation of GaN after deposition may be responsible for an increase in defect density. The identification of the particular defect present is possible, in principle, by study of annealing behaviour in an atmosphere of Ga or N. However slow self-diffusion rates in GaN are thought to frustrate attempts at such annealing studies (14). Liquid phase epitaxy of GaN in a mixed melt of Ga and Bi has permitted a variation of NH_3 pressure over GaN which produces a decrease in carrier concentration with increased NH_3 pressure (37). This is evidence for the residual donor being the N vacancy.

Two recent reports add further evidence for this suggestion. Madar et al. (39) have grown GaN in a vapour-liquid-solid system (N_2-Ga-GaN) at pressures up to 8kbar and temperatures up to 1200°C. They report a variation of electrical properties with growth parameters, including deposition of p-type polycrystalline material, which is in agreement with the residual donor being the N vacancy. They also estimate the equilibrium pressure of N_2 over GaN at a wide range of temperatures and pressures. It reaches atmospheric pressure at 840°C, well below most reported growth temperatures, so dissociation of GaN may be expected to occur in most vapour deposition methods. A diffusion-controlled dissociation process is suggested to explain the slow rate of decomposition. Saxena et al. (40) have implanted 60 keV $^{14}N^+$ ions into GaN to a depth of 0.12μm and studied the current-voltage characteristics

of Cr-GaN Schottky barrier diodes on implanted and un-implanted material. They interpret their results as showing an electron concentration of 10^{16} cm^{-3} after implantation as opposed to 10^{19} cm^{-3} before implantation and suggest that the implanted N atoms have filled the vacancies in as-grown GaN. However they did not anneal their samples and assumed the effect of radiation damage to be negligible.

GaN is usually grown by vapour phase deposition but it is metastable at the usual growth temperatures and some dissociation takes place. This is thought to result in a N vacancy which acts as a residual donor and causes the persistent n-type conductivity of GaN.

Chapter 3.

GALLIUM NITRIDE PROPERTIES II

OPTICAL

3.1 INTRODUCTION

The elucidation of the band structure and impurity levels in GaN rests almost entirely on optical evidence, since the high electron concentration makes electrical investigations difficult. In this chapter a general discussion of optical recombination in semiconductors of both high and low purity is followed by a description of known optical processes in luminescence and absorption of GaN.

3.2 OPTICAL TRANSITIONS IN PURE SEMICONDUCTORS

The recombination of electrons and holes in semiconductors is accompanied by a release of energy. In radiative recombination this energy appears mostly in the form of a photon although one or more phonons may also be produced. The phonon involved in optical transitions is usually the longitudinal optical (LO) phonon because of its high polarisation field. In direct-gap semiconductors such as GaN, phonon cooperation is not necessary to conserve crystal momentum but phonon replicas of radiative transitions are found at energies below that of the no-phonon line in emission spectra.

In high purity semiconductors the radiative transitions may follow a number of well-defined paths (1,41). There will also be non-radiative transitions in which energy released is transferred to the electronic and

vibrational energy of the crystal. These transitions will compete with the radiative transitions and influence the intensity of the latter.

Amongst the transitions which have been identified in radiative recombination of electrons and holes are (Fig 3.1):-

1) Band-to-band transitions Excitation of electrons from the valence band to the conduction band produces a non-equilibrium population of free electrons and holes. In semiconductors with low carrier concentrations at low temperatures, direct recombination of free electrons and free holes is not normally observed. Various associative mechanisms give the dominant emission spectra.

2) Free exciton recombination The Coulombic attraction between electron and hole causes them to pair off into combined states analogous to the hydrogen atom in which the lighter electron orbits around the heavier hole. These states are known as excitons and comparison with the Bohr model yields a binding energy

$$E_x = 13.6\ (\mu/n^2\varepsilon_r{}^2 m)\ eV$$

Where μ is the reduced mass of the electron and hole, m the electron mass, and ε_r is the appropriate dielectric constant (42). Only the n = 1 transition is usually observed in electron-hole annihilation giving emission at a photon energy

$$h\nu = E_g - E_x$$

Figure 3.1

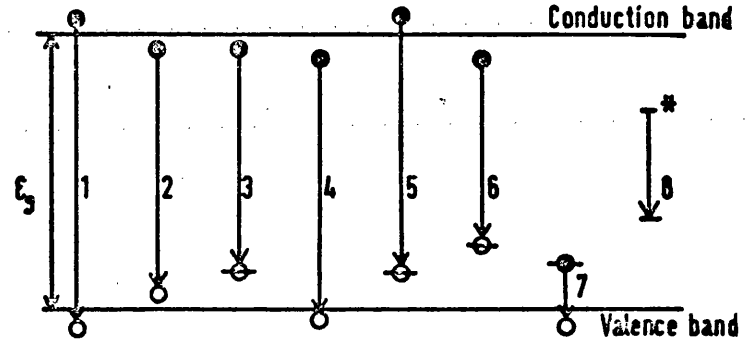

Recombination mechanisms in semiconductors.

1. Band-to-band $h\nu > \mathcal{E}_g$
2. Free exciton $h\nu = \mathcal{E}_g - \mathcal{E}_{ex}$
3. Bound exciton $h\nu = \mathcal{E}_g - (\mathcal{E}_{ex} + \mathcal{E}_{loc})$
4. Bound-free $h\nu = \mathcal{E}_g - \mathcal{E}_D$
5. Free-bound $h\nu = \mathcal{E}_g - \mathcal{E}_A$
6. DA pair $h\nu = \mathcal{E}_g - (\mathcal{E}_A + \mathcal{E}_D) + e^2/4\pi\varepsilon\varepsilon_0 r$
7. Impurity ionisations $h\nu = \mathcal{E}_A$
8. Local centre, excited state - ground state.

3) Bound exciton recombination At low temperatures, one of the components of an exciton may be trapped at a neutral donor or acceptor site. The recombination energy is less than that for the free exciton by an amount E_{loc}, the binding energy of the exciton to the impurity giving:-

$$h\nu = E_g - E_x - E_{loc}$$

In general E_{loc} is about $0.1E_D$ or $0.1E_A$ where E_D, E_A are the donor or acceptor ionisation energies, as appropriate. Recombination of an exciton trapped on a neutral acceptor is termed an I_1 line and, on a neutral donor an I_2 line. These are much sharper than free exciton lines and are easily ionised at temperatures above a few Kelvin.

Other excitonic complexes (analogous to H_2^+, H_2 etc.) may occur whose components are electrons, holes and charged impurities (41).

4) Recombination at isoelectronic traps These are formed where the impurity atom is in the same group of the periodic table as the host atom it displaces in the lattice. They form electrically inactive centres to which excitons can be bound. Interaction between neighbouring sites gives complex sharp line spectra in both emission and absorption at low temperatures.

5) Band-impurity transitions Electrons in the conduction band may be trapped by a neutral acceptor level above the valence band giving a free-bound transition

$$h\nu = E_g - E_D$$

The donor ionisation energy E_D may be estimated for hydrogenic donors in which a conduction electron of mass m^* orbits round the charged donor as

$$E_D = 13.6 \ (m^*/m\varepsilon_r^2)$$

Where ε_r is the static dielectric constant.

Since $E_A > E_D$ for hydrogenic impurities the donors will be ionised first and free-bound transitions are more probable than the bound-free transition at:-

$$h\nu = E_g - E_A$$

These lines will appear only when the impurities are ionised.

6) Donor-Acceptor (DA) pair transitions At low temperatures where impurities are not ionised, an electron trapped on a donor may recombine with a hole trapped on an acceptor leaving ionised impurity centres between which there is a Coulombic interaction dependent on the pair separation, r, giving a recombination energy

$$h = E_g - (E_A + E_D) + e^2/4\pi\varepsilon_r\varepsilon_o r$$

Where ε_r is the static dielectric constant.

Well-defined line spectra are found in high purity material. The time-dependence of luminescent line-shape through the varying recombination rates of pairs at different separation with different orbital overlaps, gives a way of identifying D-A pair spectra where sharp lines are not found. At high temperatures, D-A pair

luminescence will be quenched by a free-bound transition as the donors become ionised.

7) Deep centres Transitions to levels deep in the energy gap will occur at:-

$$h\nu = E_g - E_i$$

Where E_i is the impurity ionisation energy.

8) Local transitions A situation may arise where both the ground state and an excited state of a deep level occur within the band-gap. Transitions may then occur at this impurity centre.

3.3 OPTICAL TRANSITIONS IN HIGHLY IMPURE SEMICONDUCTORS

The above spectra are found in high purity material. In less pure material the electric fields of ionised impurities, and the strain fields due to crystalline imperfection cause major changes in the spectra. Local electric fields act in the opposite direction on electrons and holes and tend to dissociate excitonic pairs, making direct recombination of electrons and holes more probable. Strain fields do not tend to dissociate excitons. High n- or p-type carrier concentrations pin the Fermi level in the conduction or valence bands causing shifts in emission peaks. Interaction between neighbouring impurity centres will lead to a broadening of the impurity levels. At high impurity concentrations the impurity levels will become degenerate with the conduction or valence band and it will be no longer possible to talk of localised impurity levels.

An approximate value for the concentration of hydrogenic impurities N_{min} at which this occurs is (43)

$$N_{min} = 3 \times 10^{23} (m^*/m\varepsilon_r)^3 \text{ cm}^{-3}$$

Estimated values of carrier effective mass m^* and static dielectric constant ε_r in GaN (3) lead to values

$$N_D \cong 2 \times 10^{18} \text{ cm}^{-3} \text{ for donors}$$

$$\text{and } N_A \cong 1 \times 10^{20} \text{ cm}^{-3} \text{ for holes}$$

Thus a donor band degenerate with the conduction band may be expected in most GaN material but an acceptor band is not likely to be formed. When the donor band is degenerate with the conduction band major changes occur in optical transitions.

At any point in the crystal the separation of conduction and valence bands is constant at E_g but the electric fields of charged impurities will cause them to vary spatially through the crystal (Fig 3.2). Electron and hole wavefunctions decay exponentially with distance into the bandgap at constant energy and tunneling-assisted transitions at energies less than those in unperturbed material become possible (44). One effect of the presence of charged impurities is to broaden spectra by this process.

The perturbation of the band edges produces a tail to the density of states as shown in Fig 3.2b. Where the material is predominately of one conductivity type, the Fermi level will be located within the appropriate band tail

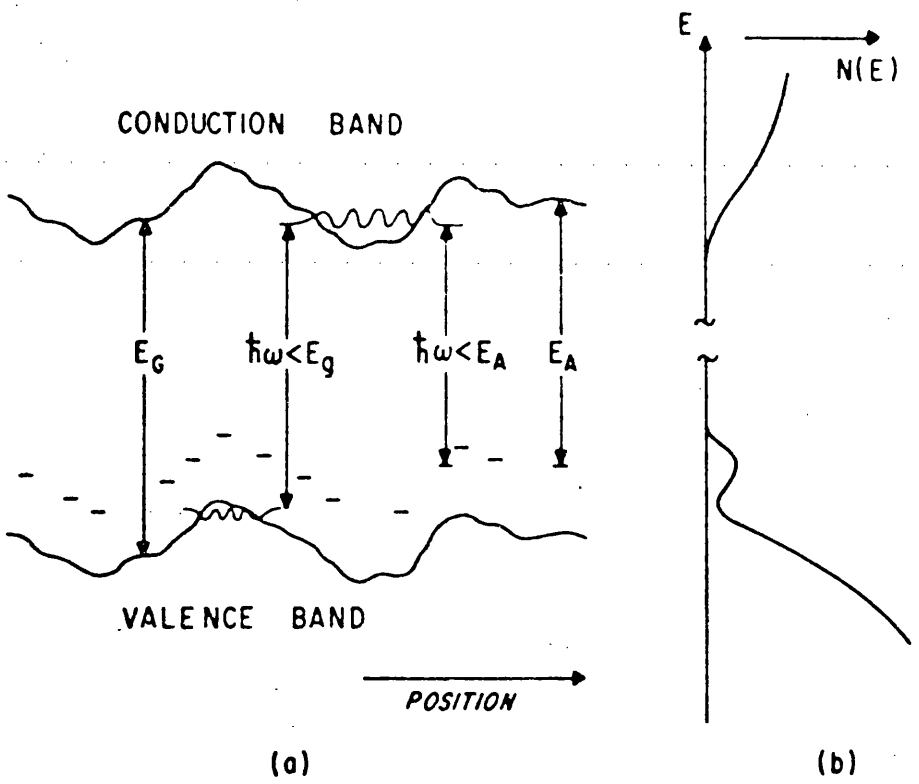

Figure 3.2 a) Variation of energy gap with position in the presence of charged impurities. Tunneling assisted transitions may occur.

b) The resulting density of states diagram. (41)

and the carriers will be degenerate. This gives a carrier concentration which varies only slowly with temperature and hence metallic conductivity. The optical transitions will be from the occupied conduction band tail in n-type material to vacant acceptor or valence band states. The variation of intensity within any emission band will give a peak at the photon energy corresponding to the maximum electron density in the conduction band. This is the product of the density of states in the band tail and of the occupancy of these states which is determined by the Fermi level. The Fermi level increases with increasing electron concentration and band-to-band or band-to-acceptor transitions will therefore have peak energies which increase with electron concentration (45). In addition the Fermi function is strongly temperature dependent and this may lead to variations in peak photon energy with temperatures which are very different from those anticipated from the change in energy gap (46).

High carrier concentrations are produced by high concentrations of charged impurities. The electric fields of these impurities deform the band edges. This permits tunneling-assisted transitions which broaden emission and other spectra. The resulting band tailing produces a number of changes in emission spectra from those of high purity material. Transitions involving donors become transitions from the conduction band tail and the variation of Fermi level with carrier concentration and temperature governs the peak photon energy of the emission.

3.4 GALLIUM NITRIDE - ABSORPTION

Early estimates of the nature and size of the band gap in GaN came from studies of the edge absorption (28,47), but the data were difficult to interpret accurately. The strength of the edge absorption is high, rising to over 10^4 cm^{-1} near the band gap. This suggests a direct transition, but the dependence of absorption coefficient, α, on photon energy is not of the form

$$\alpha \propto (h\nu - E_g)^{1/2}$$

expected from a direct transition between parabolic bands (2).

Instead in the near-gap region (3.4 to 3.0 eV at room temperature) an exponential increase in the absorption is found:-

$$\alpha \propto \exp(h\nu/E_o)$$

with a constant E_o of the order of 30 meV.

This type of dependence is found in a number of experimental situations (48). In the direct-gap semiconductor GaAs it has been correlated with the presence of a tail of states below the conduction band minimum (49). Dow and Redfield (50) describe a model involving tunneling-assisted transitions permitting the creation of excitonic electron-hole pairs at energies below that of the normal free exciton energy $E_g - E_x$. They deduce a value for the absorption coefficient below the free exciton energy of the form:-

$$\alpha \propto \exp(- (E_g - E_x - h\nu)/E_o)$$

where the constant E_o is given by:-

$$E_o = 7.5 \times 10^{-13} \varepsilon_r^{\,2} (m/\mu)^2 N_D^{\,2/3} E_x$$

N_D is the concentration of ionised donors (in cm^{-3})

μ is the reduced mass of the electron-hole pair

E_x is the exciton binding energy.

Camphausen and Connell (51) use the static dielectric constant for ε_r and find that calculated values of N_D in GaN are of the same order of magnitude as the electron concentration, so the exponential absorption edge can be explained as the perturbation of the band edges by the charged defects producing the electrons in the conduction band.

In addition to the near-gap exponential absorption, Pankove (3) identifies three other regions in the absorption spectra of GaN (Fig 3.3).

At photon energies around 3 eV a second exponential absorption

$$\alpha \propto \exp(h\nu/E_1)$$

is found with E_1 rather larger than E_o.

Between 3.0 and 1.5 eV there is a broad shoulder in the absorption spectrum which shows a variation with photon energy of the form

$$\alpha \propto (h\nu - 1.7)^2$$

which is a dependence expected of a transition from a

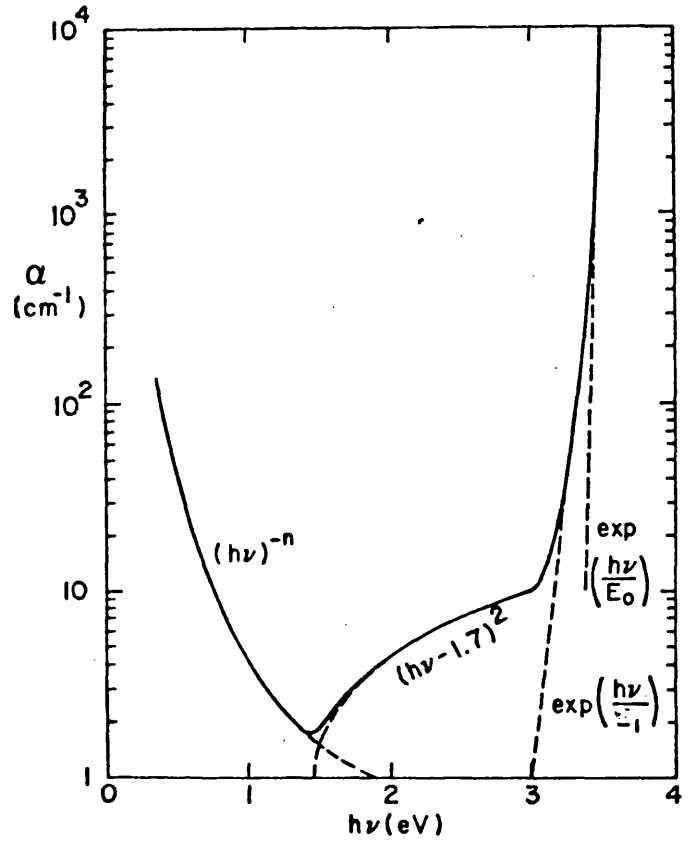

Figure 3.3 Optical absorption in GaN (3)

deep centre within the forbidden gap.

Below 1.5 eV the absorption coefficient rises rapidly with decreasing photon energy following a dependence of the form

$$\alpha \propto (h\nu)^{-n}$$

which is expected from free carrier absorption. The value of the index n depends on the mechanism by which conductors are scattered. Scattering by acoustic phonons gives n = 1.5, by optical phonons gives n = 2.5 and by ionised impurities n = 3 to 3.5. Values of n for GaN vary from 2.5 to 3.9 (52) which suggests that in most samples ionised impurities are the dominant scattering mechanism.

The free carrier absorption will reach a maximum near the plasma energy which has been estimated at 0.6 eV for a sample with an electron concentration of 5.8×10^{19} cm^{-3} (53). At these values there will be contributions to the absorption from the vibrational modes of the lattice which have energies of the order of 0.1 eV (54,55).

3.5 GALLIUM NITRIDE - LUMINESCENCE

1) Undoped The near-gap luminescence of low conductivity GaN can be split into two distinct regions. The region between 3.5 and 3.3 eV is dominated by a number of sharp spectral lines in both compensated and nominally pure material. These have been variously identified with the recombination of free excitons near 3.475 eV at 1.6 K; with the recombination of excitons bound to donors and

acceptors near 3.470 and 3.455 eV respectively (1.6 K) and with a number of unidentified transitions. Phonon replicas at about 90 meV below these lines are identified with the LO phonon whose energy has been estimated at 91.5 meV (54). Other replicas at separations near the TO phonon energy of 70 meV and an unidentified 14 meV energy are also reported (Fig 3.4). The excitation energies appropriate to these states have been measured.

Below 3.3 eV the low-temperature luminescence is dominated by a DA pair line near 3.27 eV and its 90 meV LO phonon replicas (Fig 3.4). Above about 30 K the donors are thermally excited and this becomes a free-bound transition at slightly higher energies (6). This transition is quenched above 80 K by a competing non-radiative transition and is not seen above 200 K.

The lowest energy band gap has been determined as 3.503 eV at 1.6 K from photoluminescence excitation spectra (10). The valence band is in fact split into three by the spin-orbit and crystal-field perturbations of the wurtzite lattice (7). Associated with these three band gaps are three exciton energies found in reflectance (7) and photoluminescence (10) spectra. These are at energies of 3.4751, 3.4815, and 3.493 eV at 1.6 K for the A, B, and C excitons respectively.

The energy gap decreases with increasing temperature in a way that can be approximated by (9):-

$$E_g = (3.503 + (5.08 \times 10^{-4} T^2)/(T - 996)) \text{ eV}$$

Figure 3.4 Near-gap luminescence in GaN

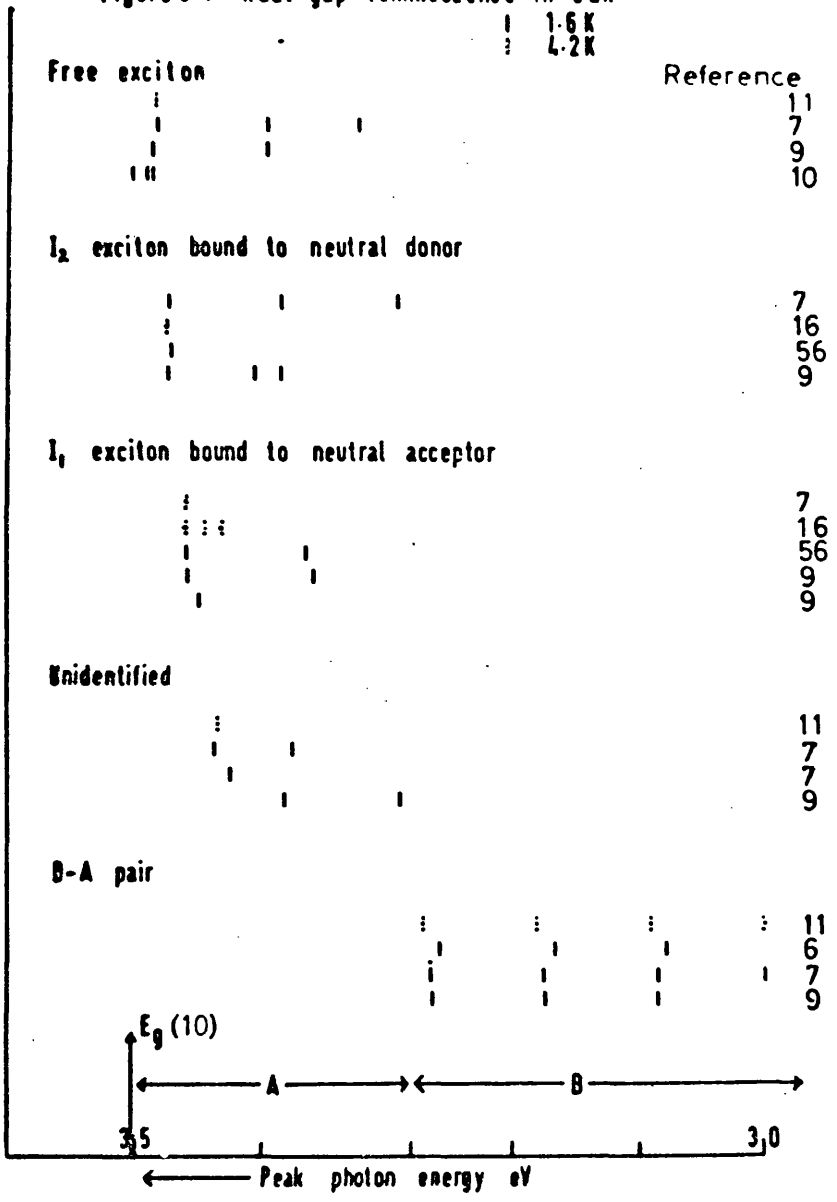

and all the near-gap emissions have peaks which follow this dependence.

In material with higher carrier concentrations the perturbation of the band edges by the ionised residual donors gives broad bands in the spectra. At carrier concentrations of the order of 10^{19} cm^{-3} two broad bands can usually be identified (Fig 3.5). (The sharp lines near 1.8 eV are the red emission from Cr impurities in the α - Al_2O_3 substrate, excited by the near-gap emission of GaN).

The first, in the range 3.5 - 3.3 eV is known as the A-band. Its peak photon energy may depend on carrier concentration (40) moving to higher values as electron concentration increases and the Fermi level moves to higher energies within the tail of states. Or it may be fixed near an impurity band below the gap energy, peaks are commonly found near 3.47 eV and 3.43 eV at low temperatures. The intensity of the A-band falls only slowly with increasing temperature (Fig 3.6).

The second band, the B-band, is found at photon energies below 3.3 eV and is associated with free-bound transitions, broadened by tunneling. It is quenched with increasing temperature in a manner similar to that observed in low carrier concentration material. Its intensity and shape also vary with carrier concentration (52). At low carrier concentrations the B-band is strong, relative to the A-band, and separate phonon replicas may be resolved. As the carrier concentration increases, the ratio of B-band

Figure 3·5

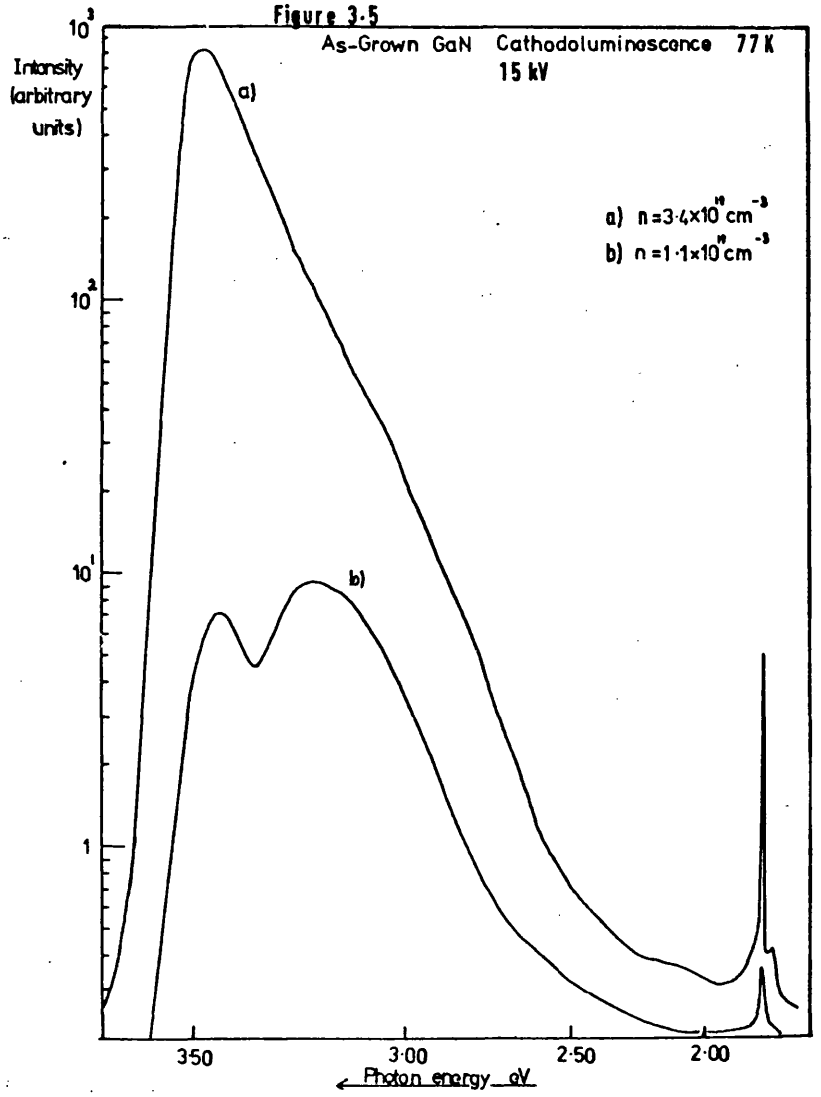
As-Grown GaN Cathodoluminescence 77 K
15 kV
Intensity (arbitrary units)
a) n=3·4x10^18 cm^-3
b) n=1·1x10^18 cm^-3
a)
b)
10^3
10^2
10^1
1
3·50
3·00
2·50
2·00
Photon energy eV

Fig. 3·6

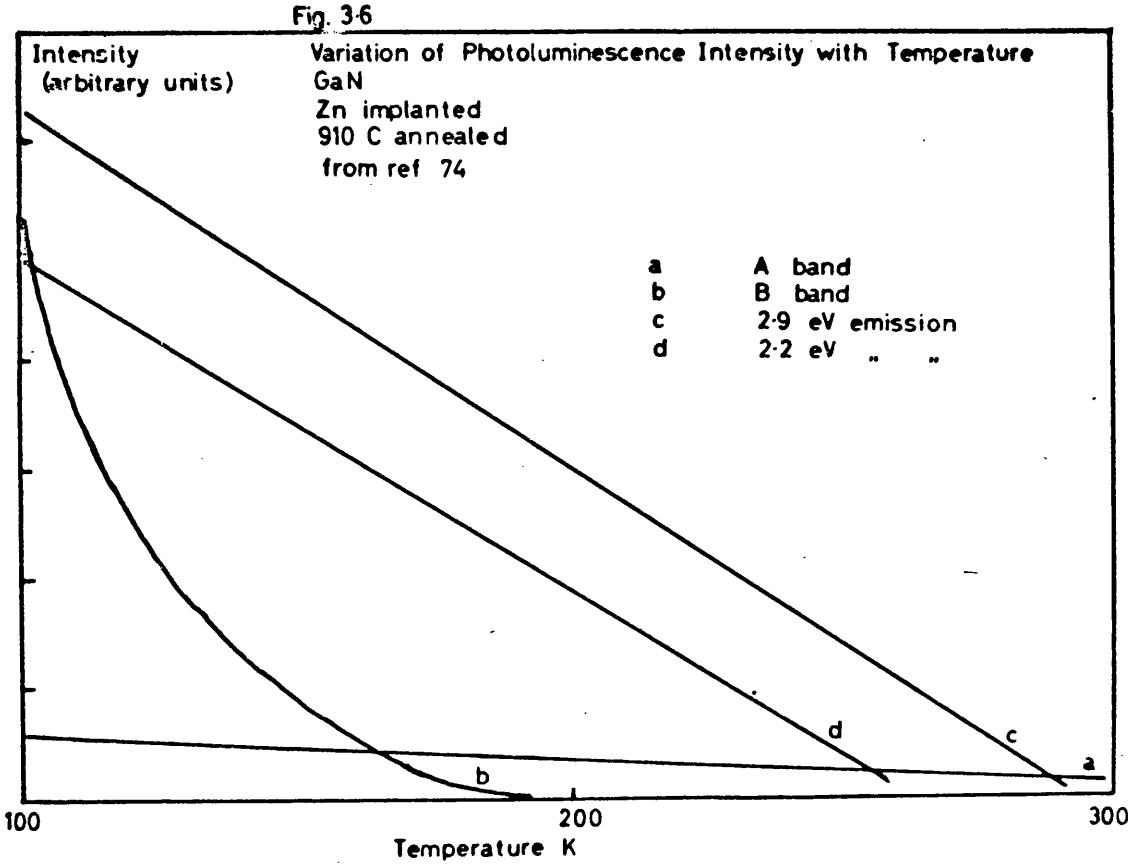
Intensity
(arbitrary units)
Variation of Photoluminescence Intensity with Temperature
GaN
Zn implanted
910 C annealed
from ref 74
a A band
b B band
c 2·9 eV emission
d 2·2 eV " "
a
b
c
d
100
200
300
Temperature K

intensity to A-band intensity decreases until at carrier concentrations of around 4×10^{19} cm^{-3} the B-band is not resolvable from the A-band tail (Fig 3.5) although the low energy component is still quenched at high temperatures. The relative size of the A and B-bands can be used as a measure of carrier concentration (52).

2) Doped Studies of impurity luminescence in GaN have been principally concerned with the introduction of possible acceptor species which might reduce the carrier concentration (3). Some studies have also been made of activators in GaN phosphors (57,58).

Compensating impurities which give semi-insulating GaN include Zn, Mg, Be, Li, and Hg. These impurities give luminescent bands which have half-widths of several hundred meV and whose peak photon energies do not shift with the energy gap as temperature changes, instead remaining almost constant. Fig 3.7 shows the peak photon energies of these impurity emissions and also those for Cd, whose low solubility does not permit carrier compensation, and a number of GaN phosphors.

The compensating impurities are thought to give deep acceptor levels which are associated with the valence band (59,61). Transitions from the conduction band to an acceptor level pinned to the valence band are normally expected to show the same temperature dependance as the energy gap, but in the presence of band tailing a peak photon energy almost independant of temperature is possible (45). Pankove et al. (59) have suggested a mechanism in

Figure 3·7 Deep impurity luminescence in GaN

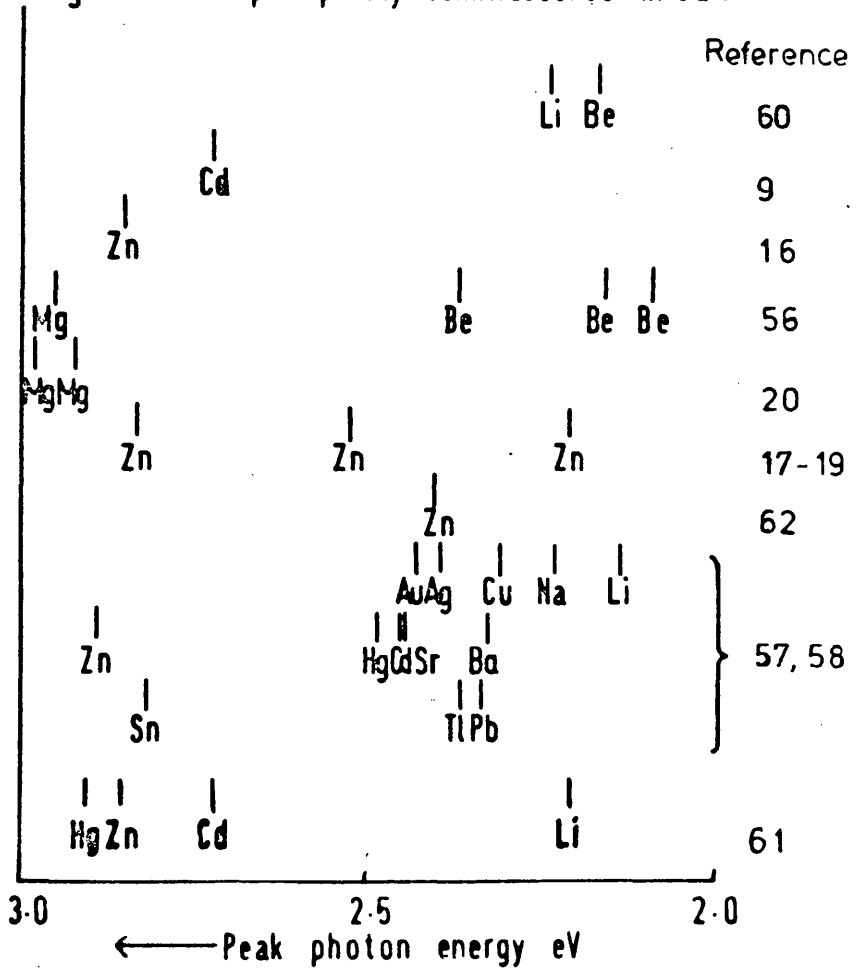

which electrons, excited into the conduction-band trough near a donor, tunnel into the neighbourhood of an ionised acceptor and recombine (Fig 3.8). They propose a fast non-radiative capture of holes on the acceptor and another non-radiative process whose strength increases with Zn concentration which causes direct band-to-band recombination quenching the Zn band at high concentrations.

A number of investigations have been made of the donor and acceptor excitation energies in GaN. A donor 30 meV below the conduction band may be the N vacancy and an acceptor at 200 meV is also found (6). Wide ranges of energies for the deep acceptor in Zn and other impurities have been reported. Pankove et al. describe photoluminescence emission spectra of Zn doped GaN whose peak photon energy varies from 1.8 to 2.9 eV (59) and it may be that Zn is involved in a number of different types of centre.

3) Electroluminescence In the absence of p-type material a p-n junction diode cannot be made, but other junction configurations have been used. Schottky-barrier diodes have only had limited success, because GaN has a work function higher than that of most metals (19). Luminescence has been produced at a wide range of photon energies using metal-insulator-semiconductor diodes. A layer of semi-insulating acceptor-doped GaN can be grown epitaxially on semiconducting material and a metal layer (usually In) deposited on the surface (18). Zn-doped GaN can give electroluminescence throughout the visible spectrum (15-18,62) and Mg- and Be-doped diodes have also been made

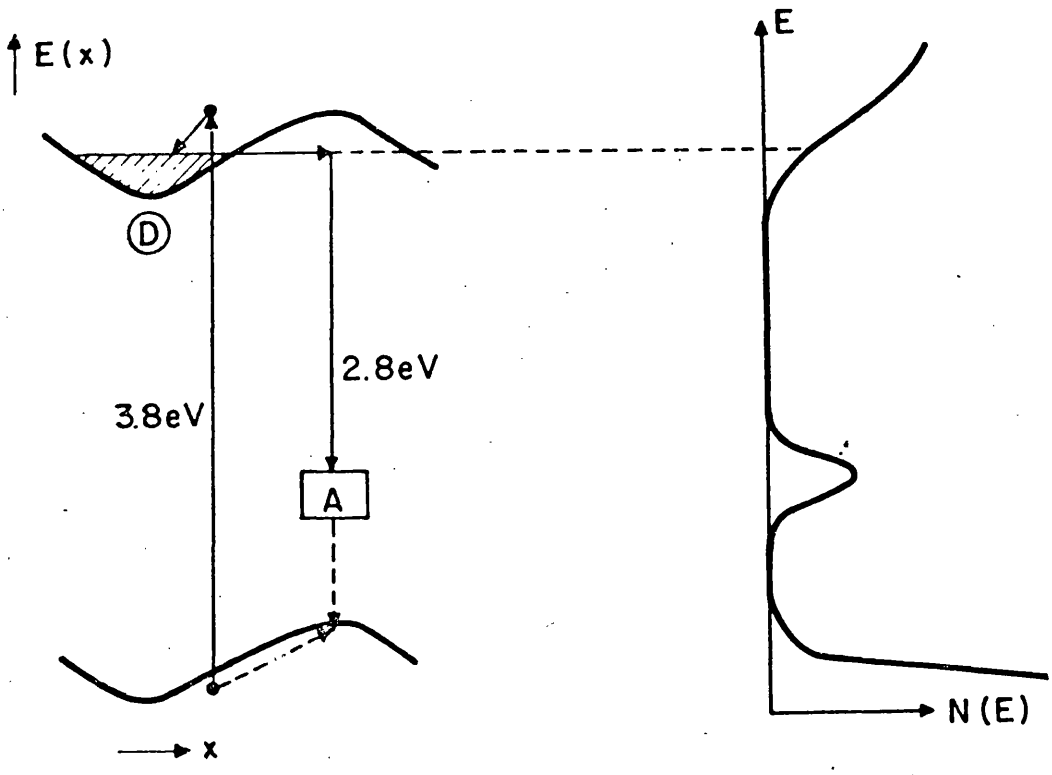

Figure 3.8 Model for the photo-luminescence process and distribution of states in Zn-doped GaN (59)

(20,60). GaN is therefore a promising LED material in which device operation has been demonstrated as feasible.

Chapter 4.

DOPING OF GALLIUM NITRIDE

4.1 SELF COMPENSATION

A prime requirement in GaN growth is for a method of including an acceptor species in sufficient concentration to convert the material to p-type. To do this acceptor levels must be shallow enough to trap thermally excited electrons from the valence band. The species must be sufficiently soluble to compensate the existing donor species and must not self-compensate by forming donors on other lattice sites, or complexes with native donors to compete with the p-type doping.

As seen above, the group II B elements and Li do give shallow acceptor levels. The dominant luminescent features are associated with deeper acceptor levels 0.6 to 1.2 eV above the valence band. The electrons in the conduction band are trapped at these levels giving insulating material, but the complex levels are too deep for thermal excitation of holes into the valence band.

A similar situation to that in GaN is found with many II-VI compounds which can only be grown of one conductivity type. GaN, because of its high ionicity, is expected to resemble II-VI compounds more than other III-V compounds. Failure to change n-type material into p-type by doping with acceptors may be due to one or more processes (64); native donors may form in equal concentration to the introduced acceptors, the solubility of donors may be too low to compensate the residual donors already present, the acceptor species may also act as a donor on

another lattice site, or native defects may migrate to form electrically inactive complexes with the introduced acceptors. For instance in CdS, only the Li donor has sufficient solubility to compensate native donors, but this is included as an interstitial donor as well as an acceptor on a Cd site (65), and thus the Li dopant compensates itself.

One or more of these mechanisms may be responsible for the difficulty experienced in obtaining p-type GaN.

4.2 CHOICE OF DOPANT

In a III-V semiconductor, atoms present substitutionally on a lattice site will act as acceptors if they have fewer valence electrons than the atom they replace, and donors if they have more. Thus possible donor species are group VI or VII atoms on the anion sublattice and group IV atoms on the cation sublattice; possible acceptors are group II or I on the cation sublattice and group IV on the anion sublattice. Impurities of the same group as the host may form isoelectronic traps which are electrically inactive but which are of interest because of the high optical efficiencies associated with recombination at them (1). Williams (66) lists ionisation energies of impurity levels in GaAs which follow the above pattern.

Simple substitutional doping as above is not the only possibility. Impurities may enter the lattice as interstitials, in which case the above behaviour is approximately reversed. Groups I-III will act as donors, groups V-VII as acceptors and group IV will be amphoteric;

the interstitial atom tending to an inert gas configuration. In the presence of native defects or residual impurities, complexes which have a behaviour radically different to that above are likely to form (66).

An important restriction on the solubility of an impurity as a simple substitutional dopant is its size relative to that of the host atom it replaces. If the covalent radius of a substituent species is more than a few tenths of an Angstrom above that of the host atom its solubility is likely to be low (65,67).

Fig 4.1 shows the structure of GaN with the host atoms and interstitial site marked. The radii of other elements relative to lattice sites in GaN are displayed in Fig 4.2. The strain energy imposed on the lattice by inclusion of a large atom limits the equilibrium concentration of the dopant, although these restrictions may be relaxed if the dopant is present in a complex centre with lattice vacancies. With a small anion as in GaN it seems possible that many species which might be expected to go on the anion lattice because of their high electronegativity; that is group V isoelectronic traps and group VI and VII donors, may, if they are included at all, be included as interstitials or complexes, which may be acceptors or donors.

Thus it seems possible that acceptor impurities might come from any group in the periodic table and a wide-ranging study of doping in GaN is needed to resolve this possibility.

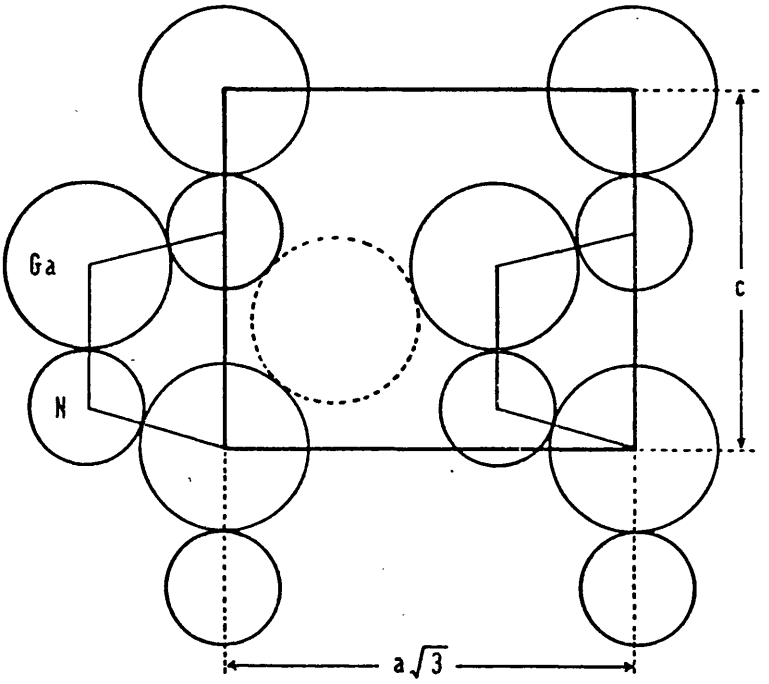

Figure 4.1 Wurtzite structure $11\bar{2}0$ plane showing

Ga r_A = 1.26 Å

N r_B = 0.71 Å

interstitial site r = 1.11 Å

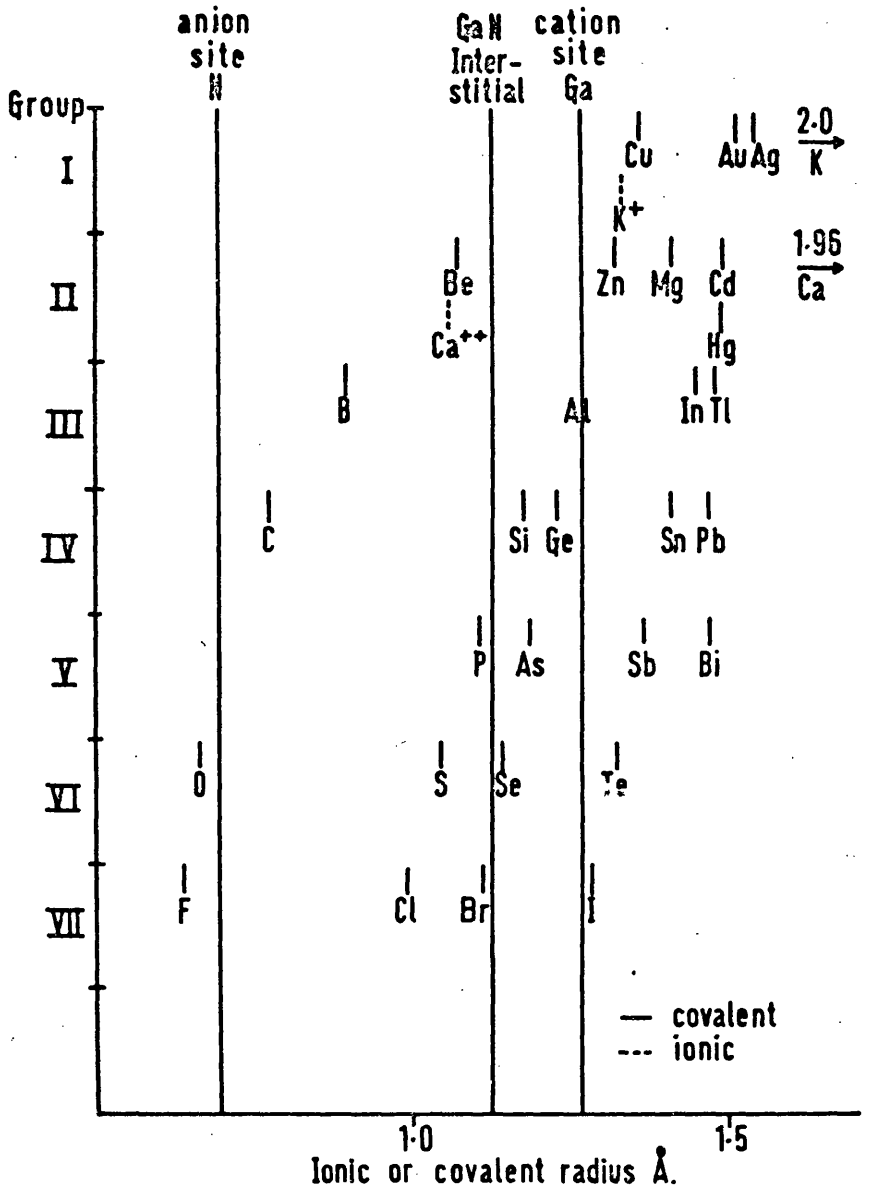

Figure 4.2 Covalent and ionic radii of the elements.

4.3 METHODS OF DOPING

Almost all reported doping of GaN has been achieved by inclusion during the growth process. Grimmeis et al. (58) included dopants in their Ga melt during melt growth of phosphors. Doped single crystal GaN has been produced by inclusion of Zn in a Ga melt in liquid phase epitaxy (33) and most commonly by inclusion as a vapour stream, directly or from a volatile compound, in the chemical vapour deposition of GaN (16-20,56,59). The only dopants producing major changes are the acceptors described above. Doping with C (33) and Ge (41) may reduce carrier concentration slightly. Ge forms a precipitate at high concentrations and is not incorporated appreciably in the lattice. Similar results have been reported for Zn doping (18).

Diffusion of dopants into semiconductors is commonly used for doping after growth. Little success has been reported with this technique at temperatures up to those at which dissociation of GaN becomes significant. GaN has been doped with a radioactive Zn isotope at 900°C but the calculated diffusion coefficients are about three factors of ten less than in other III-V compounds (68). In view of the metastable nature of GaN at this temperature this does not seem a particularly promising technique.

A method of doping after growth which offers some advantages is ion implantation (69). Ions with energies of around 10 to 100 keV are accelerated onto the material to be doped, and stopped after penetrating a short distance by atomic and electronic collisions with the target

material. Advantages of ion implantation are that the isotope used can be selected with high purity by a mass spectrometer, the target temperature is low, and the depth and number of implanted ions can be closely controlled. Impurity concentrations initially in excess of chemical equilibrium values may be introduced. The drawbacks of the method are that the crystal lattice is extensively damaged by the collision processes and must be annealed at elevated temperatures to restore crystal order, and that the usual depth of the implanted layer is low (less than 1μm).

Ion implantation has been successful in producing type conversion in a number of III-V and II-VI compounds (70) including ZnTe, normally p-type, converted to n-type by implantation of 400 eV F^+ ions (71). It has also been used satisfactorily for introducing N (72) and Bi (73) isoelectronic traps into GaP. It is therefore a promising technique for implanting acceptor and other species into a material such as GaN where normal doping methods are unsuccessful.

Studies have been made of the luminescence of Zn^+ ions implanted in GaN (63,74). After annealing a broad emission band is seen near 2.9 eV. This is similar to the results produced by doping during crystal growth (3). The luminescence of GaN implanted with Si^+ and Ar^+ ions (74) and the electrical properties of GaN implanted with N^+ ions (40) have also been investigated.

Ion implantation would seem to be a promising method for the extension of the range of impurities studied in GaN.

4.4 INVESTIGATION OF IMPLANTED LAYERS IN GALLIUM NITRIDE

As-grown GaN is strongly n-type. Implanted impurities may give deep levels which will trap electrons and reduce the carrier concentration. There are considerable practical difficulties in determining the carrier concentration in the shallow implanted layers which are around 30 nm deep.

If a reduction in electron concentration is produced by an implanted impurity it will give a layer of low conductivity which overlays a thick unimplanted layer of high conductivity. Direct conductivity measurements by the Van der Pauw or four-point probe methods are not sensitive to small reductions in conductivity in thin surface layers and will not yield useful data. Only if a p-n junction region is present, isolating the layer from the underlying material, are direct conductivity measurements applicable.

A p-n junction is not necessary before electrical investigation becomes possible. Insulating layers of Zn-doped GaN have been used to fabricate MIS (metal-insulator-semiconductor) junctions and investigations have been made of conduction characteristics and electroluminescent emission in such junctions (15-20). However these MIS junctions have been made with insulating layers of the order of 1μm thick. Attempts to make MIS diodes with 30nm thick Zn implanted layers in GaN resulted in "punch-through" of the narrow insulating layer (63) resulting in direct contact between the semiconducting

GaN and the metal layer, although N implanted layers 0.12μm thick gave rectifying action only partially modified by the underlying semiconductor (40). Direct methods of measurement of carrier properties cannot be applied to shallower implanted layers of the kind discussed here.

Indirect optical methods for measurement of carrier properties are available. One such method which has been applied to GaN involves studies of infra-red absorption and reflection (53). There are three contributions to the infra-red spectra; that from vibrational modes of the lattice, that from the free carriers, and the bound-electron contribution from all higher energy transitions. Normal incidence reflectivity spectra show minima in the range 10^2 to 5×10^3 cm^{-1} (0.01 to 0.6 eV) whose positions depend on the relative strengths of the absorption from free carriers and lattice phonons and hence can be correlated with carrier concentration (53). Unfortunately specular reflectance measurements were not available in the energy range of interest. Similar correlations exist between absorption spectra and carrier concentration but here the spectra will be dominated by the bulk material which is around 10μm thick and contributions from the thin implanted layers will be less than the errors in measurement of bulk absorption.

The luminescent spectra of GaN vary considerably with carrier concentration (see 3.4 above).

The spectra for high electron concentrations above about 2×10^{19} cm^{-3} are typified by a strong A-band and a

B-band which appears only as a low energy tail to the A-band (52). The peak photon energy of the A-band is thought to show a shift with decreasing carrier concentration to lower values which is due to the penetration of the Fermi level into the conduction band (52). As carrier concentration is reduced the A-band intensity falls and the B-band becomes visible as a separate resolved band (7,52). At very low concentrations below 1×10^{18} cm^{-3} the B-band shows separate phonon replicas and the A-band shows the sharp features which are identified with specific luminescent processes (see 3.5 above).

Both photo- and cathodoluminescence originate from a region near the crystal surface (see chapter 6 below) and therefore are highly suitable for the investigation of shallow implanted layers. In addition cathodoluminescence has the advantage of giving luminescence from different depths at different electron voltages. Some indication of changes in carrier concentration may be inferred from the variation from reference to implanted samples. A reduction in A-band intensity, especially if accompanied by a clearly resolved B-band at LNT, may indicate a reduction in electron concentration. However care must be taken in so interpreting such a change. The radiation damage introduced during implantation will, even after annealing, tend to lower the luminescent efficiency in implanted samples, and only reductions in A-band intensity greater than that due to damage admit of the possibility of carrier compensation. Furthermore the

implanted species may act as a competing non-radiative recombination centre causing loss in luminescence without carrier compensation. Changes in electron concentration may also be correlated with shifts in the peak photon energy of the band-to-band recombination. Here care must be taken to ensure that shifts in A-band peak photon energy are in fact due to these Fermi level effects and not due to the presence of a new impurity level or band.

If a new energy band is suspected it may show differences in temperature variation of intensity or peak photon energy from that of the A-band. The A-band peak photon energy normally moves to lower values as the conduction band approaches the valence band with rise in temperature. Impurity states associated with the valence band, or with tunneling-assisted transitions such as that proposed for Zn-doped GaN (59), do not change rapidly with temperature. The A-band intensity also falls slowly with increasing temperature, unlike the B-band which is quenched by a non-radiative process and is not seen above about 200 K in any samples. Excitation spectra may also show the presence of impurity levels above or below the energy gap. The excitation spectrum of semiconductor luminescence normally has a sharp edge near the energy gap value and any variation from this pattern indicates a transition to an impurity level.

Direct electrical methods of investigation of conduction are difficult to apply to very thin surface layers such as are produced by ion implantation. Of the optical

methods possible luminescence was chosen since some information exists on the influence of carrier concentration on luminescence in GaN. An additional advantage of cathodoluminescence is that it provides a way of investigating variation of luminescence with depth.

Chapter 5.

ION IMPLANTATION

5.1 DISTRIBUTION OF IMPLANTED ATOMS

Singly charged ions at energies of a few tens or hundreds of keV are used in ion implantation. In the target material they lose energy by collisions with the target atoms. Twc processes are involved; nuclear collisions with the target nuclei, and electronic collisons with the electrons distributed in the target lattice. According to the theory of Lindhard, Scharff and Schiott (75) the rate of energy loss, or stopping power, for electronic collisions is proportional to $E^{1/2}$ where E is the incident ion energy at any moment, whereas the nuclear stopping tends to the constant value given by Rutherford scattering at high energies and follows a more complex behaviour at low energies where the nuclei are partially shielded. Thus at high energies the energy loss is almost entirely due to electronic stopping but at low energies nuclear stopping dominates (Fig 5.1).

The ion track will be almost linear at high energies where scattering is mostly against the much lighter electrons but below some energy E_c the nuclear stopping will dominate and the ion is brought to a halt by scattering against the target nuclei. It will experience considerable deflection in these nuclear collisions and follow a random path.

The resulting distribution of the implanted ion species is expected to be a Gaussian distribution of

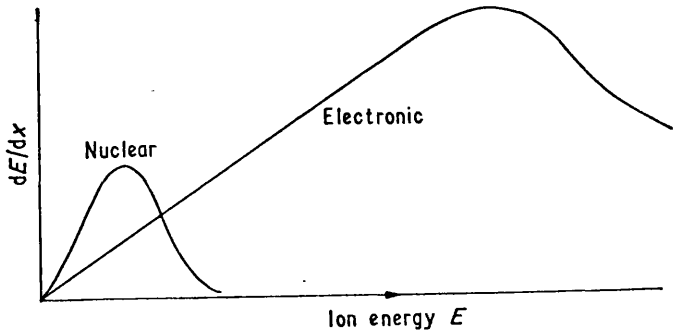

Figure 5.1 The behaviour of the nuclear and electronic contributions to the rate of energy loss dE/dx of implanted ions, as a function of ion energy E (69)

concentration N_i with depth of penetration, x (69):-

$$N_i = N_o \exp\left\{ - \frac{(x-R_p)^2}{2\Delta R_p^2} \right\}$$

where R_p is the mean projected range, measured parallel to the direction of implantation, and ΔR_p is the standard deviation in R_p. R_p and ΔR_p both increase with incident ion energy. Theoretical calculations give values of R_p and ΔR_p as a function of ion energy, ion atomic number Z_1 and target atomic number Z_2 (69). Fig 5.2 shows experimental distributions for ^{85}Kr in amorphous Al_2O_3. The parameters of these distributions are in good agreement with theoretical predictions especially for lower energies.

In crystalline material an important qualification to the above is the phenomenon known as channelling (77). If the ions are incident parallel to a prominent crystallographic zone axis there will be open paths in the lattice down which ions may penetrate without nuclear collision to many times ΔR_p, until stopped by collision at a crystal defect. LSS theory applies in principle only to amorphous material, but if the target is orientated at more than 7^0 from all major zone axes channelling will not occur. Fig 5.3 shows the influence of channelling on the distribution of ^{85}Kr in single-crystal aluminium.

5.2 DAMAGE PRODUCED BY ION IMPLANTATION

Nuclear collisons will cause a recoil in the target atom and the knocked-on atom will initiate a cascade of secondary collisions. A damaged zone of about 3nm

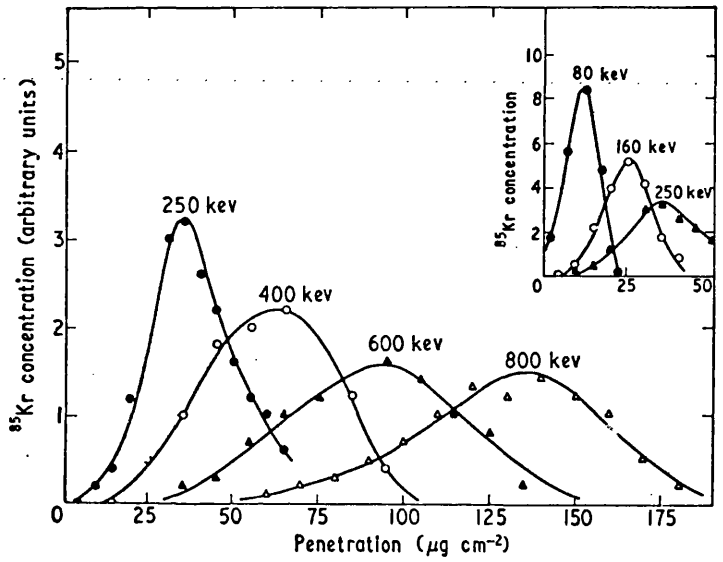

Figure 5.2 Range distribution for ^{85}Kr ions of various energies implanted in amorphous Al_2O_3 (76)

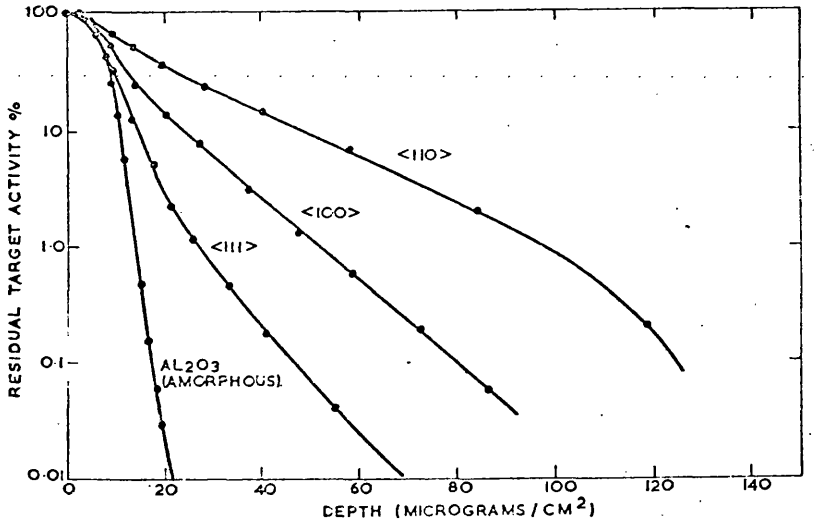

Figure 5.3 Integral range distribution of 45 keV ^{85}Kr ions implanted into single crystal aluminium and amorphous Al_2O_3 (77)

diameter in which the material is essentially amorphous is produced, and at some critical ion dose the zones overlap and an amorphous layer is produced (78). The absorbed ion energy causes local increases in temperature or thermal spikes, which cause partial annealing. In Si the amount of damage is roughly halved at room temperature and at higher temperatures (above 150°C) no amorphous layer is observed due to self-annealing. This effect is more noticeable in polar semiconductors such as GaAs. The cause is thought to be charge-enhanced diffusion where electron-hole pairs are trapped on the defects produced by the damage and these charged defects migrate more rapidly than uncharged defects (69).

A simple model giving the ion dose Φ_c needed to produce an amorphous layer at low temperatures has been proposed (79). The energy E_n absorbed in nuclear collisions, which are the only ones producing atomic displacements, is taken as:-

$$E_n = E \quad : \quad E < E_c$$

$$E_n = E_c \quad : \quad E > E_c$$

where E_c is the energy at which the nuclear and electronic stopping powers are equal, that is where

$$\left(\frac{\partial E}{\partial x}\right)_n = \left(\frac{\partial E}{\partial x}\right)_e$$

From the expressions in Dearnaley (69)

$$E_c = \left\{ \frac{166\ M_1^{\ 3}\ (Z_2^{\frac{2}{3}} + Z_1^{\frac{2}{3}})^2}{Z_1^{\frac{1}{3}}\ (M_1 + M_2)^2} \right\}$$

where M_1, Z_1, and M_2, Z_2 are the mass and atomic numbers of the incident and target nuclei respectively.

An energy E_d of about 25 eV (69) is needed to produce one Frenkel defect in a covalent semiconductor so the number of defects produced by one ion is of the order of E_n/E_d. If the depth of the damaged zone is taken as $2.5\Delta R_p$ and the critical dose Φ_c is taken as the number of ions per unit area which will produce a concentration of defects equal to N_o, the original atomic concentration then:-

$$\Phi_c = 2.5\Delta R_p N_o E_n/E_d$$

This value of Φ_c gives a reasonable estimate of the critical dose needed to produce an amorphous layer in Si at low temperatures (79). The room temperature value is about twice Φ_c in Si.

Whether the area is wholly amorphous or consists of separate highly damaged zones, the damage must be annealed out. Fig 5.4 shows some of the situations that might be produced by a single collision. The various types of damage might anneal out at a number of temperatures but not until good crystal order is recovered will the luminescence and other properties approach those in unimplanted material.

5.3 ION IMPLANTATION - EXPERIMENTAL DETAILS

Ion implantation of GaN wafers was carried out by Todkill at the GEC Hirst Research Centre, Wembley.

The apparatus used was a Danfysic 98000 implantation gun with a model 910 "Scandinavian" type ion source. A vapour stream of the element to be implanted is obtained either directly form a gas cylinder, as a volatile compound

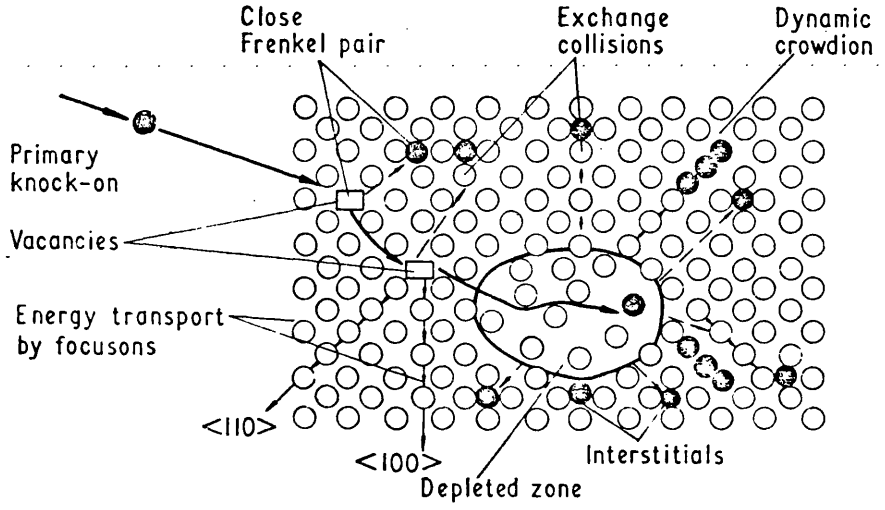

Figure 5.4 Possible damage events produced during ion implantation (80)

heated in a small furnace, or by ion exchange. The vapour is bled into the source chamber where it is ionised by collision with electrons emitted from the heated filament and accelerated into helical paths by an axial magnetic field. A positive ion plasma is held at the exit aperture of the source by a small negative potential and a potential of up to 100 kV strips ions off this plasma and accelerates them towards the target. The desired ion beam is selected by crossed magnetic and electric fields. Ion beams of up to 150μA may be obtained and can be scanned across extended target areas by a raster voltage applied to deflection coils. Table 5.1 gives the ion sources used in this work. Ions are included from every group of the periodic table except the inert gases. Attempts were made to establish ion beams for the possible acceptor species Cd, Mg, Na, and Li but without success.

The isotope used was the most abundant isotope except for ^{29}Si which was used in preference to the more abundant isotope ^{28}Si which may be polluted with $^{14}N_2^+$ ions with the same charge/mass ratio. Possible pollution with $^{28}Si^{++}$ ions prevented implantation with $^{14}N^+$ ions which might have reduced the N vacancy concentration.

The GaN samples used have carrier concentrations of around 10^{19} cm^{-3} due to a residual native defect. To compensate this defect impurity concentrations of at least the same order of magnitude are needed.

The parameters which can be varied are the accelerating voltage, which controls the depth of the implanted layer,

Table 5.1

Group	Isotope	Method	Source Material
I	^{39}K	Furnace	KBF_4 at 250°C
II	^{40}Ca	"	$CaCl_2$ "
	^{64}Zn	"	$ZnCl_2$ "
III	^{11}B	"	KBF_4 "
	^{27}Al	ion exchange	$ZnCl_2$ from furnace over Al
IV	^{12}C	"	present in vacuum system
	^{29}Si	"	" " "
V	^{31}P	Furnace	P_2O_5 at 250°C
	^{74}As	"	As_2S_3 "
VI	^{32}S	"	As_2S_3 "
VII	^{19}F	"	KBF_4 "
	^{35}Cl	"	$ZnCl_2$ "

and the ion flux, which controls the concentration of the implanted species. The implanted depth is lowest for the heaviest ions, so the depth available on this machine for the heaviest ion chosen (23nm at 82 keV for As) was taken as standard and the accelerating voltage was reduced for lighter ions to give the same range.

Each GaN wafer was cut into four parts. Three of the resulting samples were then implanted at different ion fluxes so that N_o, the peak concentration of the implanted species, was about 10^{18}, 10^{19} or 10^{20} cm^{-3} (except for Zn and Ca where N_o was 10^{19}, 10^{20} or 10^{21} cm^{-3}). These values were chosen so as to span residual donor concentration assumed equal to the carrier concentrations of around 10^{19} cm^{-3}. The fourth sample was reserved as a reference.

Table 5.2 lists values of ion beam energy E, from which range R_p and scatter ΔR_p are calculated from tables, and Q, the charge density incident on the most heavily implanted sample. From Q is calculated the peak concentration in all three samples. Fig 5.5 shows the actual distribution predicted for $^{11}B^+$ and $^{75}As^+$, the lightest and heaviest ions implanted.

5.4 HEAT TREATMENT

Implantation produces extensive crystal disorder within the implanted layer, and the material must be annealed to reduce this disorder.

In previous work on material from HRC a 15 minute anneal at 900°C was used (74), which is well below the growth temperature of 1050°C. Higher temperature annealing is reported for RCA-grown implanted material (63).

Table 5.2

Implanted Ion Species	Energy E keV	Range R_p nm	Scatter ΔR_p nm	Maximum Dose Q Ccm^{-2}	Peak Concentration N_o cm^{-3}		
^{11}B	13	23	13.3	89.6	1.7×10^{18}	$\times 10^{19}$	$\times 10^{20}$
^{12}C	15	"	12.1	86.7	1.8×10^{18}	$\times 10^{19}$	$\times 10^{20}$
^{19}F	23.5	"	11.6	76.7	1.65×10^{18}	$\times 10^{19}$	$\times 10^{20}$
^{27}Al	34.5	"	10.8	68.7	1.6×10^{18}	$\times 10^{19}$	$\times 10^{20}$
^{29}Si	37	"	10.8	68.0	1.55×10^{18}	$\times 10^{19}$	$\times 10^{20}$
^{31}P	40	"	10.8	69.0	1.6×10^{18}	$\times 10^{19}$	$\times 10^{20}$
^{32}S	42	"	10.8	64.0	1.5×10^{18}	$\times 10^{19}$	$\times 10^{20}$
^{35}Cl	45	"	10.7	62.0	1.45×10^{18}	$\times 10^{19}$	$\times 10^{20}$
^{39}K	51	"	10.5	57.6	1.35×10^{18}	$\times 10^{19}$	$\times 10^{20}$
^{40}Ca	53	"	10.4	560	1.35×10^{19}	$\times 10^{20}$	$\times 10^{21}$
^{64}Zn	44	15	6.3	497	2.0×10^{19}	$\times 10^{20}$	$\times 10^{21}$
^{74}As	82	23	9.5	42.7	1.1×10^{18}	$\times 10^{19}$	$\times 10^{20}$

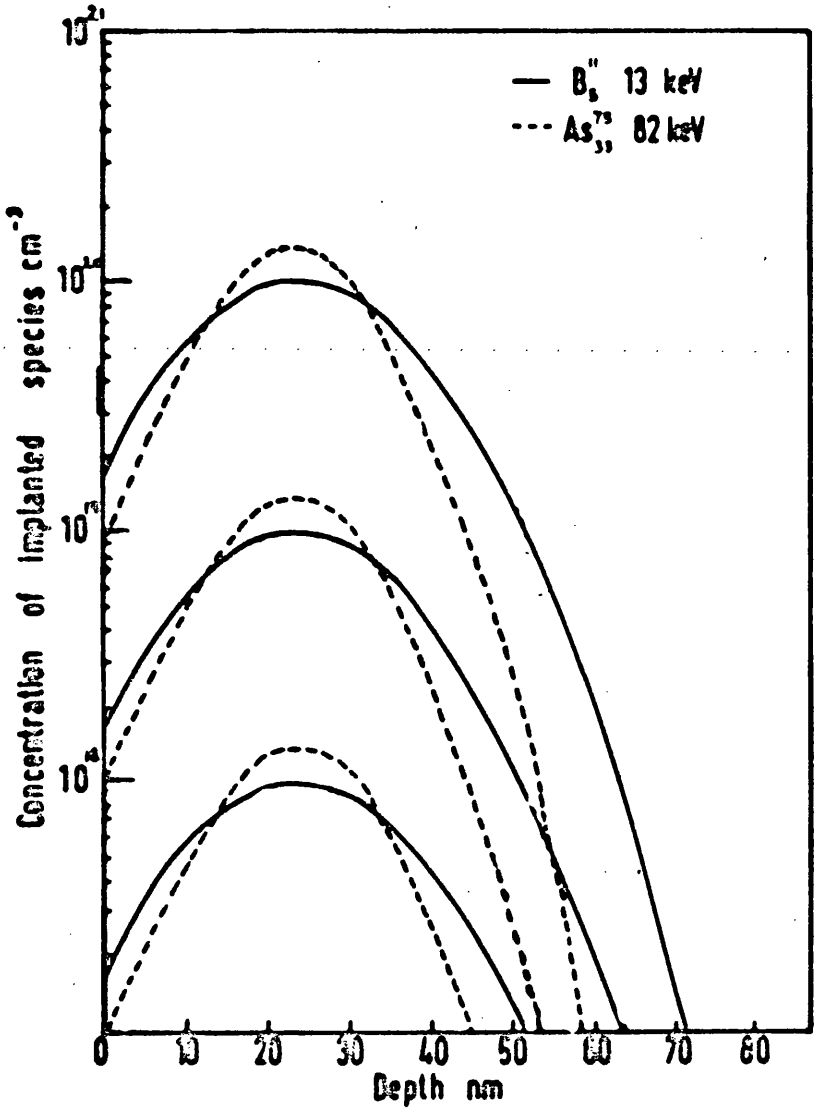

Figure 5·5 Penetration of implanted species in GaAs calculated from tables in ref 69

Since at temperatures above about 600°C GaN begins to lose N (13) the annealing must be carried out in a stream of ammonia to inhibit reactions of the type

$$GaN = V_N + Ga + \frac{1}{2} N_2$$

A flow of 600ml/hr. of dried technical grade ammonia was therefore passed through the quartz annealing furnace (Fig 5.6). The samples were introduced on a quartz spatula at the cool end of the furnace and atmospheric gases swept out by the ammonia stream. The spatula was then moved to the hot zone where samples were usually annealed for 15 minutes before being removed from the hot zone and allowed to cool. Some samples were annealed for rather longer times to test the completeness of the annealing process. The effect of a number of annealing treatments between 600°C and 930°C was investigated.

5.5 DISCUSSION OF IMPLANTATION AND ANNEALING

The initial degree of damage depends on the mass and energy of the implanted ions. Presence of a considerable defect concentration will quench luminescent emission by providing competing non-radiative paths. The observed luminescence intensity compared to the reference sample gave an indication of the extent of damage. For the 10^{18} cm^{-3} sample of the lighter elements considerable luminescence was observed, but for the 10^{20} cm^{-3} implants of the heavier elements no luminescence was observed except for cathodoluminescence at high electron energies where the electrons penetrate to the underlying undamaged layer.

Fig.5·6 Annealing Furnace for GaN wafers

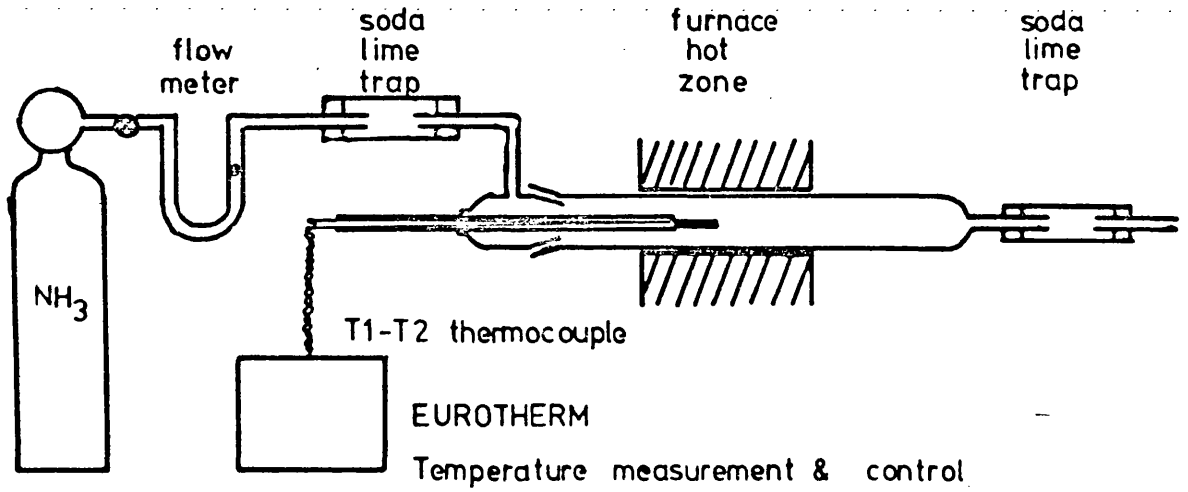

At high ion fluxes amorphous layers may be formed. Fig 5.7 shows the critical dose Φ_c needed to produce an amorphous layer at OK (see 5.2 above) and the greatest flux Φ_{max} incident on the 10^{20} (or 10^{21}) cm^{-3} sample. With the exception of the 10^{21} cm^{-3} Zn and Ca implants the ratio of Φ_{max} to Φ is always less than 2. It has been found that room temperature implants in Si do not give amorphous layers unless this ratio is in excess of 2 (79).

Since self-annealing is more noticeable in compound semiconductors such as GaAs (69) it seems likely that complete destruction of crystal order does not take place in GaN. Supporting evidence for this comes from glancing angle electron diffraction photographs of GaN implanted at 85 keV with a peak concentration of 10^{20} cm^{-3} Zn^+ ions (81) which show no patterns due to amorphous material. This is not conclusive however because the penetration depth of electrons at glancing angles is less than R_p.

The annealing cycles carried out give recovery of luminescent efficiency in all cases, but there are two factors which restrict the maximum annealing temperature. Diffusion constants will increase with temperature and the implanted species may be lost from the surface or precipitated at crystal defects, and the GaN material which is metastable at the annealing temperatures used may begin to dissociate.

Diffusion of impurities in one dimension is governed by Fick's 2nd Law

$$\left(\frac{\partial n}{\partial t}\right) = \frac{\partial}{\partial x}\left\{ D\left(\frac{\partial n}{\partial x}\right)\right\}$$

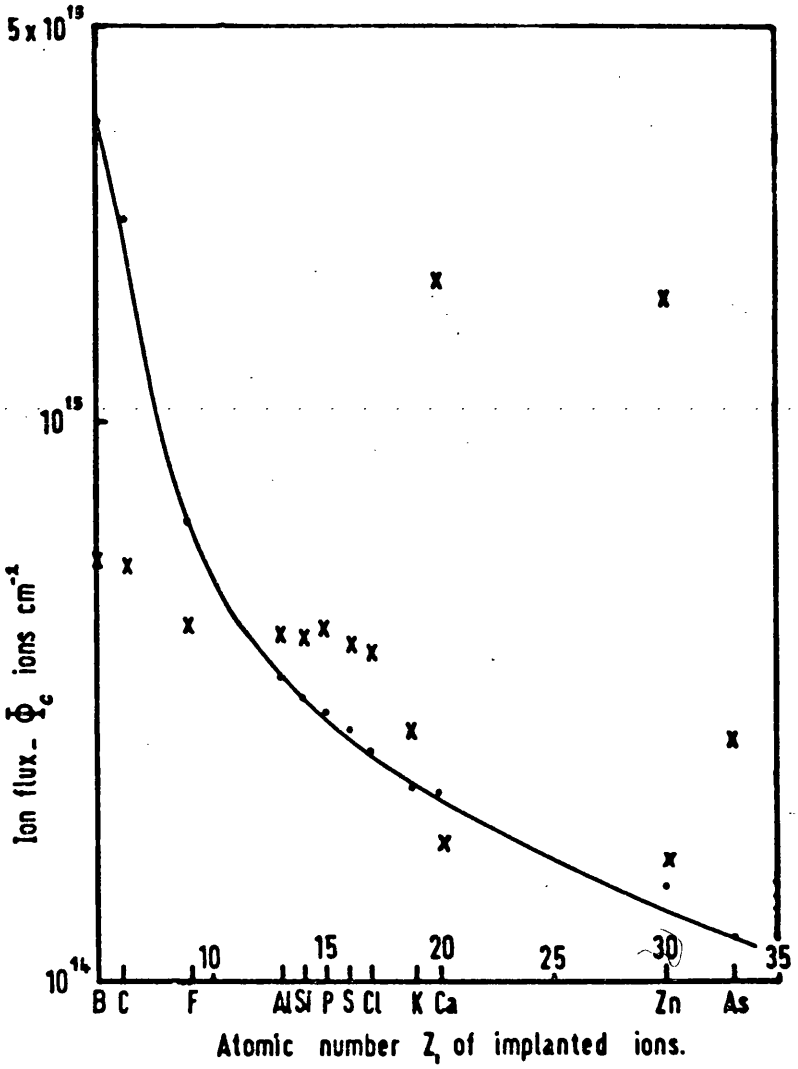

Figure 5·7 Critical dose to produce amorphous layers in GaN

Continuous curve Φ_c = 0°K critical dose.

x = greatest flux Φ_{max}.

If the initial distribution is Gaussian as is the case for ion-implanted impurities and the diffusion coefficient, D, is assumed constant after a time t the distribution will be given by:-

$$n(t) = n_o \sqrt{\frac{t_o}{t + t_o}} \exp\left\{ - \frac{(x - R_p)^2}{4D(t + t_o)} \right\}$$

with $\Delta R_p = \sqrt{Dt_o}$

Loss of impurity from the surface is neglected.

Measurements of the diffusion coefficient of Zn in GaN show that diffusion is extremely slow (68). The 900°C value of D is 10^{-20} $m^2 s^{-1}$; several factors of ten less than diffusion coefficients in GaAs and other III-V compounds.

Substitution of this value yields a new standard error of the distribution after a 15 minute anneal:-

$$\Delta R_p' = \sqrt{D(t + t_o)} \cong \Delta R_p + 0.5nm$$

So in undamaged GaN, diffusion of Zn is not great. It is however quite feasible that diffusion coefficients are much higher in radiation-damaged GaN and in fact evidence is presented below for diffusion of implanted Al and P atoms during annealing. Some variation of diffusion coefficient with impurity element is also expected.

Electron microprobe measurements made by Love of the department of Materials Science at Bath University investigated loss of potassium from K-implanted GaN. A large atom such as K may be expected to diffuse slowly, but since the relative concentration of impurity in the

10^{20} cm^{-3} samples is less than 0.01 atom percent within the penetration depth of 8 kV electrons (0.3μm) it was necessary to choose an element near the peak sensitivity of the detection system.

Measurements were made on a JEOL JXA-50A electron microscope using a PET analysing crystal and a beam voltage of 8 kV. Continuous scanning did not yield a resolvable peak at the wavelength of potassium K_α X-rays so the setting was first determined using a KCl crystal and then 10s counts were made at the peak position and offset to high and low wavelengths. This enabled significant deviations from the background value to be detected. The 10^{20} cm^{-3} sample was halved, one half only was annealed and the intensity of the potassium X-rays compared for the two samples. Table 5.3 summarises the deviations from background of the counts at the potassium K_α wavelength in units of one standard deviation.

There is no evidence for loss of potassium atoms from GaN:K, and only a slight indication that precipitation at slip bands may be occurring.

A systematic scan for impurity atoms within the range of the instrument was carried out. Some annealed specimens showed a marked peak at the wavelength for Si, considerably stronger than that for K. This may come from SiO_2 leached from the silica annealing tube. The Si impurity was not concentrated on slip bands, or on regions of yellow luminescence (see below). No other impurity element was detected at a level of 0.1 - 1%.

Table 5.3

Anneal Temp.^{0}C	Annealed GaN:K	unannealed GaN:K	unimplanted GaN
-	11.7	9.2	- 0.8
600	9.4	5.6	1.1
900	8.9	9.3	0.4
930	10.5	9.6	1.5
"	13.0 *		

* counts taken for X-rays from a slip band.

After the first few annealing cycles deterioration of surface quality becomes apparent in all four samples. The interference bands in the low wavelength absorption spectrum are no longer resolved (see below). The slip bands become decorated with etch pits on the surface of the crystal (Fig 2.3). Some etch pits show a dark head and a long tail (Fig 5.8). These are similar to the much larger tails seen on high temperature (1200^{0}C) grown GaN which are caused by the formation of Ga droplets due to dissociation (87).

A yellow luminescence band near 2.2 eV is seen in all implanted samples and may also appear on the reference sample. This yellow luminescence is associated with crystal damage (see below).

Although diffusion of implanted impurities was not found in the one specimen where direct measurements were carried out it may explain the variation of luminescence

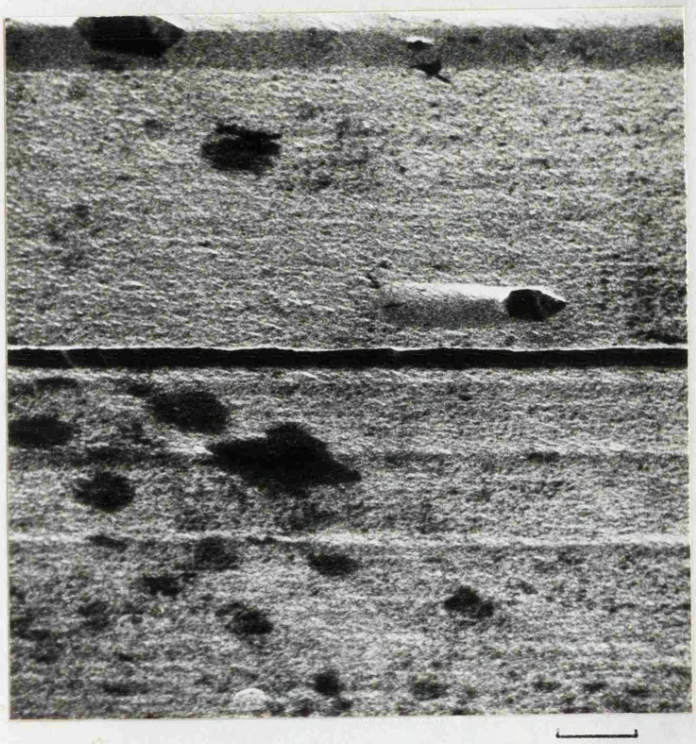

Figure 5.8 Surface damage in GaN after annealing at 930°C

with annealing in some other samples. Si and possibly O are deposited on the crystal surface during annealing.

Chapter 6.

OPTICAL INVESTIGATION OF IMPLANTED LAYERS

EXPERIMENTAL DETAILS

6.1 INTRODUCTION

After implantation the room temperature (RT) absorption spectra and room temperature, liquid nitrogen temperature (LNT) and liquid helium temperature (LHeT) luminescence spectra were recorded for each set of three implanted samples and one reference sample. All four samples were then annealed at a series of constant temperatures between 600°C and 930°C. The normal annealing time was 15 minutes but some anneals were repeated for up to 12hrs to see if any further change in properties was produced.

Each annealing treatment was followed by the recording of RT absorption and RT and LNT luminescence spectra. The variation of luminescence with temperature was recorded in more detail on a number of occasions. Low temperature spectra were recorded when liquid helium was available. The earlier spectra were records of photoluminescence (PL) excited by a He-Cd laser on loan from the HRC. When the cathodoluminescence (CL) rig at the University of Bath was built it became possible to record CL for electron beam energies of 8 and 15 keV. The varying penetration of electrons at these energies gave some indication of the distribution of luminescent centres.

After the final anneal the GaN layer on the reference sample was sand-blasted to a clover-leaf shape. Ag paste contacts were added and measurements of room temperature

carrier concentration and mobility made by the Van der Pauw method. Electrical investigation of the narrow implanted layers was not possible since "punch through" occurred between the contacts and the underlying unimplanted GaN.

An opportunity to investigate excitation spectra was offered after the annealing was completed. This would have been better done after a lower temperature anneal as the luminescence had begun to decrease at the highest annealing temperatures.

It was also possible to have some samples irradiated with thermal neutrons at AERE Harwell. This gave an opportunity to study radiation damage effects.

The annealing of one sample was studied using the scanning electron microscope.

6.2 CATHODOLUMINESCENCE

Cathodoluminescence measurements were carried out on an apparatus built at Bath University as part of this work.

The beam source was a GEC T984 electrostatically focussed electron gun with an alkali metal cathode (Fig 6.1). The gun was chosen for the ease with which the heater and cathode assembly can be replaced. The alkali metals are deposited on the cathode as the carbonate, which is inert, but before use they are converted to the oxides by heating. The oxide converts to the hydroxide on contact with damp air and electron emission is then drastically reduced. Dry nitrogen was admitted to the sample chamber whenever it was exposed to atmospheric pressure to minimise this effect. There was however an unavoidable decrease in electron emission during the working life of a gun.

The sample holder and anodes a_2 and a_4 were held at earth potential. The cathode was supplied with a negative voltage of 7-20 kV from an Oxford Instruments power unit. A high voltage enclosure held a 12 V wet battery to supply the heater voltage via a constant voltage circuit, and control voltages for the grid, first anode and focussing anode, also via constant voltage circuits, from 90 V dry batteries. Their voltages could be continuously varied and were displayed on voltmeters in the HT enclosure. Table 6.1 lists the values available.

Table 6.1

Electrode	voltage relative to cathode
h	6.3 to 10 V
g	-1 to 90 V
a_1	0 to 540 V
a_3	-90 to +270 V

The vacuum chamber was made from 8in. mild steel tubing with four Edwards 2in. brass flanges welded on at right angles. The whole was cadmium plated to minimise outgassing. The top of the chamber carried a needle valve to admit nitrogen gas to the chamber, Penning and Pirani gauge heads and a stainless steel sleeve designed to carry an Oxford Instruments CF100 constant flow cryostat (Fig 6.2).

The electron gun was mounted in a glass tube with six wires sealed through it to carry the electrode voltages.

Figure 6·1
Electron gun and vacuum chamber

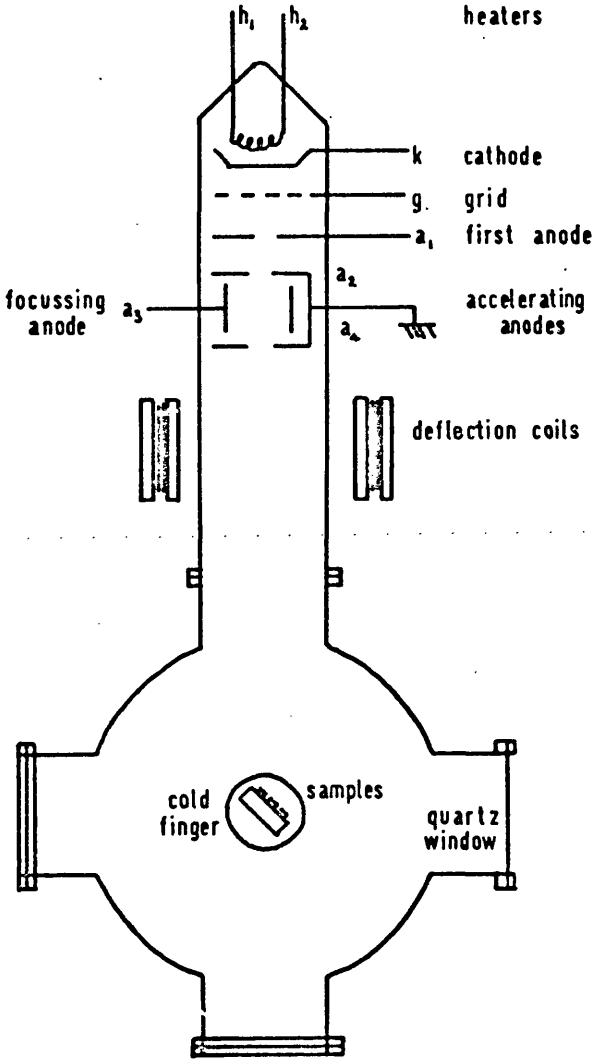

Figure 6·2
Electron gun and cryostat assembly

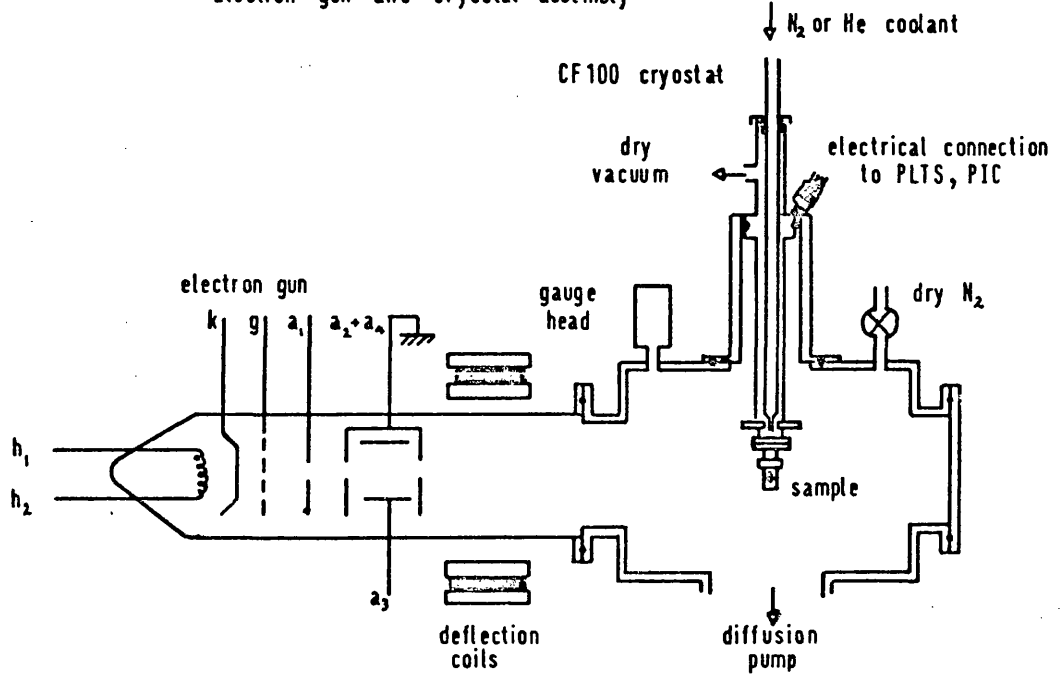

This fitted into a plated brass cone which bolted onto one of the flanges. Up to ten GaN wafers were mounted with silver dag (a suspension of Ag in methyl isobutyl ketone) on the cold finger of the cryostat at 60^0 to the electron beam and viewed through a quartz window at right angles to the electron beam. This arrangement prevents any specularly reflected light from the gun filament emerging with the desired luminescence. The position of the beam was varied over the sample holder by means of a pair of coils free to rotate about the brass cone carrying the gun tube, and a rheostat controlling the deflection coil current.

The emitted light was collected by a 150mm focal length quartz lens of 50mm diameter and focussed on the entrance slits of a Barr and Stroud VL1 monochromator (Fig 6.3). With quartz prisms this has a dispersion of 0.25mm/nm at 360nm (3.5 eV) and 0.05mm/nm at 720nm (1.8 eV). Its f/11 optics are fully flashed by the collecting lens. The light emerging from this monochromator was detected by an EMI 9558Q photomultiplier with a dynode chain wired for DC detection with its anode at earth and cathode at -1.2 kV. The anode current of the photomultiplier was passed through a 1 Megohm load resistor and the resulting voltage measured by a Phillips P2440 voltmeter. A 100 mV full-scale-deflection display signal was recorded on a Servoscribe chart recorder. The wavelength drum was motor driven at 4 minutes per degree of arc, a complete spectrum from the band edge of GaN at 3.5 eV to the limit of the S20 photomultiplier response (about 1.6 eV) taking about six minutes. A marker pulse was recorded on the chart recorder every

Figure 6.3
Cathodoluminescence apparatus

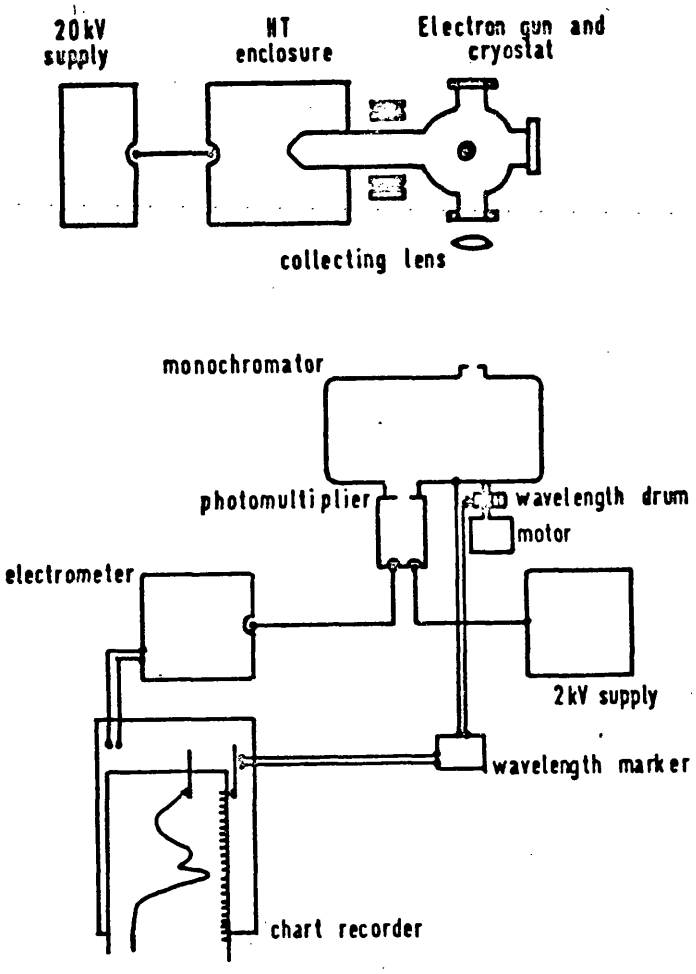

minute of arc.

The detection system was calibrated by means of a tungsten filament standard lamp, calibrated for colour temperature at the GEC HRC Lamp division. The resulting correction factors for various slit widths were incorporated in a computer program to correct the spectra for photomultiplier response, and reflection and transmission losses in the monochromator, and to plot graphs of the spectra.

The sample temperature could be varied between 8 K and 310 K by choosing appropriate liquid helium or nitrogen coolant pumping rates, and utilising the Oxford Instruments PID (proportional, integral, and derivative) controller supplied as part of the cryostat package. The temperature was monitored by an Oxford Instruments CLTS (Cryogenic Linear Temperature Sensor), which is a grid of resistance wires with a nearly linear temperature coefficient from 4 K to 300 K. The temperature was controllable to ± 0.2 K in the range 8-40 K and to ± 2 K in the range 40-300 K. Excitation intensity was variable by using either the grid or the heater voltage control to alter the beam current. Beam currents were measured using a Faraday cylinder in place of the cryostat and a Levell Multimeter. Normal operating currents were around 1μA over spot sizes of 0.5mm diameter at 15 kV, and 300nA at 8 kV.

An important parameter in the investigation of cathodoluminescence of thin surface layers such as those produced by ion implantation, is the penetration depth of the exciting electrons.

A number of investigations of energy loss by electrons with initial energies in the range 5-50 keV in gases (82) and solids (83), have shown that a range beyond which very few electrons penetrate can be defined, and if this range is normalised by the density of the target material a universal range R_G is found which is related to the incident beam energy E as:-

$$R_G = aE^{7/4}$$

Multiplication of data for R_G (82), by the density of GaN gives the maximum depth of penetration of electrons in GaN as a function of E (Fig 6.4). The maximum depth of penetration of electrons in GaN is thus about 1μm at 15 keV and 300nm at 8 keV. The energy lost by the incident electron beam goes into the creation of electron-hole pairs in the semiconductor conduction and valence bands.

The maximum energy loss occurs at about half the penetration depth and the resulting excess electrons and holes will diffuse out until annihilated in some recombination process.

The region in which luminescence is excited by the electron beam is therefore determined by the energy loss of the incident beam and the diffusion of the carriers produced. The diffusion length of holes in n-type GaAs is 0.65μm at an electron concentration of 3×10^{18} cm^{-3} (84) and will be less at higher electron concentrations. If similar values hold in GaN the peak luminescence originates at a depth of 0.15 μm at 8 keV and 0.5μm at 15 keV, and the depth of the layer from which luminescence originates is

Figure 6·4

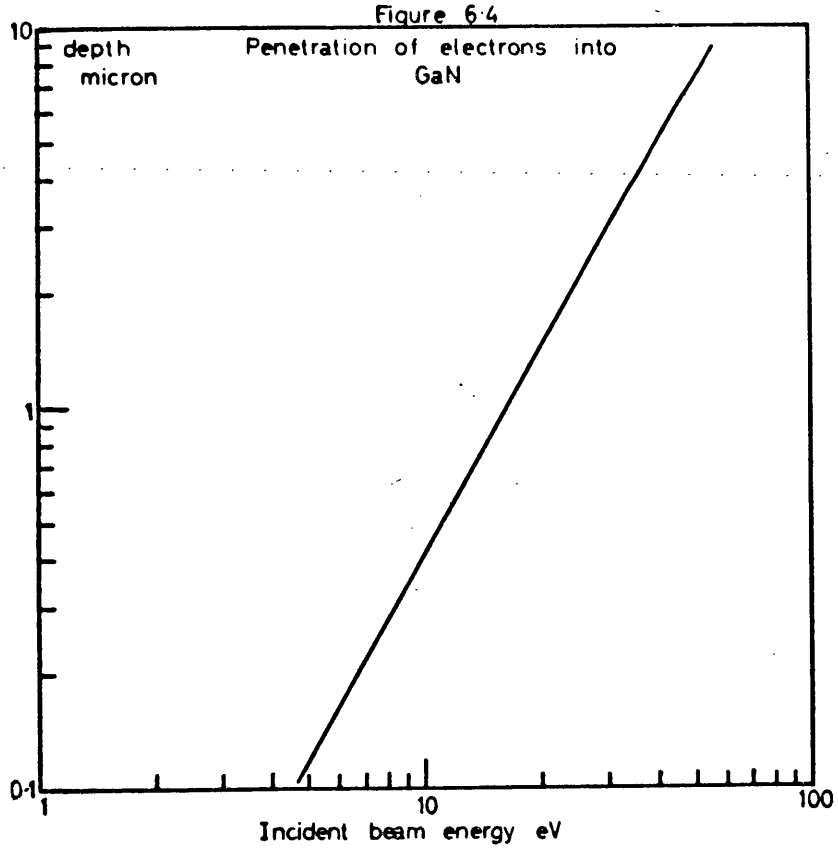
10
depth
micron
Penetration of electrons into
GaN
1
0·1
1
10
100
Incident beam energy eV

a few hundred microns.

The implanted layers are of the order of 0.1μm thick along the direction of the beam so some luminescence from the unimplanted layer will be produced even at 8 keV.

However the weak luminescence observed from implanted samples before annealing, when crystal damage quenches luminescence from the implanted layer itself, indicates that the greater part of 8 keV cathodoluminescence originates in the implanted layer. At 15 keV the majority of the luminescence will originate from below the original implanted layer. The variation of luminescence with exciting electron voltage gives an indication whether the luminescent centres are in the implanted layer or deeper.

An appreciable amount of power is generated in the excited region. A beam current of 1μA at 15 kV delivers 15 mW of power into 0.25×10^{-4} cm^3 of material. No appreciable heating occurs though as is shown by the value of the high energy slope in the near band-edge luminescence; this is always near kT in value.

The number of excess electron-hole pairs produced, Δn, can be estimated (41).

$$\Delta n = \frac{J E \Gamma}{e E_p d}$$

E_p the energy needed to produce an electron-hole pair in GaN is about 10.5 eV and, taking a penetration depth d of 1μm at 15 kV and the lifetime Γ of 10^{-6} sec. found for deep luminescence in Zn-doped GaN (60) the non-equilibrium pair density will be, at a current density

$$J = 40 \times 10^{-6} \text{ A cm}^{-2}$$

$$\Delta n = 4 \times 10^{15} \text{ cm}^{-3}$$

Since the assumed lifetime is for tunneling assisted free electron to deep donor transitions, and the lifetime for band-to-band transitions will be less, the excess electron concentration is not enough to cause appreciable band broadening in high n-type material.

Self-absorption of deep luminescence will occur, but this will only be effective near the band edge where the absorption coefficient is high.

If an absorption coefficient of the form:-

$$\alpha = \alpha_o \exp (- (E_g - E_x - h\nu)/E_o)$$

is assumed with E_o about 30 meV (see above) the luminescence from a depth d is reduced in intensity by a factor

$$I / I_o = \exp (- \alpha d)$$

Taking α_o about 10^4 cm^{-1} and d = 10^{-4} cm we see that when $(E_g - E_x - h\nu) = 4E_o$

$$I / I_o = .98$$

Thus self-absorption is negligible about 0.12 eV below the exciton energy $(E_g - E_x)$ which is about 3.44 eV at 300 K (9) for luminescence from 1μm deep, and since this will only be a fraction of the total luminescence, self-absorption corrections are not very critical. This conclusion is supported by the experimental results (see below).

Cathodoluminescent excitation generates electron-hole pairs to a depth beyond that of the implanted layers. The effect of the luminescence from undoped material is small at 8 keV, and will not be shifted appreciably by self-absorption. Band filling effects are not expected.

6.3 PHOTOLUMINESCENCE

Photoluminescent spectra were excited by an RCA LD2148 He-Cd laser operating at 325nm (3.7 eV). It gives 3 mW of power in a 0.9mm diameter beam which is then focussed onto the sample giving a high power density which generates electron-hole pairs. These diffuse from the excited area and recombine to give luminescence. The samples were mounted in the cold-finger of the CF 100, in the manufacturers vacuum jacket. Samples were angled at 60^0 to the laser beam to reduce specularly reflected laser light and increase the path length in the surface layer. The laser light was filtered of non-coherent light from the discharge tube by two interference filters and a pin-hole reduced scattered laser light.

At 325nm the absorption coefficient of GaN is around 2×10^5 cm^{-1} (3), and thus 95% of the incident radiation is absorbed in a layer 0.1μm thick at normal incidence, or 50nm at 60^0 incidence. Diffusion of the resultant electron-hole pairs increases the excited volume, but photoluminescence is still expected to give a better spectrum of the implanted layer than 8 kV cathodoluminescence.

6.4 ABSORPTION SPECTRA

Room temperature absorption spectra were recorded before and after each annealing treatment on Unicam SP700

spectrometers at Bath and at HRC.

The maximum absorbance detectable is 2 and this limits the maximum absorption coefficient measurable to:-

$$\alpha = (2 \ln 10)/x$$

which is about 10^4 cm^{-1} for samples 5μm thick. This is not high enough to show the levelling off expected above the direct energy gap at about 3.4 eV (RT).

The transmitted intensity depends upon energy losses by absorption, reflection, and by scattering from the surfaces of the GaN layer and from the substrate. The recorded absorbance must be corrected for reflection losses. Multiple reflection occurs at the GaN surface, the substrate surface and the GaN substrate interface. Data were corrected using a computer program based on an approximate expression for energy losses and refractive index data from the literature (86,87).

Allowing for the light scattered from imperfections on the crystal surface is much more difficult. Before annealing GaN shows growth facets a few microns in area and striations located on the slip bands caused by thermal mismatch during cooling from the growth temperature. After annealing the slip bands become heavily decorated with etch-pits which will further add to the scattering (Fig 2.3).

Since samples were smaller than the aperture of the SP700 spectrometer mounts were made which cut off part of the incident and reference beams. The spectrometer was balanced accordingly. The range of photon energies available was from 3.5 eV to 0.525 eV (28,000 to 4200 cm^{-1}).

6.5 EXCITATION SPECTRA

Excitation spectra of implanted GaN samples and of undoped and growth doped GaN were recorded at the luminescence facility of the HRC.

The excitation source used was a Wotan XBO 150W/4 Xenon arc lamp and the exciting photon energy was selected by a Hilger-Watts Monospek 600 monochromator. Light from the monochromator was focussed through a quartz window onto the sample, mounted on the cold finger of a stainless steel nitrogen dewar perpendicular to the incident light. Spectra were recorded at RT and LNT. The emitted light was collected through a second quartz window at 45^0 and focussed onto the entrance slits of the detecting monochromator, a second Monospek 600. The resulting signal was detected by an EMI 9558Q photomultiplier tube with an S20 response. The photomultiplier voltage was amplified by a Brookdeal phase sensitive detector operating at 100Hz, the frequency of the arc, and recorded together with wavelength values on a Nuclear Enterprizes data logging system. The exciting or the detecting monochromator could be scanned so the system was suitable for recording of excitation or emission spectra.

This system was designed for use with phosphors where sharp spectral lines are expected. The luminescent band widths found in the GaN samples investigated varied from 50 meV for the sharpest A-band to 250 meV for impurity bands. The monochromators had diffraction gratings with a dispersion of 0.6mm/nm in the first order and maximum slit widths of 1.5 and 3.0mm for the exciting and detecting monochromator respectively. The pass bands are therefore 7 and 14 meV at

3 eV and only a small part of any emitted band can be detected. This reduced the effective luminescence, particularly from shallow implanted regions and, despite the high light collecting power of the f5.6 optics it was difficult to record satisfactory spectra for ion-implanted GaN.

A further complication is that the Xenon arc source has a spectrum with strong structure in the range 430 to 500nm (2.9 to 2.5 eV) which covers most of the impurity bands of interest in GaN. Spurious features due to this structure, and to grating ghosts of the exciting wavelength made analysis of weak spectral features difficult especially in the 2.9 to 2.5 eV range.

Chapter 7.

OPTICAL INVESTIGATION OF IMPLANTED LAYERS

RESULTS

7.1 INTRODUCTION

In this chapter the main results of optical investigations of ion-implanted and other GaN samples are described. A general section in which common features of the observed luminescence are described is followed by a section in which results for each implanted impurity are presented separately.

For each set of samples the thickness and carrier concentration of the original layer is recorded together with some of the parameters of the implantation from 5.3 above. A table then gives the annealing temperature and time, and also the type of luminescence recorded and the main temperatures at which measurements were carried out. A description of the salient points in the development of the luminescence with annealing is then followed by a graph of the LNT cathodoluminescence spectrum after the 900^{0}C anneal and others where necessary.

In further sections the luminescence of neutron-irradiated samples, some relevant excitation spectra, and the absorption spectra are described. A brief reference is made to measurements on $Ga_{1-x}Al_xN$ alloys.

7.2 GENERAL FEATURES OF THE LUMINESCENCE

The reference samples all showed a near-gap emission (the A-band) at a peak photon energy in the range 3.49 to 3.43 eV at LNT, 3.45 to 3.36 eV at RT. This peak energy

showed variations of the order of 10 meV across each individual sample. At LNT the luminescence extended to photon energies as low as 2.5 eV. In two samples a separate B-band was resolvable. In the remainder the A-band intensity was much greater and the B-band appeared only as a tail to the A-band (Fig 3.5 above). In either case the B-band intensity fell rapidly with increasing temperature. Fig 7.1 shows the temperature dependence of intensity of the A-band, a clearly resolved B-band, and the 3.27 eV luminescence in the tail of the A-band from a different part of the same sample. The A-band intensity fell slowly with increasing temperature. The B-band and 3.27 eV luminescence intensity fell more rapidly above about 150 K, both activation energies are close to the value of 120 ± 20 meV observed in other material (74). Below 150 K the rate of decrease of intensity tended towards the value of 30 meV reported for the change from D-A pair luminescence to a free-bound transition in purer material (6). This behaviour indicates that the tail of the A-band may be regarded as an unresolved B-band, quenched by a similar non-radiative transition.

The near-gap luminescence in implanted samples showed the same features as the reference sample before annealing, but the intensity was reduced. This reduction was least for low ion energies and at low temperatures and greatest for heavy ions at room temperatures, luminescence being barely detectable at the highest doses. Fig 7.2 shows a common feature of LHeT photoluminescence after implantation. A peak near 3.50 eV in the unimplanted sample is identified

Figure 71 Temperature dependence of photoluminescent intensity

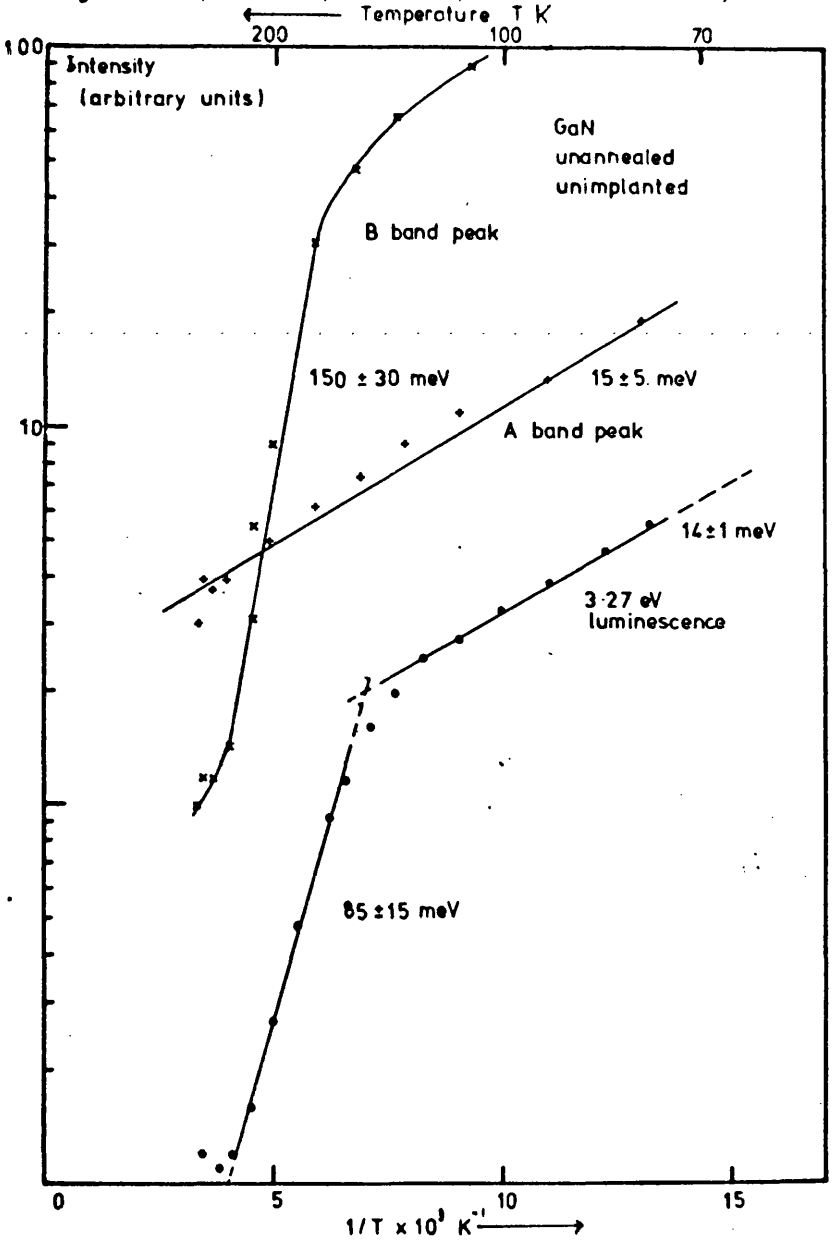

Figure 7·2

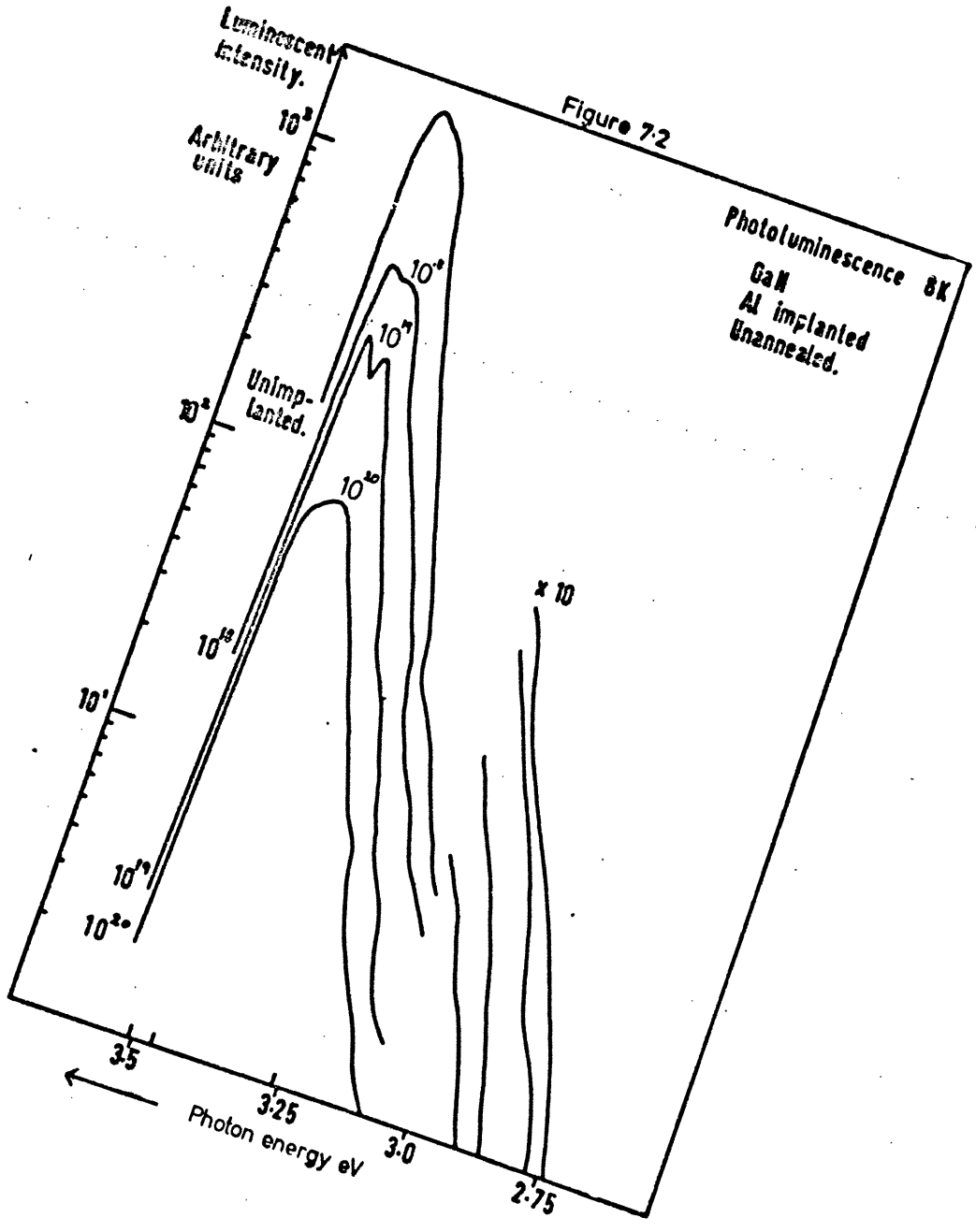
Luminescent intensity.
Arbitrary units
10^3
10^2
10^1
10^{-1}
10^{-2}
Unimp-lanted.
10^8
10^7
10^6
x 10
Photoluminescence 8K
GaN
Al implanted
Unannealed.
3·5
3·25
3·0
2·75
Photon energy eV

with band-to-band recombination. As the ion dose increased a peak near 3.47 eV became relatively stronger and dominated the near-gap emission in the most heavily implanted sample. These two peaks broadened rapidly with increasing temperature and could not usually be resolved at LNT.

The major effect of low-temperature annealing on luminescence was to reduce the band-to-band peak intensity relative to the 3.47 eV peak which became the dominant feature of the luminescence (Fig 7.3). Annealing at higher temperatures produced a considerable variation in peak photon energy of the A-band. In the more heavily implanted samples a broad band near 3.44 eV at LNT was most common. LHeT spectra showed little change from LNT.

After annealing the A-band luminescence in implanted samples was generally less intense than that in the reference sample. This loss in intensity is due to a competing non-radiative transition which may occur at a defect-impurity atom complex or at a defect alone. The number of defects initially produced depends on that proportion of the ion energy dissipated in nuclear collisions which alone cause atomic displacements, although the energy dissipated in electronic collisions may determine the amount of self-annealing which takes place (88).

Fig 7.4 shows the relation between the reduction in intensity of the LNT A-band 8 kV cathodoluminescence of a number of samples, relative to that of the reference sample, after the 900°C anneal and the energy causing atomic displacements. The measure of the latter was taken as the product of the energy per ion dissipated in nuclear

Figure 7.3

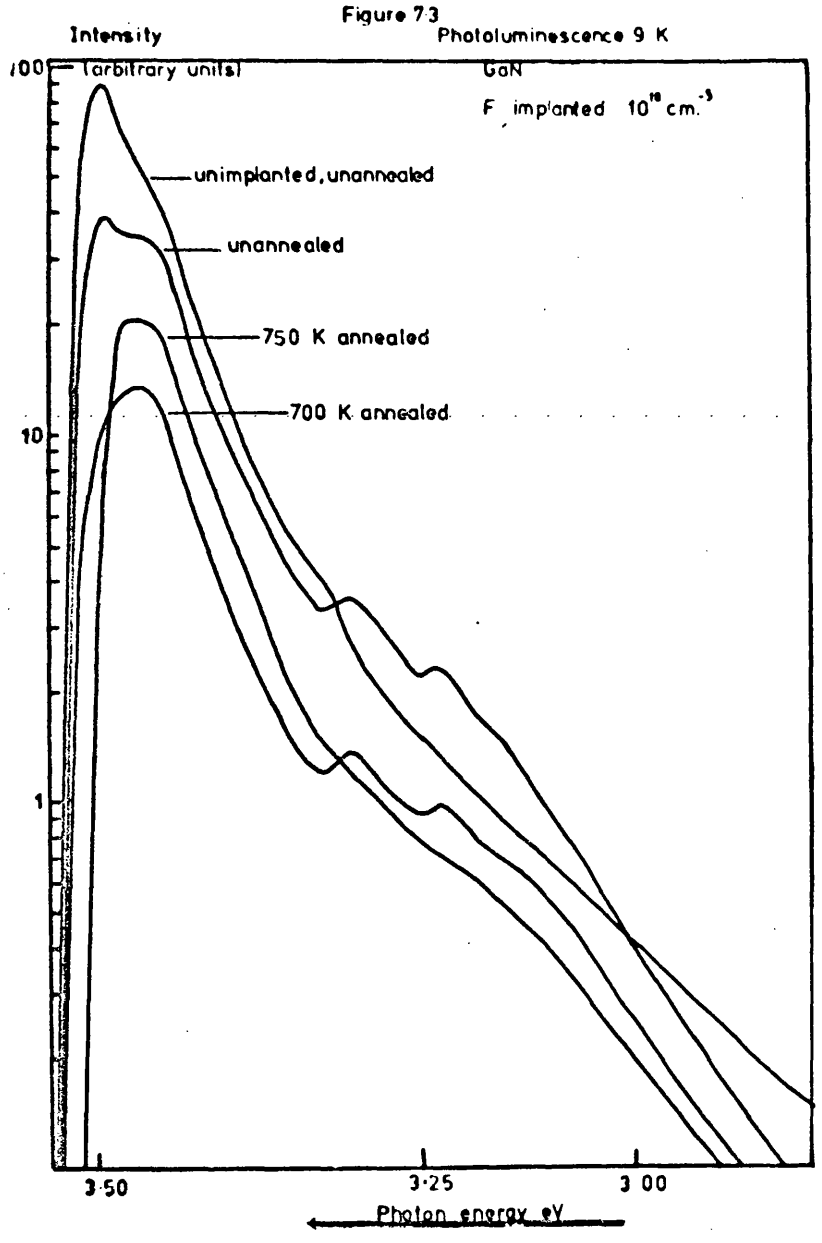
Intensity
(arbitrary units)
Photoluminescence 9 K
GaN
F implanted 10^{18} cm.$^{-3}$
unimplanted, unannealed
unannealed
750 K annealed
700 K annealed
100
10
1
3·50
3·25
3·00
Photon energy eV

Fig 7·4

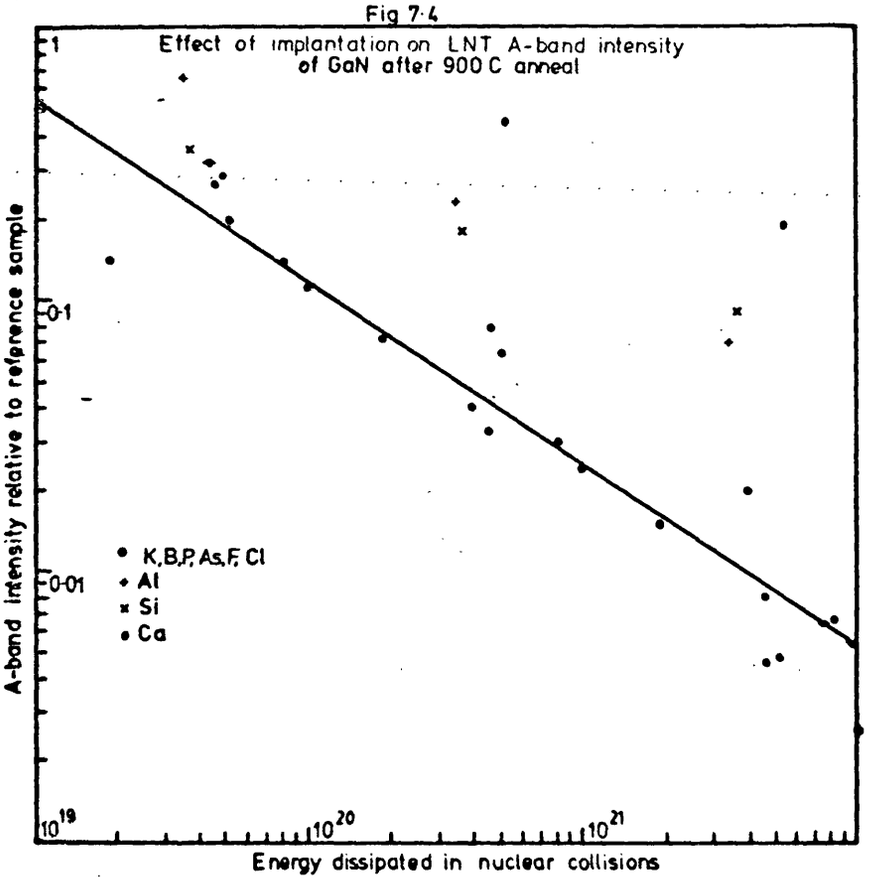
Effect of implantation on LNT A-band intensity
of GaN after 900 C anneal
1
0·1
0·01
A-band intensity relative to reference sample
• K,B,P,As,F,Cl
+ Al
× Si
• Ca
10^19
10^20
10^21
Energy dissipated in nuclear collisions

collisions, defined as in 5.2 above, and the peak concentration of implanted ions N_o, which is proportional to the number of ions implanted. There is a close correlation (r^2 = - 0.91) between the reduction in intensity, I / I_o, and the energy dissipated, E_n, for the six species K, B, P, As, F and Cl which follow a power law of the form:-

$$I / I_o = a E_n^{-0.66}$$

Of the remaining six species four, Ca, Zn, Al and Si, show less reduction than the others and two, C and S, show an increase in A-band intensity. This suggests that the implanted species in the first case have no effect on the A-band luminescence and that reduction in A-band intensity is due solely to a non-radiative process at unannealed defects. In the remainder of cases the implanted species may be involved in an optical transition within the A-band, this is probably the case for C and S where an actual increase in intensity occurs, or may form inactive complexes with the defect responsible for quenching luminescence, reducing its concentration.

New luminescent features developed in a number of samples as the annealing progressed. These are reported individually below. One feature that appeared in all samples was a yellow band with peak photon energy near 2.2 eV. This was generally much stronger in implanted samples than in unimplanted but parts of some reference samples developed strong yellow luminescence (Fig 7.5).

Fig 7.6 shows the change in intensity of a number of luminescent bands, normalised to the A-band of the

Figure 7·5

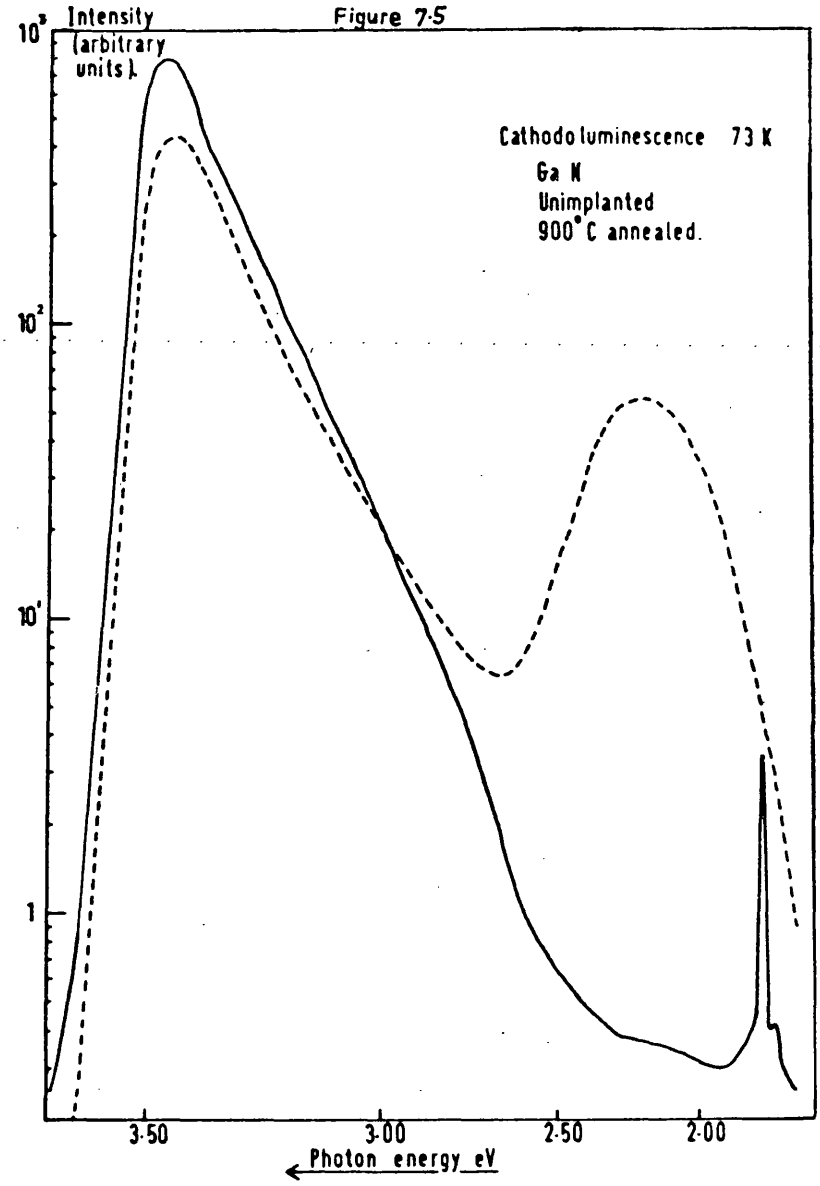
Intensity
(arbitrary
units)
10³
10²
10¹
1
Cathodoluminescence 73 K
Ga N
Unimplanted
900°C annealed.
3·50
3·00
2·50
2·00
Photon energy eV

Figure 7·6 Effect of annealing on luminescent intensity

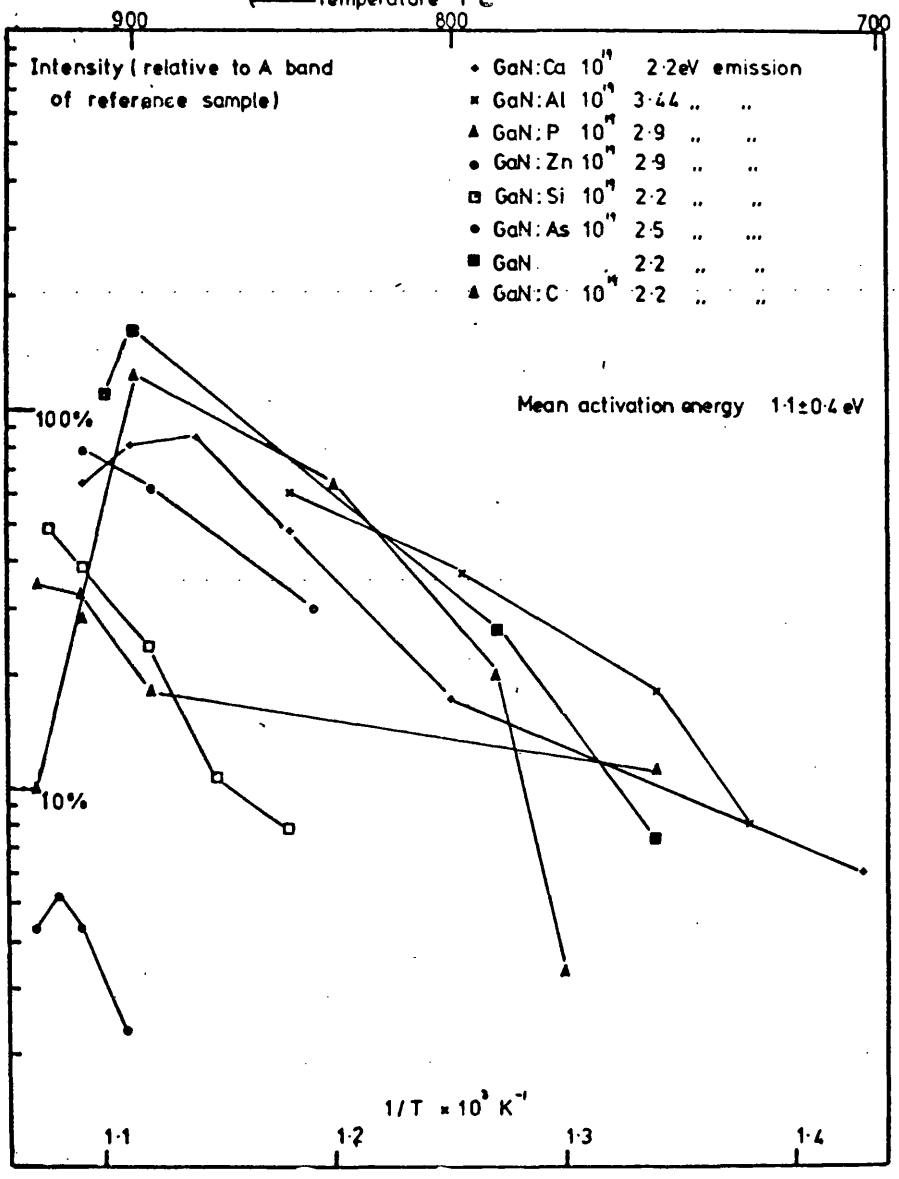

reference sample, with annealing temperature. Below 900°C the plot of relative intensity against 1/T K^{-1} shows an increase in intensity with temperature at an approximate activation energy of 1.1 eV. Above 900°C a number of features began to show a reduced intensity. The increase in intensity below 900°C may be due to the formation of defect-impurity atom complexes. Activation energies of the order of 1 eV are typical in implanted Si (88). Above 900°C surface damage was seen presumably due to dissociation of GaN. This will be accompanied by increases in defect concentration which may reduce luminescence efficiency, and by greater rates of diffusion.

Considerable variation in the intensity and peak phonon energy of luminescent peaks were observed across each sample. Normally the luminescence was recorded from a number of samples at one fixed temperature and this proceedure made it impossible to guarantee that the same spot on each sample was being excited at each different temperature. To avoid this in a number of cases the luminescence of a single sample was recorded at a series of temperatures without adjustment of the deflection coils or beam energy.

A representative selection of these measurements are shown in Fig 7.7. The temperature dependence fitted into two broad groups. The near-gap emission peak photon energies fell as temperature increased, following the band-gap as determined by Lagerstadt and Monemar (7) and by Pankove (3) with the exception of the Si and Ca doped samples. The B-band, and the lower energy emissions

Figure 7·7

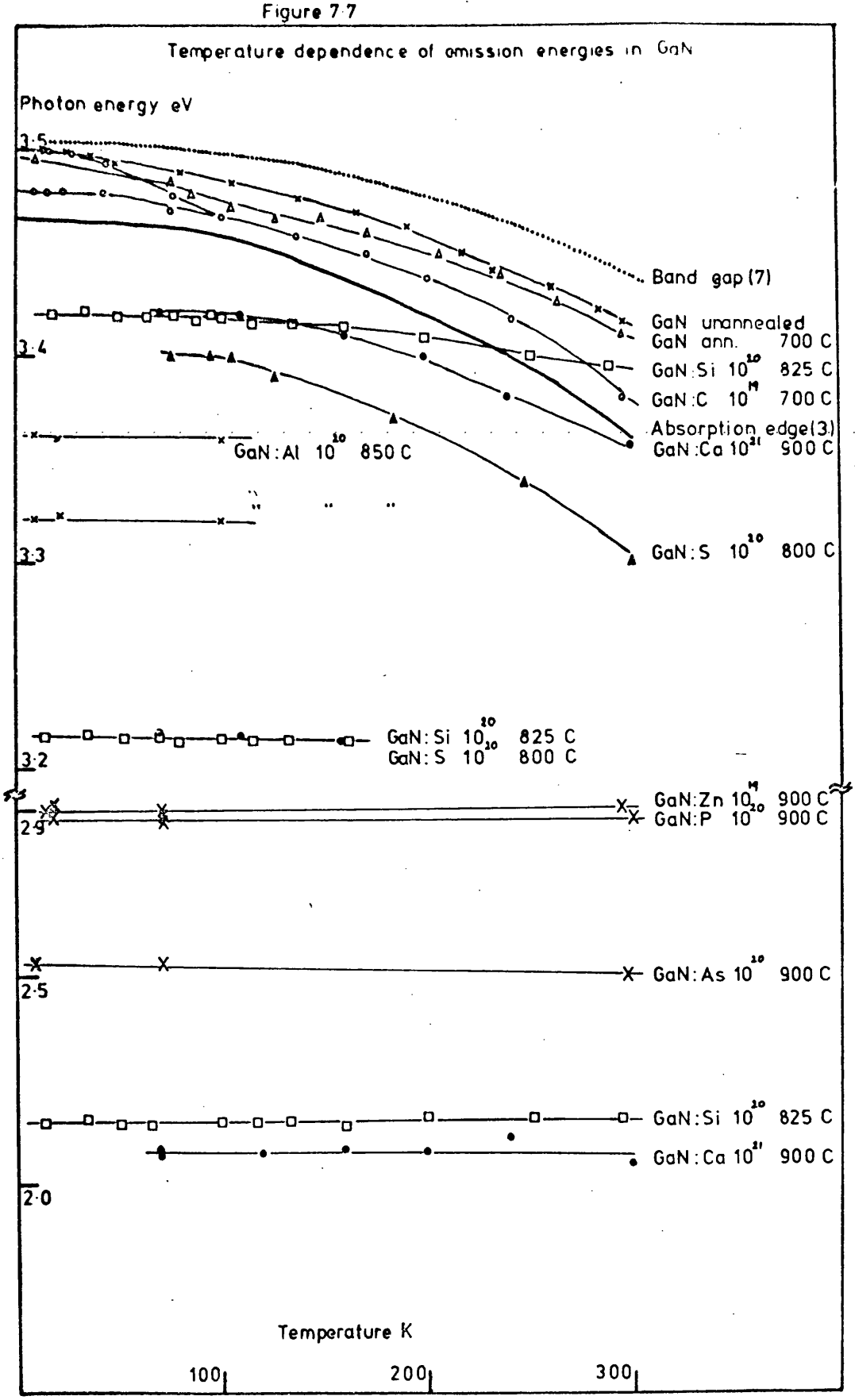
Temperature dependence of emission energies in GaN
Photon energy eV
3·5
3·4
3·3
3·2
2·9
2·5
2·0
Band gap (7)
GaN unannealed
GaN ann. 700 C
GaN:Si 10^20 825 C
GaN:C 10^19 700 C
Absorption edge(3)
GaN:Ca 10^21 900 C
GaN:Al 10^20 850 C
GaN:S 10^20 800 C
GaN:Si 10^20 825 C
GaN:S 10^20 800 C
GaN:Zn 10^19 900 C
GaN:P 10^20 900 C
GaN:As 10^20 900 C
GaN:Si 10^20 825 C
GaN:Ca 10^21 900 C
Temperature K
100
200
300

observed in Al, Zn, As, and P implanted samples (see below) and the yellow luminescence common to all implanted samples varied little with temperature.

The B-band and the sharp line spectra seen in Al-doped GaN were quenched above about 100 K and were not separable from the A-band tail.

7.3 SPECIFIC IMPLANTED IMPURITIES

(i) Potassium

Thickness 21.5μm

Carrier concentration - not measured

Implanted K^+ 51.0 keV

Peak concentrations 1.35 x 10^{18}, 10^{19}, 10^{20} cm^{-3}

Anneal Temp.^{0}C	Anneal Time	Type of Luminescence	Temperature of measurement
-	-	PL	RT and LNT
750	15 min.	PL	RT and LNT
900	"	PL and CL	RT, LNT and LHeT
930	"	CL	RT and LNT

The 10^{20} cm^{-3} sample was divided into two and one half reserved for reference in the electron microprobe investigations reported in chapter 5 above.

Group I elements on the cation sublattice are expected to be double acceptors. The covalent radius of K is large and simple substitution is improbable.

The unimplanted GaN showed no resolved B-band, and neglible yellow luminescence after annealing. The implanted layers had weak luminescence before annealing and after the 750^{0}C anneal. Some recovery is observed after the 900^{0}C anneal and a yellow band at 2.20 eV developed, most strongly for high ion dose where A-band luminescence is weakest (Fig 7.8). The spectra were similar after the 930^{0}C anneal.

The unannealed half of the 10^{20} cm^{-3} implant gave luminescence less than 0.1% of the reference for both PL and 8 kV CL. This indicates a low contribution to the total luminescence from below the implanted layer (see chapter 6).

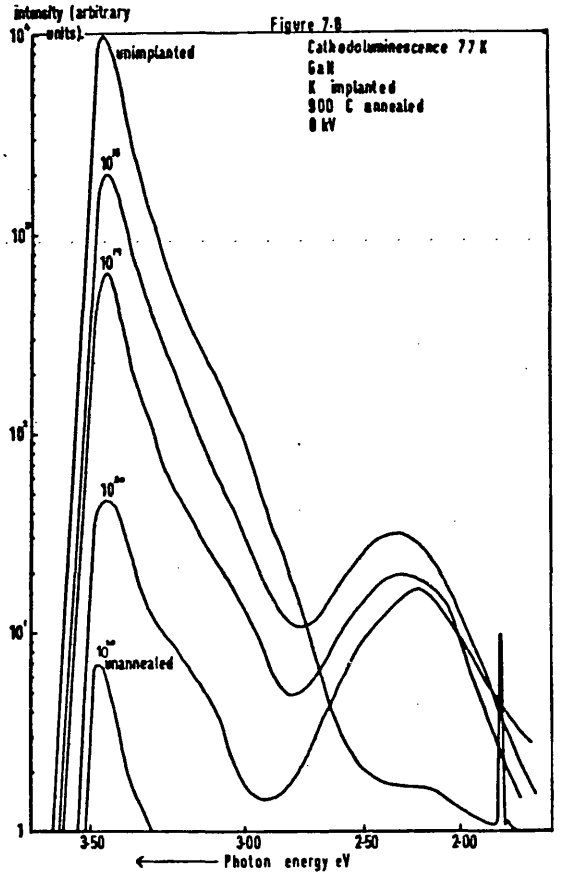
intensity (arbitrary units)
Figure 7·8
Cathodoluminescence 77 K
GaN
K implanted
900 C annealed
8 kV
unimplanted
annealed
3·50
3·00
2·50
2·00
Photon energy eV

(ii) Zinc

Thickness 4.4μm

Carrier concentration 6.5×10^{19} cm^{-3}

Implanted Zn^+ 45 kV

Peak concentrations 2×10^{19}, 10^{20}, 10^{21} cm^{-3}

Anneal Temp.^{0}C	Anneal Time	Type of Luminescence	Temperature of measurement
-	-	CL	RT and LNT
600	12 hrs.	CL	RT and LNT
700	15 mins.	CL	RT, LNT and LHeT
800	"	CL	RT and LNT
850	"	CL	RT and LNT
870	"	CL	RT and LNT
900	"	CL	RT, LNT and LHeT
920	"	CL	RT and LNT

The voltage available for Zn implantation was less than for other implants. A voltage of 45 kV gives R_p = 15nm as opposed to R_p = 32nm for the other implants.

Zinc doping of GaN by ion implantation has been reported previously (63,74). A broad band near 2.9 eV similar to that produced by more orthodox doping methods (see Fig 3.7 above) is found. The Zn impurity forms a complex acceptor level (4).

The unimplanted GaN showed no resolved B-band and no yellow luminescence. The implanted layers were only weakly luminescent after implantation and recovered gradually after successive annealing cycles. The typical Zn luminescence appeared first as a weak shoulder on the 10^{19} cm^{-3} implant after annealing at 850°C. The yellow band at 2.2 eV developed simultaneously. No Zn luminescence was observed from the 10^{20} cm^{-3} implant. The 10^{21} cm^{-3} showed heavy surface damage after the 880°C anneal, and only a weak yellow luminescence was detected subsequently.

Fig 7.9 shows the spectra after annealing at 900°C. A-band intensities are close to those of the unimplanted sample indicating a contribution to the A-band from the Zn impurity. The Zn and yellow bands at 2.88 and 2.22 eV respectively are not greatly enhanced by increasing electron voltage, indicating that both bands are limited to the implanted layer near the surface.

Figure 7·9

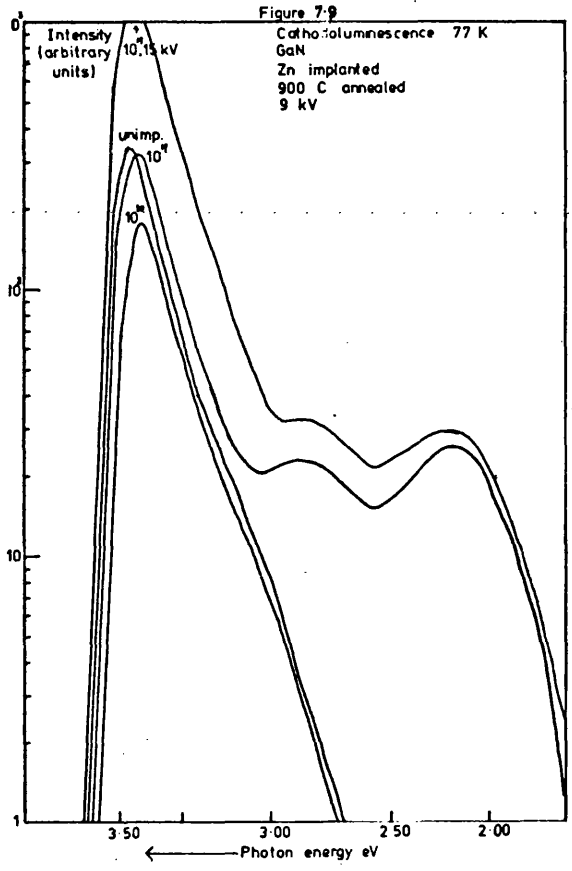
Intensity (arbitrary units)
10,15 kV
unimp.
Cathodoluminescence 77 K
GaN
Zn implanted
900 C annealed
9 kV
3·50
3·00
2·50
2·00
Photon energy eV

(iii) Calcium

Thickness 6.5μm

Carrier concentration 1.1 x 10^{19} cm^{-3}

Implanted Ca^{+} 53 kV

Peak concentrations 1.35 x 10^{19}, 10^{20}, 10^{21} cm^{-3}

Anneal Temp.^{0}C	Anneal Time	Type of Luminescence	Temperature of measurement
-	-	CL	RT and LNT
600	12 hrs.	CL	RT and LNT
700	15 mins.	CL	RT and LNT
800	"	CL	RT, LNT and LHeT
850	"	CL	RT and LNT
880	"	CL	RT and LNT
900	"	CL	RT, LNT and LHeT
920	"	CL	RT and LNT

Group II elements are known to form complex acceptor levels in GaN.

The unimplanted sample showed the low A-band intensity and clearly resolved B-band expected from its low carrier concentration.

A strong yellow band developed at annealing temperatures as low as 800^{0}C. At LNT its peak photon energy was at 2.18 eV but at RT the peak shifted to lower photon energies

at about 2.0 eV. The A and B-bands maintain their shape in the implanted samples and the fall in A-band intensity is much less than in most other samples (Fig 7.10).

Figure 7.10

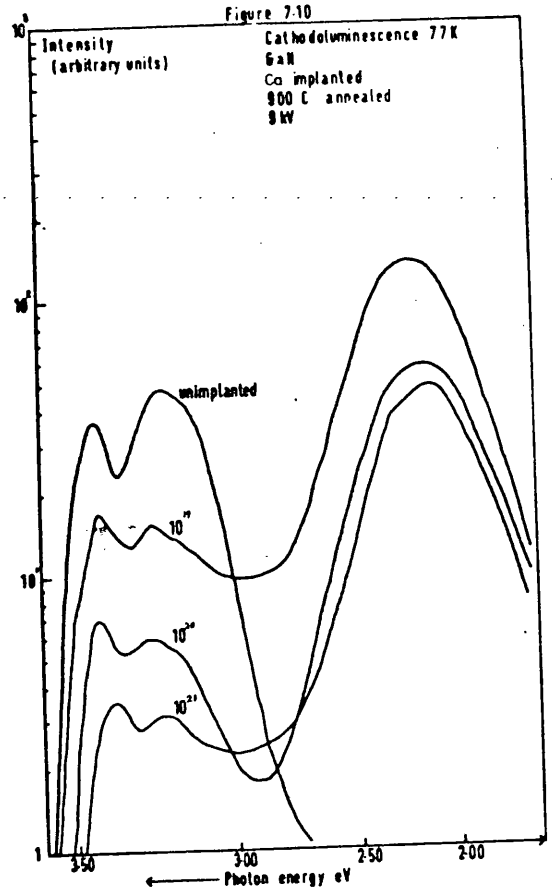
Intensity
(arbitrary units)
Cathodoluminescence 77K
GaN
Ca implanted
900 C annealed
9 kV
unimplanted
10^{17}
10^{21}
10^{21}
3·50
3·00
2·50
2·00
Photon energy eV

(iv) Boron

Thickness 10.4μm

Carrier concentration 4×10^{19} cm^{-3}

Implanted B^+ 13 kV

Peak concentrations 1.7×10^{18}, 10^{19}, 10^{20} cm^{-3}

Anneal Temp.^{0}C	Anneal Time	Type of Luminescence	Temperature of measurement
-	-	PL	RT and LNT
700	12 hrs.	PL	RT, LNT and LHeT
720	15 min.	PL	RT and LNT
800	"	PL and CL	RT and LNT
850	"	PL	RT and LNT
900	"	CL	RT and LNT
930	"	CL	RT and LNT

Group III ions may be expected to substitute for Ga on the cation sublattice.

The unimplanted sample showed no resolved B-band. After annealing at 900^{0}C some parts of the unimplanted sample showed yellow luminescence comparable to that of implanted samples.

The unannealed samples showed an A-band peak at 3.50 eV at LNT. The contribution near 3.47 eV was weaker than for heavier ions indicating a lower defect concentration. After the 850^{0}C anneal PL spectra showed a shoulder on the A-band

near 3.2 eV (Fig 7.11). All implanted samples showed yellow luminescence peaking near 2.30 eV.

After annealing at 900°C the 10^{18} cm^{-3} sample developed a pronounced B-band with a peak at 3.30 eV (Fig 7.12). Yellow luminescence near 2.2 eV was observed in all samples except 10^{18} cm^{-3}. Spectra were similar after the 920°C anneal. CL spectra at 8 and 15 kV showed similar enhancement of all luminescent features except the yellow band indicating A and B-band luminescence was not limited to the initial implanted layer.

Figure 7-11

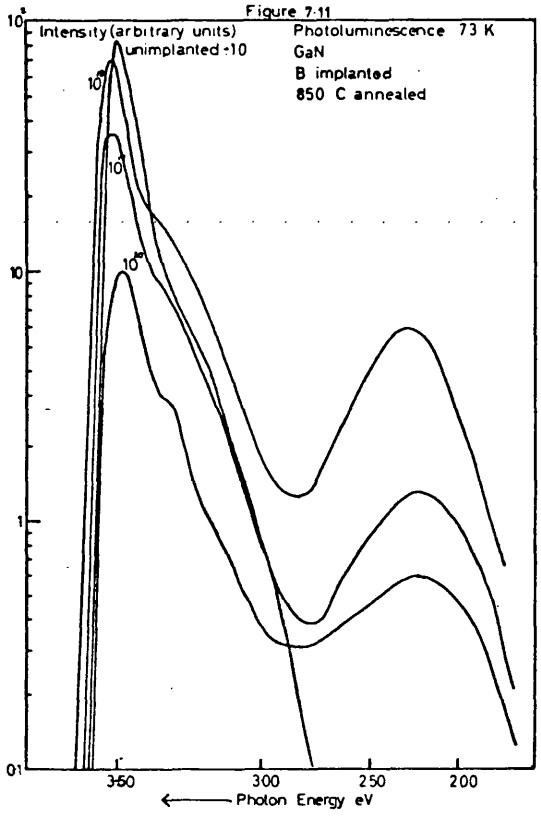

Figure 7-12

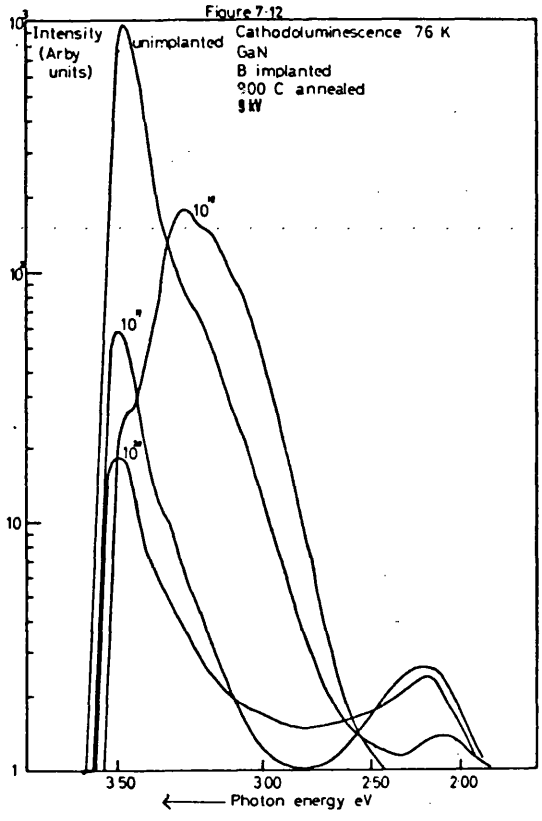

(v) Aluminium

Thickness 21.5μm

Carrier concentration 3 x 10^{19} cm^{-3}

Implanted Al^{+} 34.5 kV

Peak concentrations 1.6 x 10^{18}, 10^{19}, 10^{20} cm^{-3}

Anneal Temp.^{0}C	Anneal Time	Type of Luminescence	Temperature of measurement
-	-	PL	RT LNT and LHeT
700	12 hrs.	PL	RT and LNT
720	15 mins.	PL	RT and LNT
750	"	PL	RT and LNT
800	"	PL	RT and LNT
850	"	PL	RT LNT and LHeT
900	"	CL	RT and LNT
920	"	CL	RT and LNT
930	"	CL	RT and LNT

Group III elements may be expected to substitute for Ga on the cation lattice.

After annealing at 750^{0}C LNT spectra of the 10^{19} cm^{-3} sample showed sharp peaks at 3.33 and 3.24 eV and a shoulder at 3.13 eV (Fig 7.13). These peaks were quenched with increasing temperature like the B-band in undoped GaN and

were separated by an energy close to that of the LO phonon (92 meV)

These bands did not reappear after 800°C annealing. The 10^{20} cm^{-3} sample showed a sharp pair emission at LNT with peaks at 3.36 and 3.32 eV (Fig 7.14). This emission was also quenched like the B-band.

After annealing at 850°C the pair emission strengthened and appeared also in the 10^{19} cm^{-3} sample (Fig 7.15). The 10^{20} cm^{-3} sample also showed a sharp peak at 3.47 eV at low temperature. All pair spectra showed a dependance of peak energy and intensity like the B-band. At LNT, samples other than 10^{20} cm^{-3} showed the usual low energy tail to the A-band in the region below 3.0 eV. This was absent in the 10^{20} cm^{-3} sample. Yellow luminescence near 2.2 eV was observed at a stronger intensity in all but the 10^{20} cm^{-3} sample.

CL spectra after 900 and 920°C annealing showed a strong A-band but no sharp spectra (Fig 7.16). The relative intensity of the A-band was higher in implanted samples than for most other implants. However after the 930°C anneal sharp spectra of the type seen in photoluminescence after the 850°C anneal were observed in small regions on both the 10^{19} cm^{-3} and 10^{20} cm^{-3} implants (Fig 7.17). The pair spectra was at 3.38 and 3.34 eV (LNT) and the near gap emission at 3.50 eV (10^{19} cm^{-3}) and 3.53 eV (10^{20} cm^{-3}). These features were not seen at RT (Fig 7.18).

Al in GaN gives rise to complex spectra whose nature is not fully elucidated in these observations. A B-band type of spectra is observed in one sample but after higher temp-

erature annealing pair features appear and replace the "B-band tail". After higher temperature annealing still the features disappear over most of the sample. Strong pair spectra are accompanied by a fall in the B-band tail and the yellow luminescence.

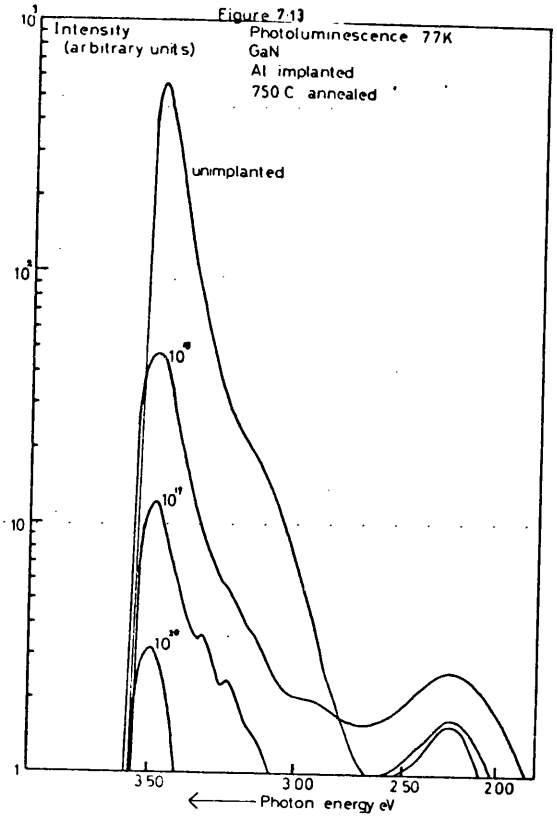

Figure 7·13

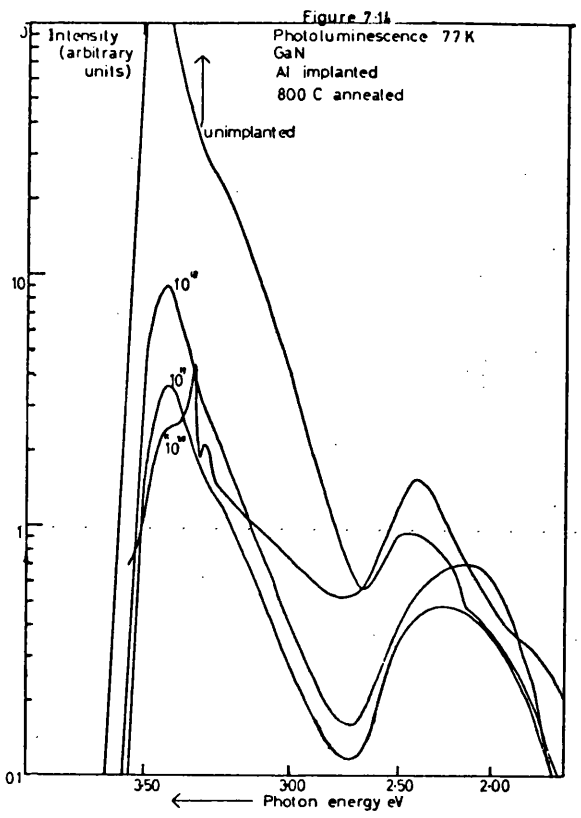

Figure 7·14

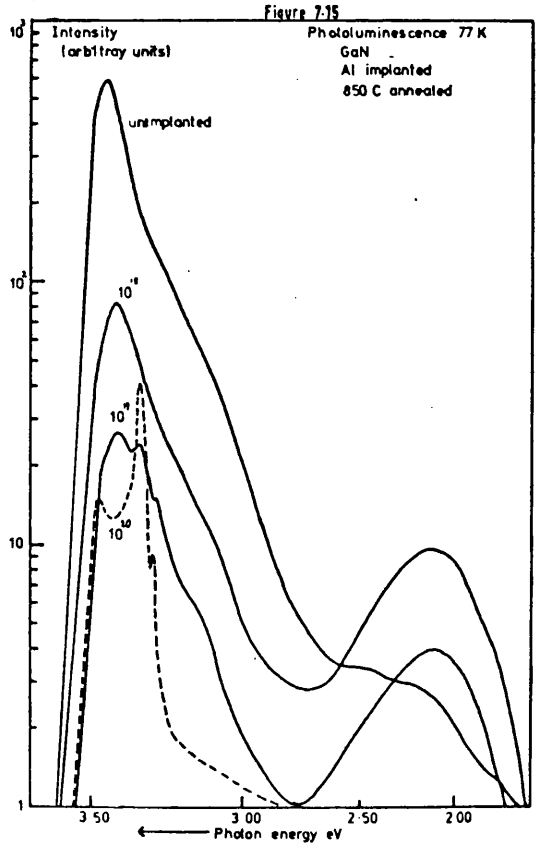

Figure 7·15

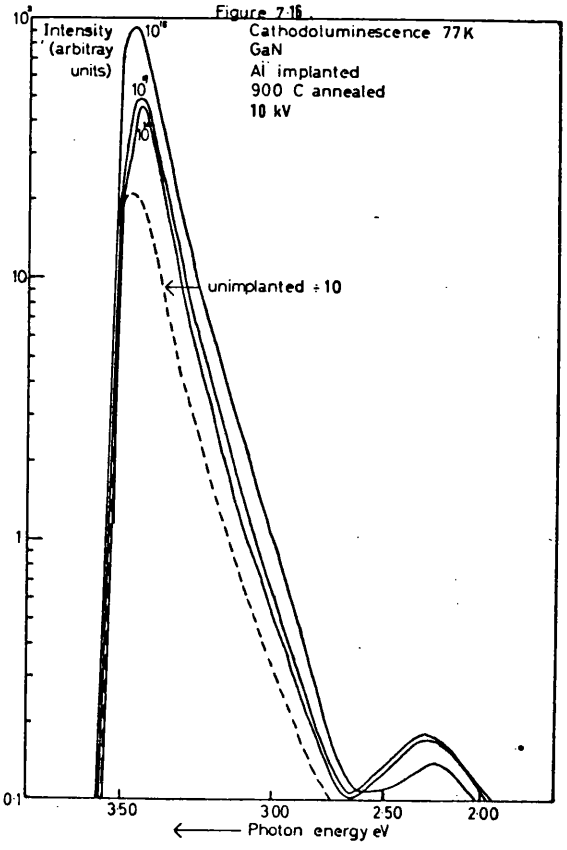

Figure 7·16

Figure 7·17

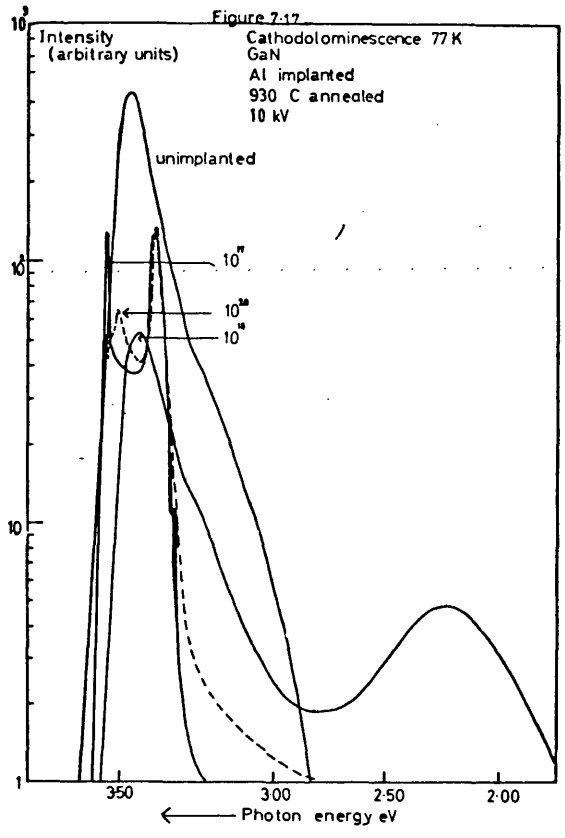

Figure 7·18

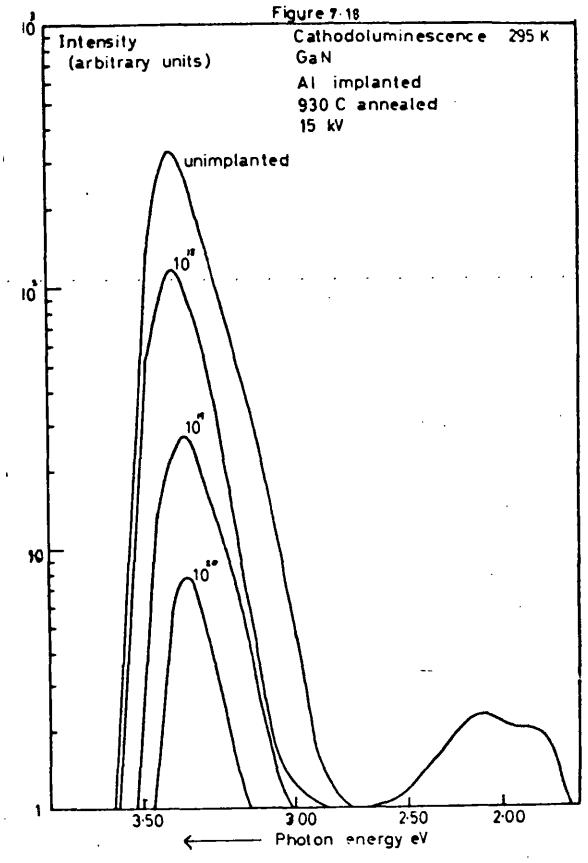

(vi) Carbon

Thickness 5.8μm

Carrier concentration 4.8×10^{19} cm^{-3}

Implanted C^+ 15 kV

Peak concentrations 1.8×10^{18}, 10^{19}, 10^{20} cm^{-3}

Anneal Temp. C	Anneal Time	Type of Luminescence	Temperature of measurement
-	-	PL	RT LNT and LHeT
700	15 mins.	PL	RT LNT and LHeT
700	7 hrs.	PL	RT and LNT
750	12 hrs.	PL	RT and LNT
770	15 mins.	PL	RT LNT and LHeT
900	"	CL	RT and LNT
920	"	CL	RT and LNT
930	"	CL	RT and LNT

Group IV impurities are amphoteric in III-V compounds. C is small enough to substitute on the anion lattice where it would act as an acceptor.

The unimplanted sample gave no B-band structure. After annealing the A-band peak in the reference sample was at 3.47 eV. The implanted samples peaks were at 3.44 eV and were stronger than the reference sample for the 10^{18} and 10^{19} cm^{-3} implants (Fig 7.19). The strong yellow luminescence

appeared at about 2.3 eV at low annealing temperatures (750°C) but after the 900°C anneal its peak had shifted to 2.20 eV. The A-band and yellow luminescence both increase in intensity with increasing electron energy (Fig 7.20) suggesting that the impurity may have diffused to greater depths. This was one of the two implanted samples giving detectable excitation spectra for the yellow luminescence, (see below).

Figure 7·19

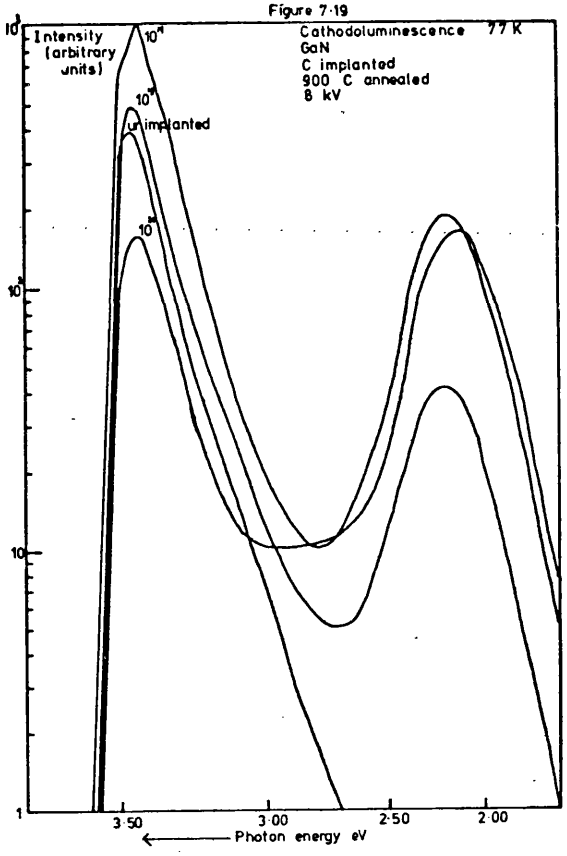

Figure 7·20

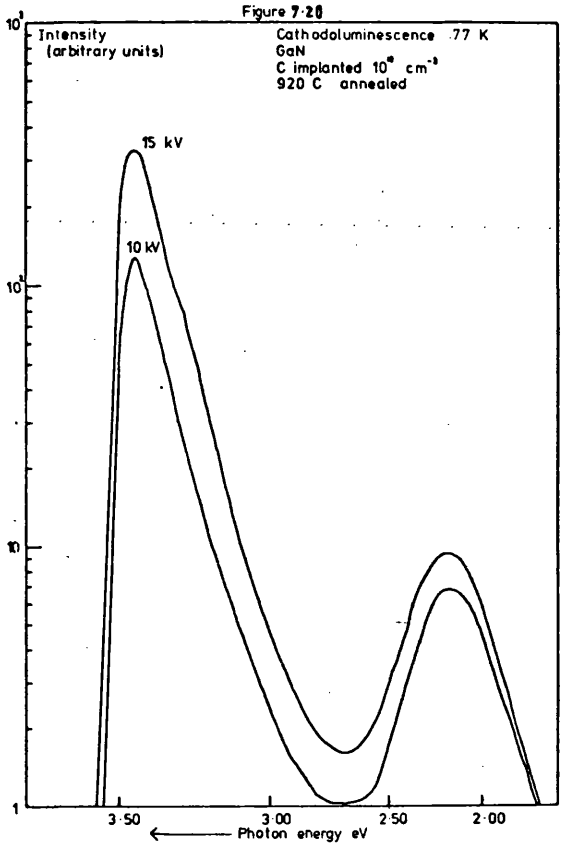

(vii) Silicon

Thickness 9.8μm

Carrier concentration 5.4×10^{19} cm^{-3}

Implanted Si^{+} 37 kV

Peak concentrations 1.6×10^{18}, 10^{19}, 10^{20} cm^{-3}

Anneal Temp. C	Anneal Time	Type of Luminescence	Temperature of measurement
-	-	PL	RT and LNT
850	15 mins.	PL	RT LNT and LHeT
870	"	CL	RT and LNT
880	"	CL	RT and LNT
900	"	CL	RT LNT and LHeT
920	"	CL	RT and LNT
930	"	CL	RT and LNT

Although Silicon (Group IV) may be amphoteric its size makes it an improbable substituent on the anion sites. A previous investigation (74) showed Si ion implanted GaN to give a strong yellow luminescence at 2.15 eV.

The unimplanted sample showed a low intensity A-band and a well-defined B-band with a peak at 3.27 eV and a shoulder at 3.19 eV, despite the high measured carrier concentration. Low temperature annealing was not carried out. The A-band intensity of implanted samples was greater

than for most implants (Fig 7.21) and a strong yellow luminescence developed. Its peak photon energy was near 2.18 eV at all temperatures and its half-width remained at 500 meV. The dependance of CL intensity on exciting electron energy shows that the yellow luminescence is limited to the surface layer (Fig 7.22).

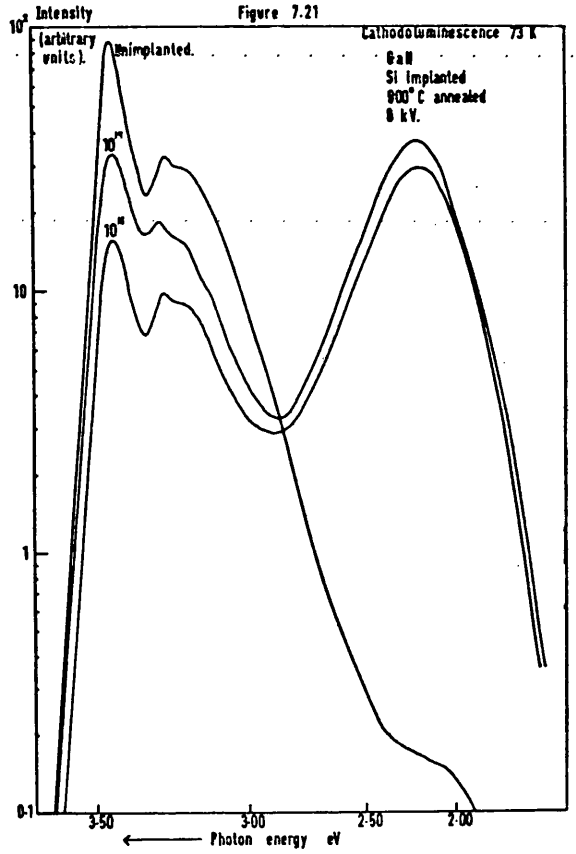
Intensity
(arbitrary units).
Figure 7-21
Cathodoluminescence 73 K
GaN
Si implanted
900°C annealed
8 kV.
Unimplanted.
10
1
0·1
3·50
3·00
2·50
2·00
Photon energy eV

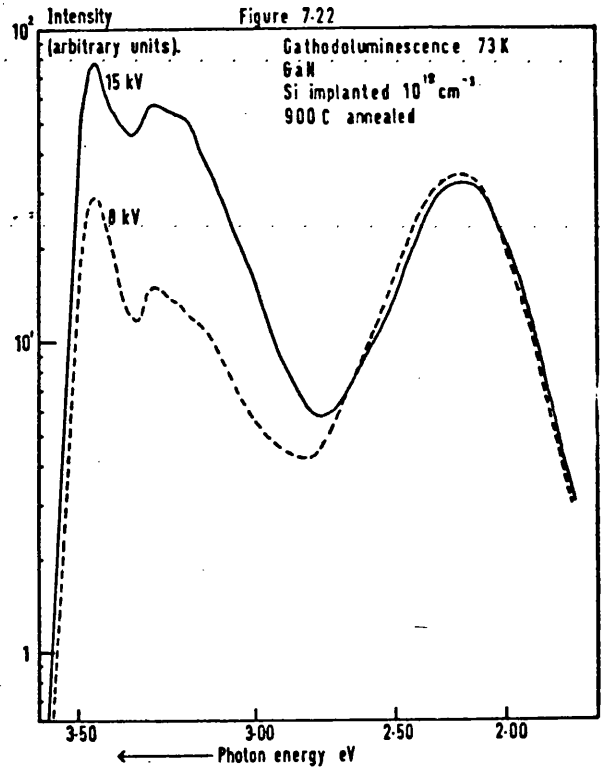
Intensity
(arbitrary units).
Figure 7-22
Cathodoluminescence 73 K
GaN
Si implanted 10 cm
900 C annealed
15 kV
8 kV
10
1
3·50
3·00
2·50
2·00
Photon energy eV

(viii) Phosphorus

Thickness 5.4μm

Carrier concentration 4×10^{19} cm^{-3}

Implanted P^+ 40 kV

Peak concentration 1.5×10^{18}, 10^{19}, 10^{20} cm^{-3}

Anneal Temp.^{0}C	Anneal Time	Type of Luminescence	Temperature of measurement
-	-	PL	RT LNT and LHeT
750	15 mins.	PL	RT and LNT
750	"	PL	RT LNT and LHeT
770	"	PL	RT and LNT
770	"	PL	RT and LNT
900	"	CL	RT LNT and LHeT
920	"	CL	RT and LNT
930	"	CL	RT and LNT

Group V impurities in III-V compounds can act as iso-electronic traps. However the large size of the P atom may prevent simple substitution on N sites.

The unimplanted sample showed no B-band structure.

A weak shoulder near 2.8 eV was detected in RT spectra after low temperature annealing, but this was masked by the tail of the A-band at LNT and below. After the 900^{0}C anneal a new strong peak was observed. At RT this was at 2.85 eV

for both 10^{19} and 10^{20} cm^{-3} implants, and no resolved peak was seen for the 10^{18} cm^{-3} implant (Fig 7.23). At LNT the 10^{20} cm^{-3} implant peak photon energy was at 2.85 eV but the 10^{19} cm^{-3} energy shifted to 2.92 eV (Fig 7.24). The LHeT peaks were similar to the LNT ones. Weak B-band structure was observed in the 10^{20} cm^{-3} implant. A yellow peak at 2.2 eV was also seen. CL at 8 kV and 15 kV (Fig 7.25) gave an almost constant yellow luminescence intensity but the A-band intensity increased strongly and the 2.85 eV band less strongly indicating yellow luminescence limited to the surface layer but some diffusion of implanted impurity. Similar spectra were seen after higher temperature annealing but the 2.85 eV band decreases in energy relative to the A-band and increases less with increasing exciting electron voltage, perhaps owing to loss of P due to out-diffusion.

The 2.85 eV band is only found in P implanted GaN.

Figure 7.23

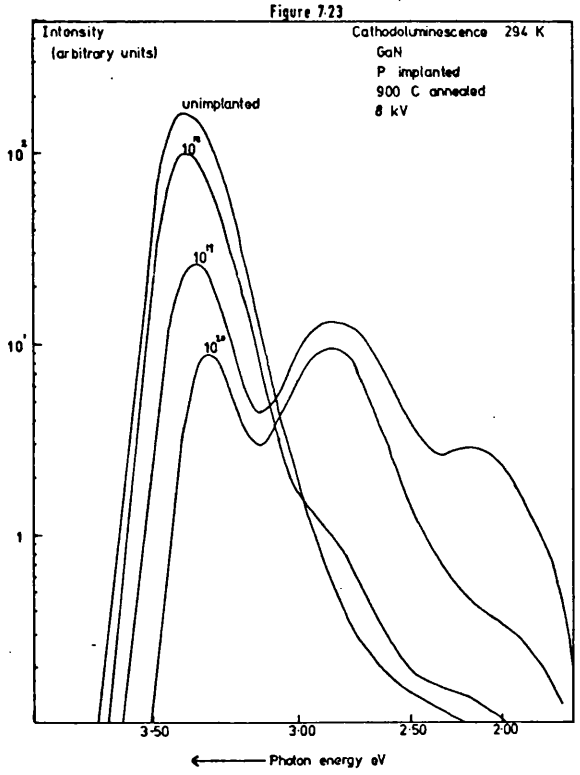

Figure 7.24

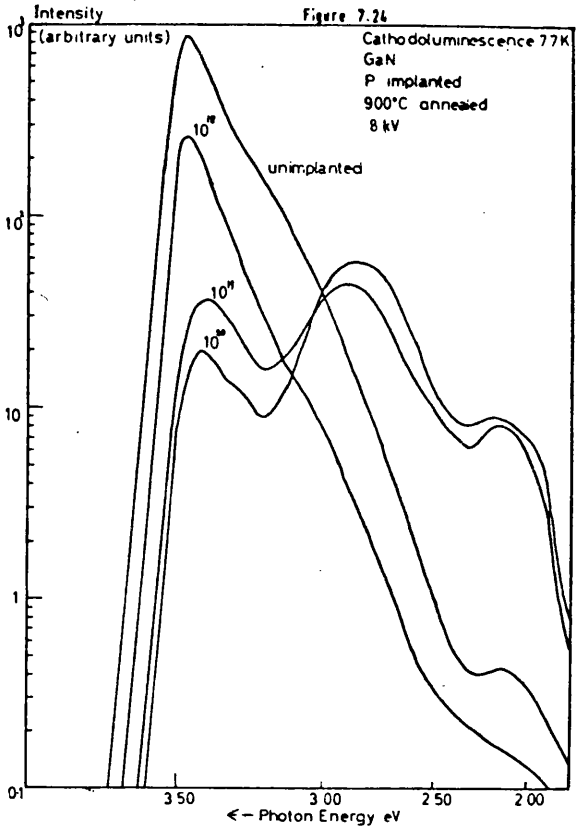

Figure 7.25

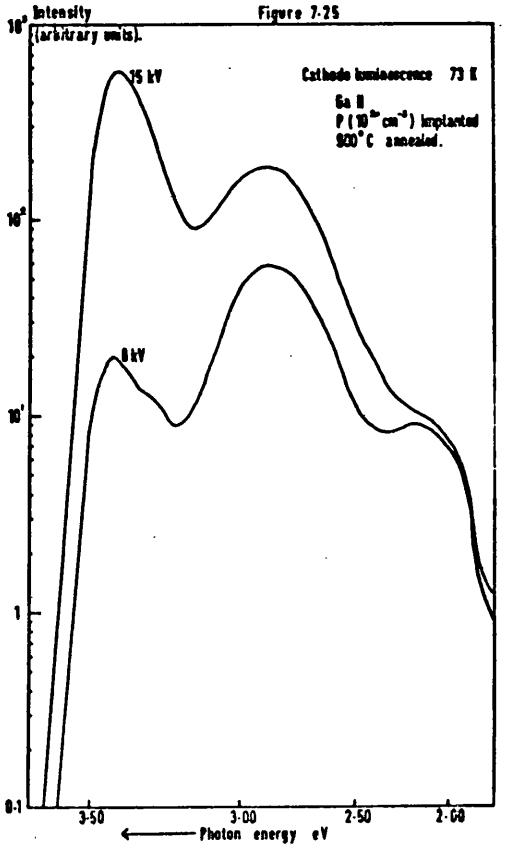

(ix) Arsenic

Thickness 9.8μm

Carrier concentration 3.4×10^{19} cm^{-3}

Implanted As^+ 82 kV

Peak concentrations 1.1×10^{18}, 10^{19}, 10^{20} cm^{-3}

Anneal Temp.^{0}C	Anneal Time	Type of Luminescence	Temperature of measurement
-	-	PL	RT LNT and LHeT
600	6 hrs.	PL	RT and LNT
750	15 mins.	PL	RT LNT and LHeT
770	"	PL	RT and LNT
900	"	CL	RT LNT and LHeT
920	"	CL	RT and LNT
930	"	CL	RT and LNT

Group V impurities in III-V compounds can act as isoelectronic traps, but As atoms are larger than P atoms so substitutional doping is less likely.

The unimplanted sample showed no resolved B-band. Some recovery of intensity was observed after low temperature annealing and a weak yellow band at 2.2 eV developed. After the 900^{0}C anneal a new band was observed. This peaked near 2.5 eV at RT (Fig 7.26) and at 2.58 eV at LNT (Fig 7.27) and LHeT in all three implanted samples. It was

accompanied by a reduction in A-band intensity and, for the 10^{20} cm^{-3} implant, by a clearly resolved B-band at LNT. The dependance of intensity on exciting electron voltage indicated that this reduction was limited to the surface layer (Fig 7.28) but that both the 2.58 eV band and the yellow band were deeper than in other samples. The 2.2 eV luminescence appeared as a low energy tail to the new band.

Further annealing reduced the 2.58 eV band intensity, partially restored the A-band intensity and increased the yellow band until it became a separately resolveable peak at 2.2 eV.

The 2.5 eV band is only found in As implanted GaN.

Figure 7-26

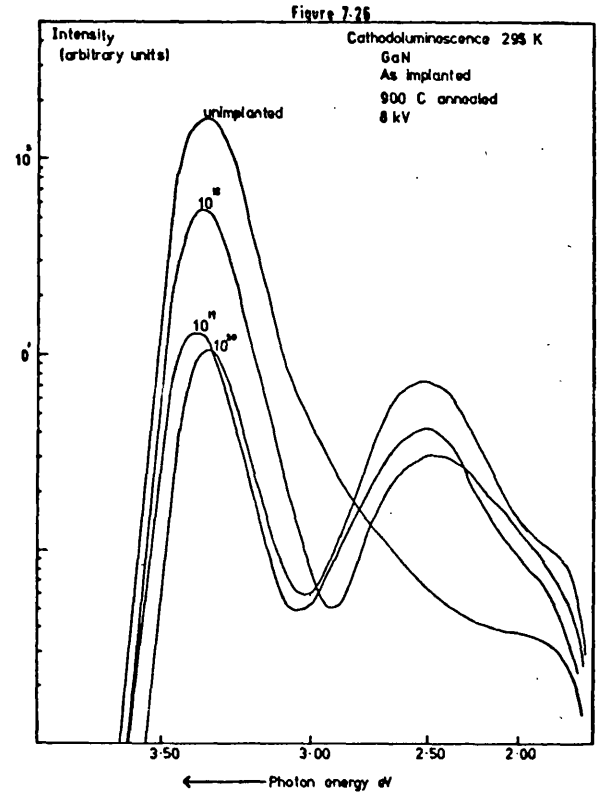

Figure 7-27

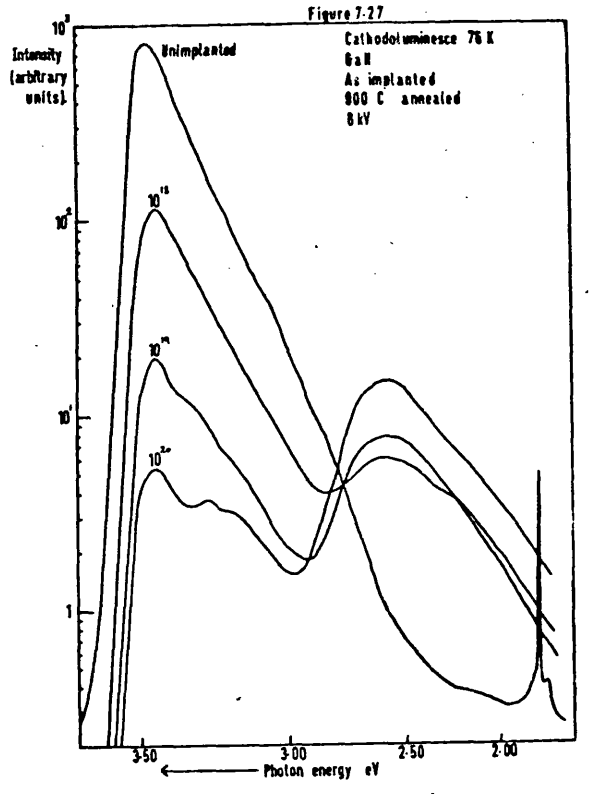

Figure 7-28

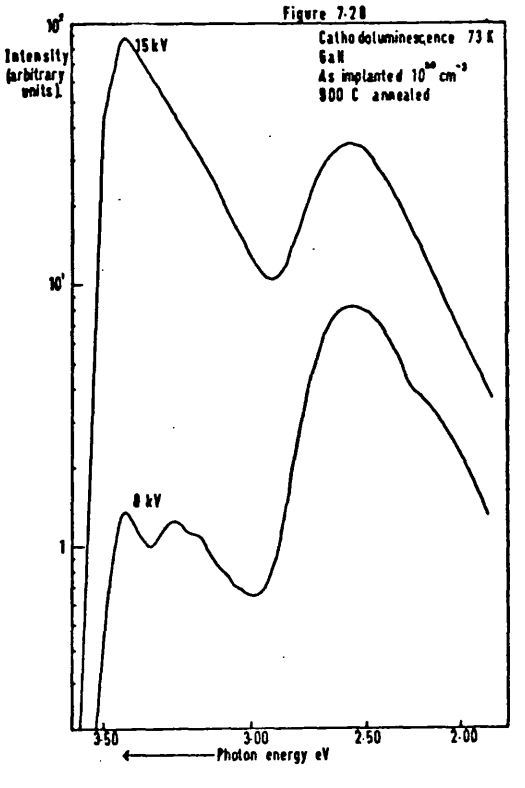

(x) Sulphur

Thickness 7.1μm

Carrier concentration 7.9 x 10^{19} cm^{-3}

Implanted S^+ 42 kV

Peak concentrations 1.5 x 10^{18}, 10^{19}, 10^{20} cm^{-3}

Anneal Temp.^{0}C	Anneal Time	Type of Luminescence	Temperature of measurement
-	-	PL	RT LNT and LHeT
750	15 mins.	PL	RT and LNT
770	"	PL	RT and LNT
800	"	PL	RT and LNT
820	"	PL	RT and LNT
900	"	PL and CL	RT LNT and LHeT
920	"	CL	RT and LNT
930	"	CL	RT and LNT

Group VI impurities in III-V compounds are donors when substituting on the anion lattice.

The unimplanted sample showed no B-band structure. Recovery of luminescent intensity was rapid. The intensity of 10^{18} and 10^{19} cm^{-3} implanted samples exceeded that of the unimplanted sample (Fig 7.29). The peak photon energy of the A-band was at 3.44 eV LNT for implanted samples as opposed to 3.47 eV for the reference sample. A weak yellow lumin-

escence at 2.2 eV developed.

Figure 7·29

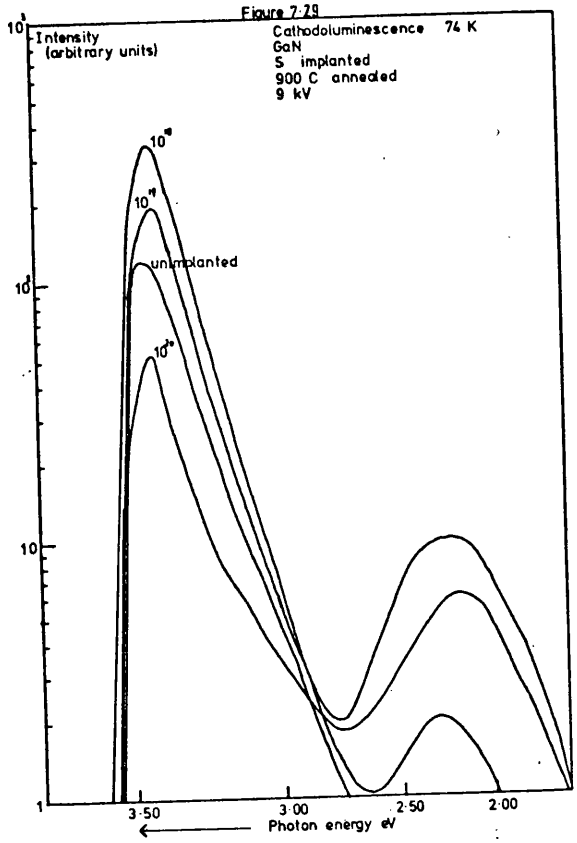
Intensity
(arbitrary units)
Cathodoluminescence 74 K
GaN
S implanted
900 C annealed
9 kV
unimplanted
3·50
3·00
2·50
2·00
Photon energy eV

(xi) Fluorine

Thickness 18.3μm

Carrier concentration 3.2×10^{19} cm^{-3}

Implanted F^+ 23.5 kV

Peak concentrations 1.65×10^{18}, 10^{19}, 10^{20} cm^{-3}

Anneal Temp.^{0}C	Anneal Time	Type of Luminescence	Temperature of measurement
-	-	PL	RT LNT and LHeT
700	7 hrs.	PL	RT LNT and LHeT
750	15 mins.	PL	RT LNT and LHeT
770	"	PL	RT and LNT
850	"	PL	RT and LNT
750	18 hrs.	PL	RT and LNT
800	15 mins.	PL	RT and LNT
900	"	CL	RT LNT and LHeT
920	"	CL	RT and LNT

Group VII impurities in III-V compounds can act as non-radiative centres, as donors or as interstitial acceptors (70).

The unimplanted sample showed no B-band luminescence. The 10^{19} cm^{-3} sample showed sharp features at 3.27 and 3.18 eV with a shoulder near 3.10 eV even before annealing.

Other samples showed no such features, then or after low temperature annealing (Fig 7.30).

After higher temperature annealing a weak shoulder began to develop near 3.2 eV in the LNT spectra (Fig 7.31) and on some parts of the 10^{19} cm^{-3} sample B-band structure could be identified. A yellow band near 2.26 eV was also detected. This structure was not limited to luminescence from the surface layer, excited by low energy electrons, but the yellow band showed a lesser increase in intensity with electron energy (Fig 7.32).

The B-band luminescence is observed only over part of one sample. It is not restricted to the original implanted layer.

Figure 7·30

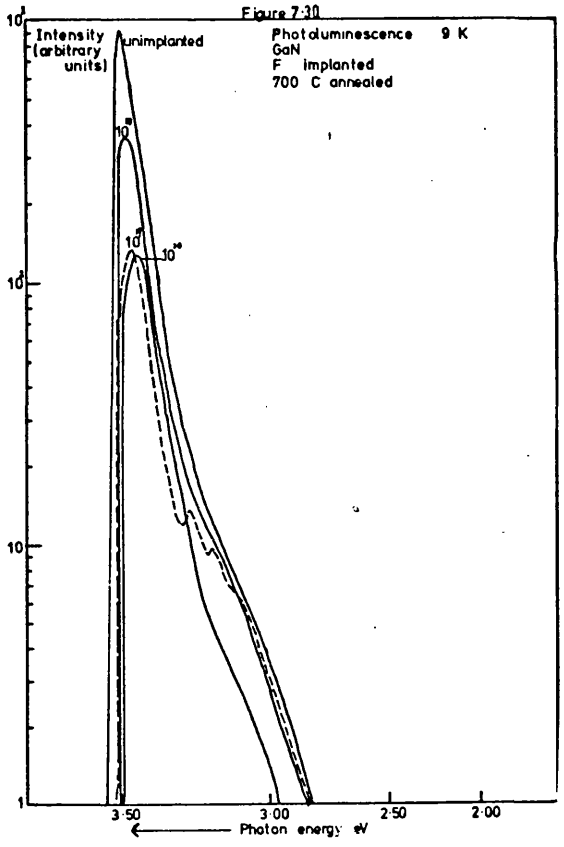

Figure 7·31

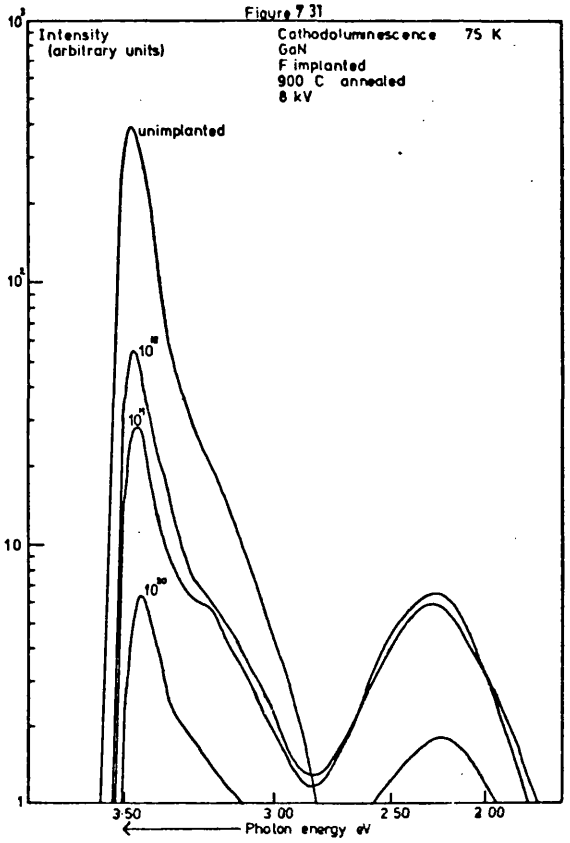

Figure 7·32

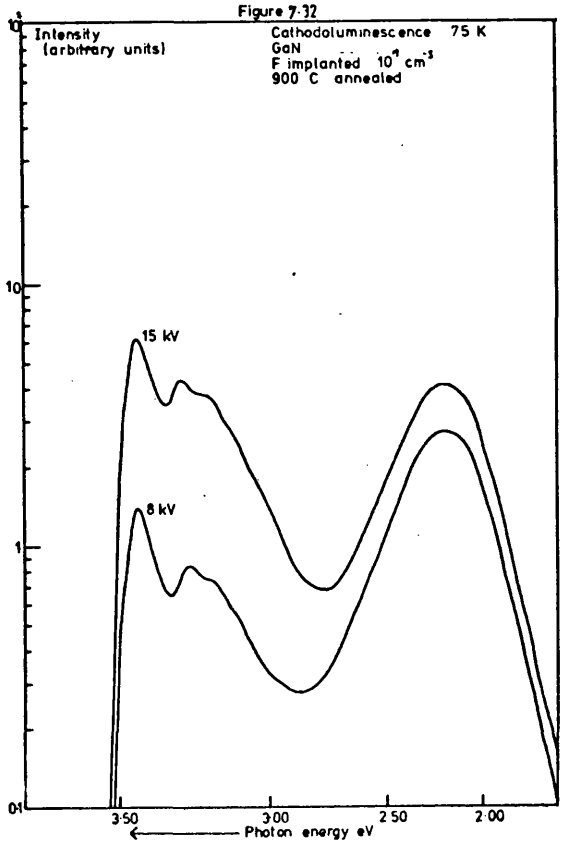

(xii) Chlorine

Thickness 7.4μm

Carrier concentration 5.9 x 10^{19} cm^{-3}

Implanted Cl^+ 45 kV

Peak concentrations 1.45 x 10^{18}, 10^{19}, 10^{20} cm^{-3}

Anneal Temp. ^0C	Anneal Time	Type of Luminescence	Temperature of measurement
-	-	PL	RT LNT and LHeT
700	10 hrs.	PL	RT and LNT
750	15 mins.	PL	RT LNT and LHeT
800	"	PL	RT and LNT
850	"	PL	RT and LNT
900	"	PL and CL	RT and LNT
920	"	CL	RT and LNT
930	"	CL	RT and LNT

Group VI impurities can act as non-radiative centres in III-V compounds, as donors or as interstitial acceptors (70).

The unimplanted sample showed no B-band structure. After annealing at temperatures as low as 750^{0}C B-band features were observed in some parts of the more heavily implanted samples. Fig 7.33 shows a strong B-band for 10^{19} cm^{-3}, 10^{20} cm^{-3} sample with a much reduced A-band int-

ensity and a resolved B-band after 900°C annealing. Yellow luminescence near 2.30 eV was strong only for 10^{18} cm^{-3} sample. After further annealing the B-band features disappeared for the 10^{19} cm^{-3} implant and became much weaker for the 10^{20} cm^{-3} implant. All samples developed a yellow luminescence near 2.28 eV. The 10^{20} cm^{-3} implant was still much less intense than the unimplanted sample (Fig 7.34). An increase in exciting electron energy gives a massive increase in A-band luminescence and the shoulder on the 10^{20} cm^{-3} implant spectrum was no longer observed. Yellow luminescence intensity was only slightly increased.

B-band features are observed. There is considerable variation in intensity and shape of spectra over each individual sample, but the features are limited to near the surface layer.

Figure 7·33

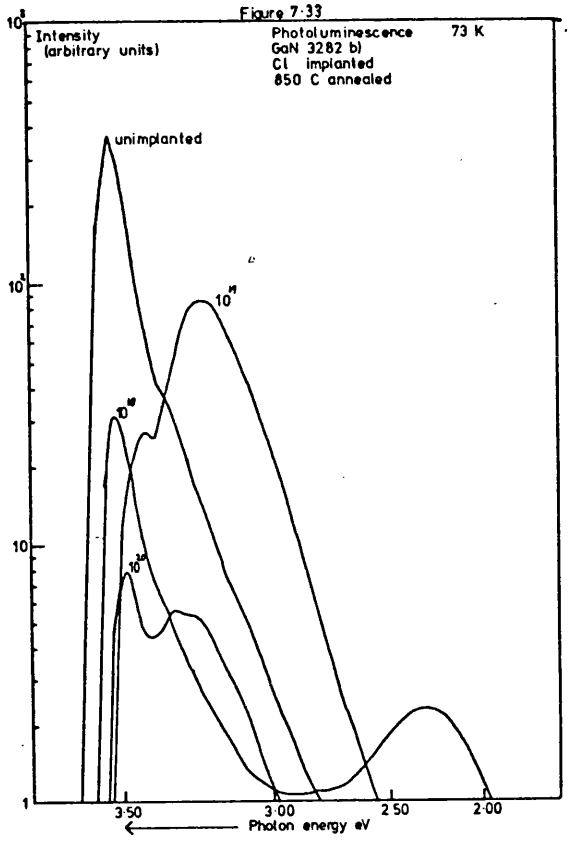

Figure 7·34

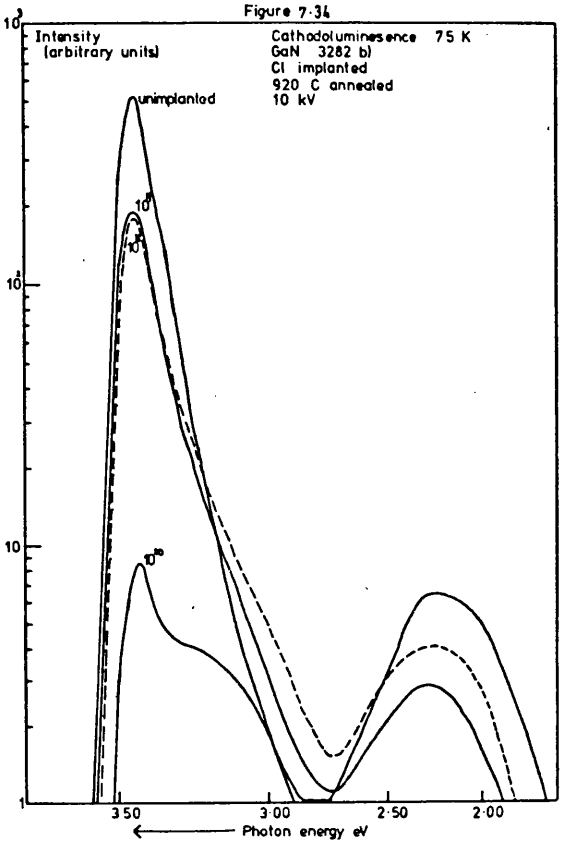

7.4 LUMINESCENCE OF NEUTRON IRRADIATED GAN

An opportunity arose to send some samples which had been implanted and annealed for activation analysis. Activation analysis is carried out by irradiating the sample with a flux of thermal neutrons and then measuring the typical energies of γ-rays and X-rays produced during the decay of unstable products of (n,γ) and (n,p) reactions.

e.g.

$$^{14}_{7}N\ (n,p)\ ^{14}_{6}C\ (\beta^-)\ ^{14}_{6}N \quad \text{(half-life 5730 years)}$$

$$^{71}_{31}Ga\ (n,\gamma)\ ^{72}_{31}Ga\ (\beta^-)\ ^{72}_{32}Ge \text{(half-life 14 hours)}$$

The only elements detected were Ga, N and those known to be in the substrate.

However neutron irradiation has two effects on the luminescence properties of semiconductors. It introduces impurity elements by reactions such as those above and extensive damage is caused by the energetic products of these reactions. (Thermal neutrons themselves with energies of the order of 25 meV at 300 K will not cause atomic displacements by elastic collision). The thermal neutron flux was 1.1×10^{17} cm^{-2} which gives concentrations of the order of 10^{16} cm^{-3} for impurities produced by this method. This concentration is likely to be too low for appreciable effects on the luminescence.

The energy released when a radioactive product decays is of the order of MeV and lattice damage produced will be high. If the optical properties are observed several half-

lives after the irradiation the samples should have damage which is distributed randomly throughout the material, instead of being concentrated in a surface layer. An investigation of the luminescent properties before and after annealing might be expected to throw some light on the influence of damage on the properties of the shallower layers produced by implantation. Unfortunately no reference samples were available for activation analysis so these results are limited to ion implanted and pre-annealed samples.

Before annealing these irradiated samples gave no luminescence. They were a dark brown colour and showed only a very weak edge absorption. Fig 7.35 shows the luminescence of some of these samples after a single anneal at 920°C. These had been implanted with 85 keV Zn^+ ions and before irradiation showed A and B-band luminescence together with the 2.9 eV Zn band and a yellow band at 2.12 eV. After annealing these features were re-established although the relative intensity of the A and B-bands were much reduced and half-widths were measured. Cathodoluminescence at 9 kV and 15 kV showed almost equal increments in the luminescence of A-band, Zn-band and yellow band indicating that both the Zn and yellow band originated from below the original implanted layer (Fig 7.36).

Fig 7.37 shows results for samples originally implanted with Si. After irradiation and a single anneal at 910°C they showed similar spectra to before irradiation. However the A-band was not resolvable and the relative intensity of the yellow band was much greater. Again the shapes of the spectra were similar at high and low electron energies.

Figure 7.35

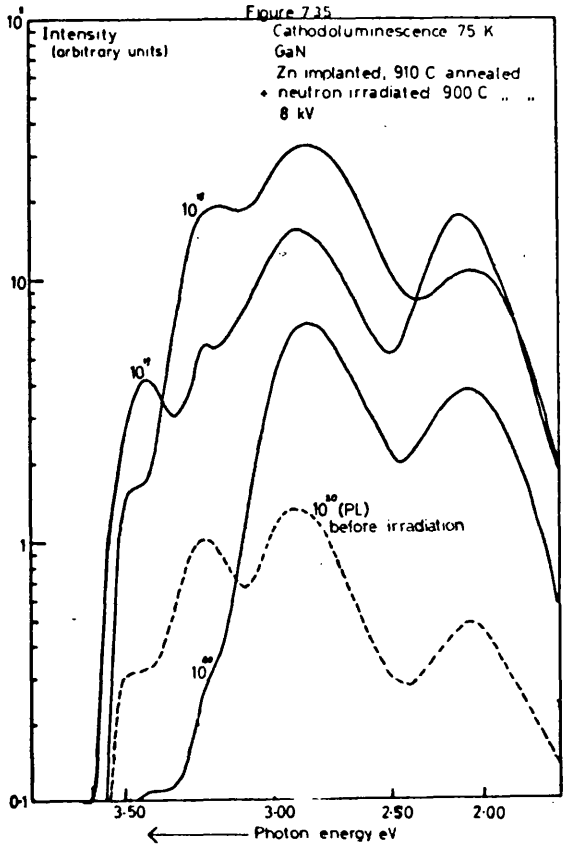

Figure 7.35

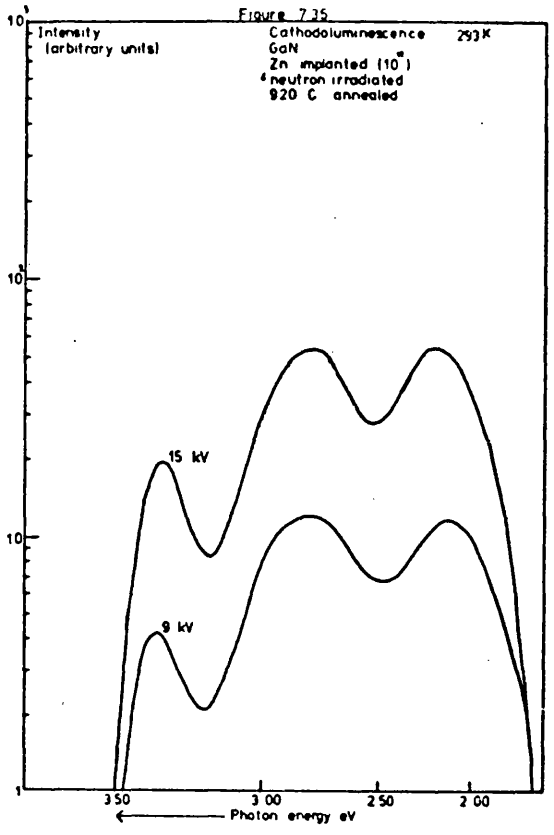

Figure 7.37

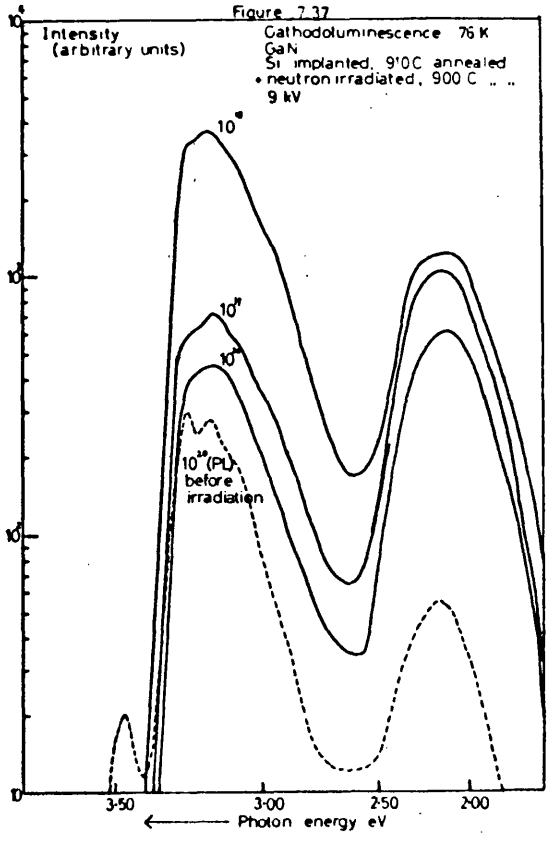

The extra damage introduced by neutron irradiation enhances both the Zn and yellow bands. The latter is particularly strong in Si implanted GaN. The luminescence is no longer restricted to the original implanted layer.

7.5 EXCITATION SPECTRA

The dependance on exciting photon energy of the principal luminescence features observed in as-grown, growth doped and implanted GaN was investigated.

Fig 7.38 shows the LNT emission spectrum of GaN doped with Zn during the growth process together with the excitation spectrum of the 2.9 eV emission. The emission spectrum showed a sharp near-gap peak at 3.464 eV and a broad peak at 2.90 eV, the typical Zn luminescence. The B-band appeared as a shoulder near 3.25 eV on the Zn-band and no yellow band was seen. The excitation spectrum, which was not corrected for photomultiplier sensitivity, showed a steady rising intensity of 2.90 eV emission as exciting photon energy decreased from above 5 eV to the band gap at 3.50 eV. The intensity then fell rapidly. This type of spectrum is typical of semiconductor luminescence excited by the creation of electron-hole pairs within the electron bands (2).

The LNT excitation spectra were recorded of the 3.20 eV emission of undoped GaN and of the 2.14 eV emission in C implanted GaN and Si implanted GaN after neutron irradiation and re-annealing (Fig 7.39). These latter were the only two implanted samples for which excitation spectra were detected. The sharp lines on the spectrum of the C implant changed their position with a small change in detected photon energy and were assumed to be grating ghosts. The same spectra were recorded at RT with the exception of the B-band at 3.20 eV which is not seen (Fig 7.40).

The table below summarises the excitation spectra and the relation of their peaks to the band edges at LNT and RT.

Table 7.1

LNT E_g = 3.500 eV

Sample	Emission	Peak Emission	Energy Difference from E_g
undoped	3.20 eV	3.488 eV	-12 meV
Zn doped	2.90 "	3.503 "	+ 3 "
Si implanted	2.14 "	3.473 "	-27 "
C implanted	2.14 "	3.575 "	+75 "

RT E_g = 3.437 eV

Zn doped	2.90 eV	3.435 eV	- 2 meV
Si implanted	2.14 "	3.416 "	-21 "
C implanted	2.14 "	3.523 "	+86 "

Figure 7.38

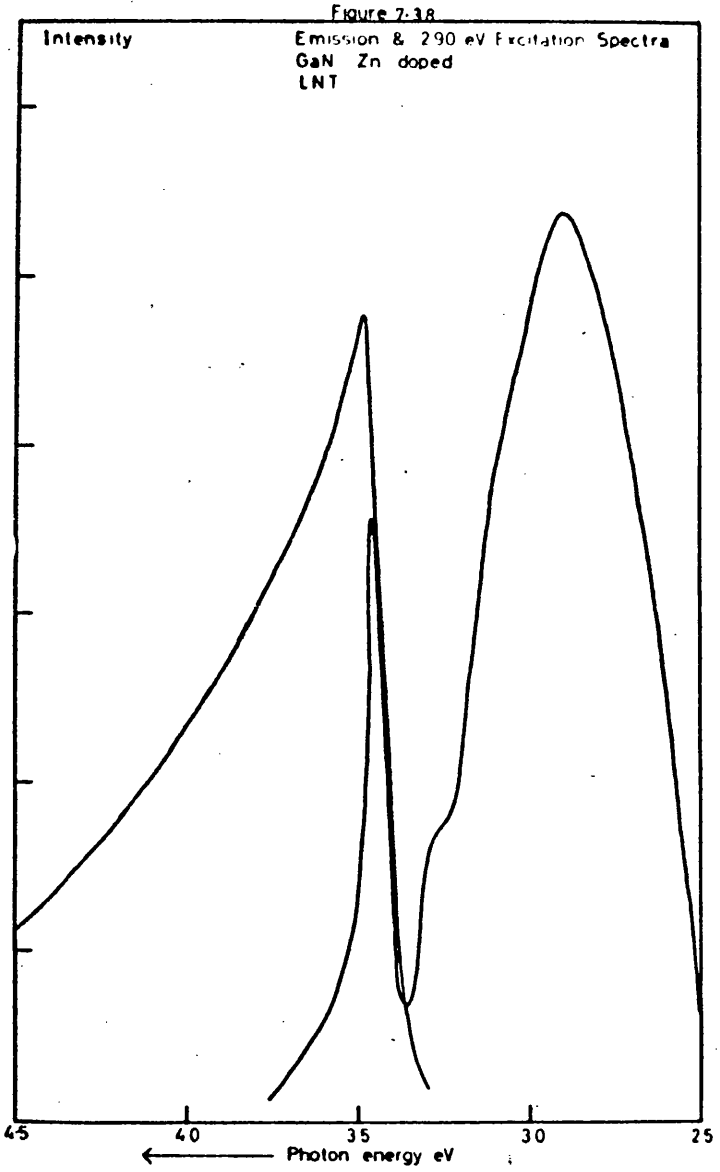
Intensity
Emission & 290 eV Excitation Spectra
GaN Zn doped
LNT
45
40
35
30
25
Photon energy eV

Figure 7·39

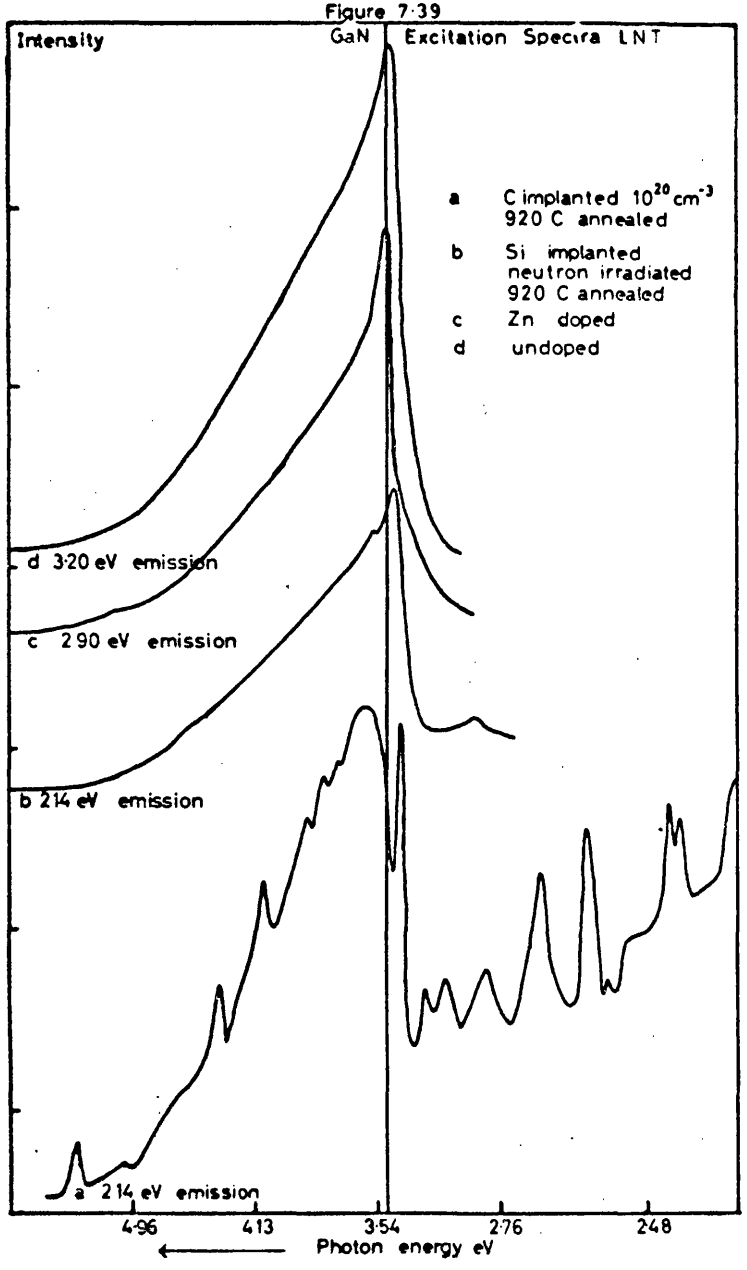

Figure 7·40

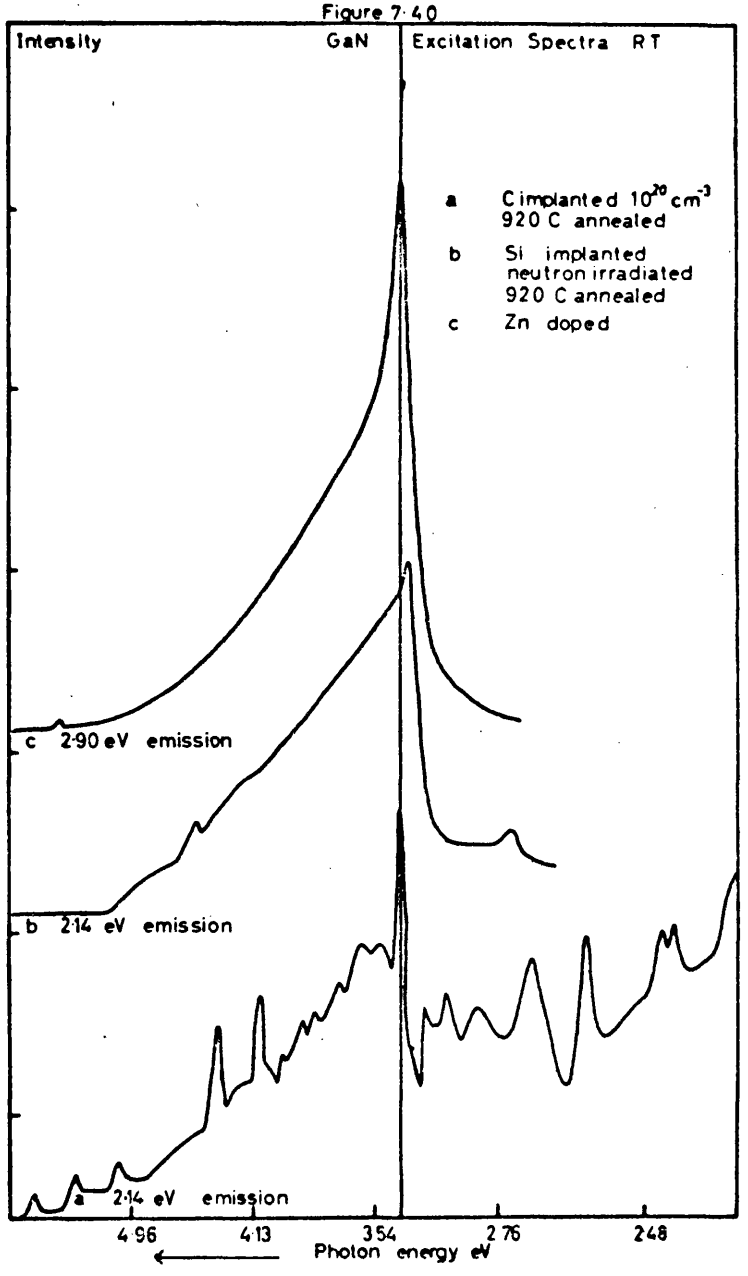

7.6 ABSORPTION SPECTRA

Fig 7.41 shows the RT absorption spectra from an unimplanted, unannealed GaN sample. The two spectra were recorded with the slip bands vertical and horizontal. The difference between them is an indication of the influence of asymmetrical scattering on the intensity recorded by the detector of the spectrometer.

Three distinct regions are identified in the spectra.

a) above 3.3 eV. The absorption coefficient increases exponentially with photon energy.

$$\alpha = \alpha_o \exp (h\nu/E_o)$$

with E_o near 30 meV.

This is a common form of relationship in disordered semiconductors (see 3.6 above).

b) below 1.0 eV. The absorption coefficient follows a power law (Fig 7.42).

$$\alpha = \alpha_o (h\nu)^{-n}$$

The index n has values associated with absorption by free carriers scattered by ionised impurities.

c) the intermediate region 1.0 - 3.3 eV. Unlike the first two regions it is here where absorption is low that the influence of scattering is observed and there is significant difference between different orientations of the same sample. An exponential relationship of the form

$$\alpha = \alpha_o \exp (h\nu/E_o)$$

can also be used to approximate to the absorption in this

region. E_o may vary from 0.5 to 2 eV. This empirical expression is reasonably successful for separating the edge and free carrier absorption contributions from the background contribution at intermediate energies.

Superimposed on the spectrum below about 2.0 eV are periodic variations in intensity due to thin film interference in the epitaxial layer. Values for thickness of the epitaxial layer of all four samples from the same slice are in close agreement with the values quoted in section 7.2 above. These values are obtained from weighing the substrates before and after growth so this is an indication of a uniform average thickness over the whole slice. However the contrast of these fringes is low; the ratio of maximum to minimum intensity varies from 1% to 4%. I_{max}/I_{min} for a layer of front surface amplitude reflection coefficient r_1 and rear surface coefficient r_{12} with absorption coefficient α and thickness d is:-

$$I_{max}/I_{min} = \frac{1 - r_1 r_{12} \exp(-\alpha d)}{1 + r_1 r_{12} \exp(-\alpha d)}$$

with $r_1 r_{12} = 0.08$

and $\exp(-\alpha d) = 0.9$

in the region of interest

$$I_{max}/I_{min} = 0.85$$

There will be further contributions from light reflected at the substrate - air interface but the above value is a reasonable first approximation.

The loss in contrast is a further indication of the

roughness which causes scattering at the sample surface.

In Fig 7.43 is shown the variation of absorption with implanted ion flux before annealing. This particular sample was almost free of slip bands and the spectra was the same for vertical and horizontal orientations. (By comparison Fig 7.44 shows the same relation for a more striated sample). A steady increase in overall absorption is seen.

The edge absorption of both samples (Fig 7.45 and 7.46) shows a similar decrease of slope with increasing ion dose. The value of E_o increases with ion dose. The free carrier absorption gives indices in the same range as those for unimplanted samples (Fig 7.48).

It is possible to plot the excess absorption of a sample after implantation (Fig 7.47) by subtracting the absorption coefficient for the unimplanted sample. The edge absorption of all samples has $E_o = 50 \pm 5$ meV and the free carrier absorption yields indices in the range $n = 3.8 \pm .5$. Thus the implanted layers have spectra of similar shapes.

The effect of annealing on absorption spectra does not follow a simple pattern. The brown colouration disappears after low temperature annealing. The intermediate region absorption shows much lower coefficients, there being least change in the unimplanted sample, but the relative positions of the curves for implanted samples being rather random. Fig 7.49 is fairly typical. The edge absorption gives values close to those of the unimplanted sample in all cases. The difference between the different sample orientations becomes more noticeable. The thin film interference bands

below 2.0 eV become less well defined, disappearing completely after two or three annealing cycles.

Figure 7.43

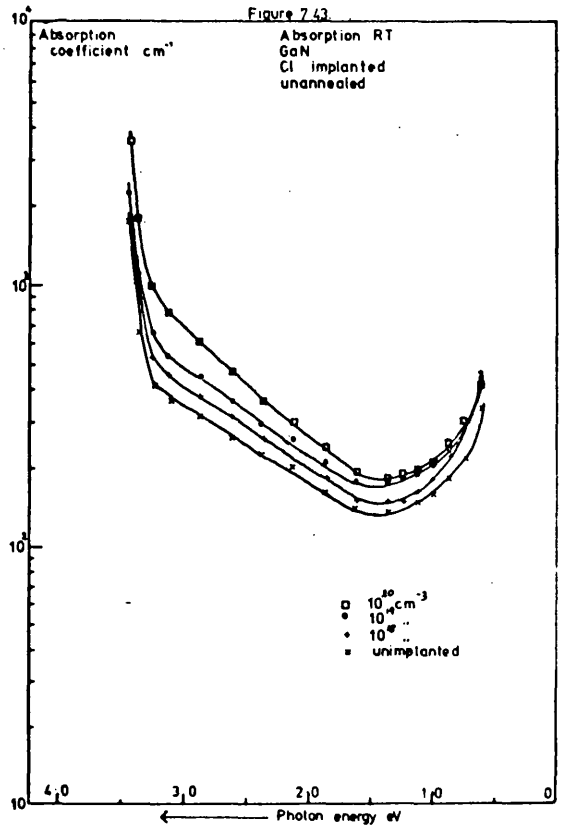

Figure 7.42

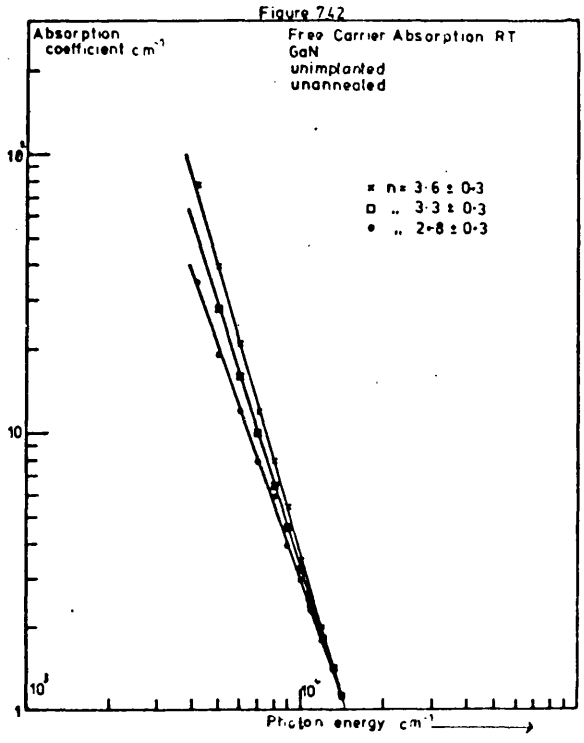

Figure 7.41

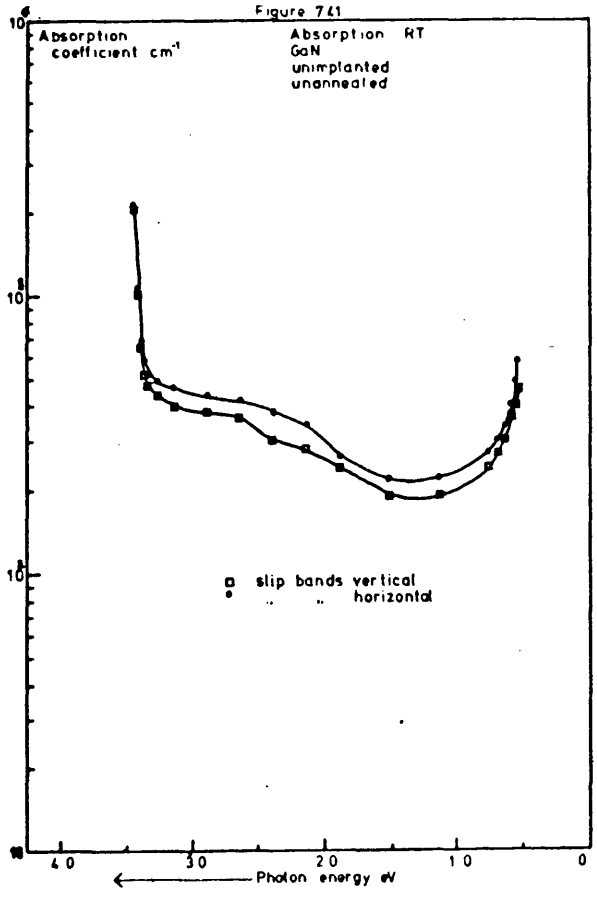

Figure 7.46

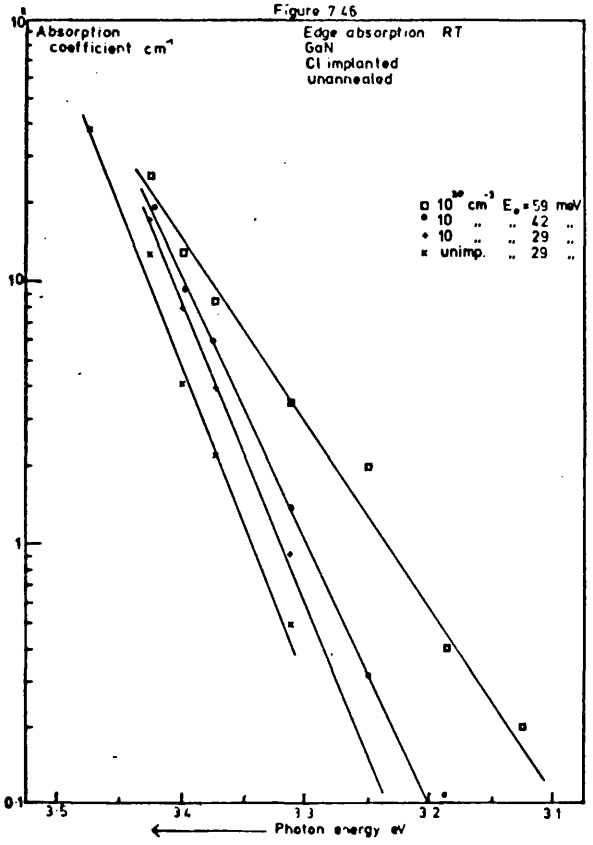

Figure 7.47

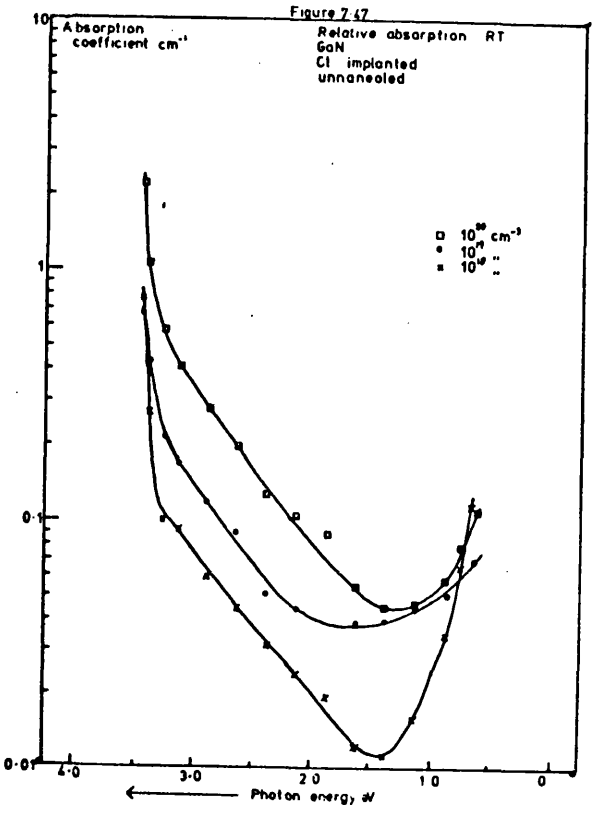

Figure 7.48

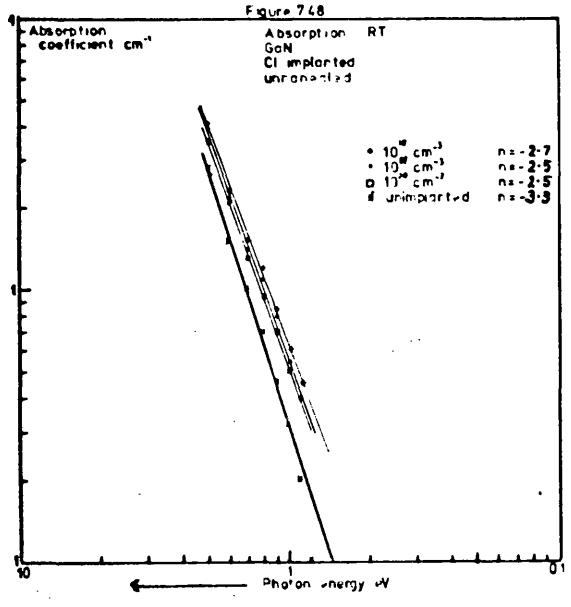

Figure 7.49

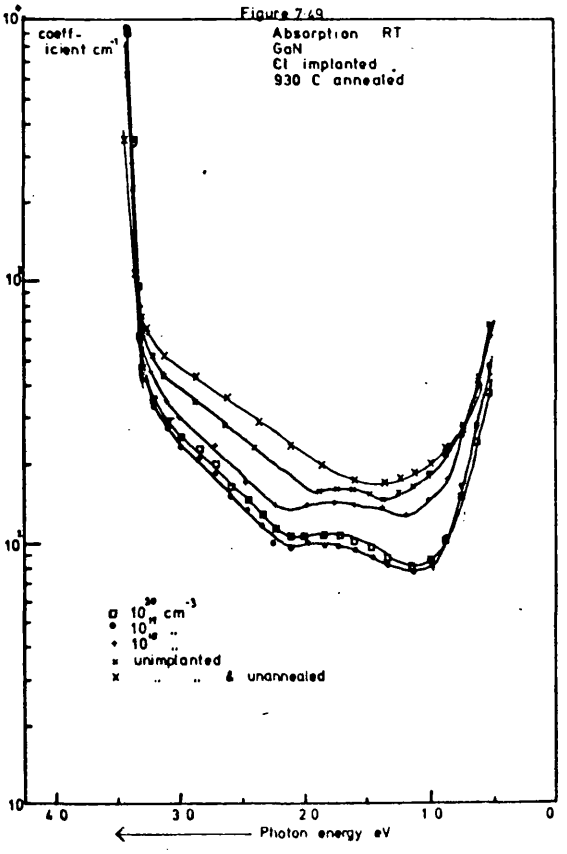

Figure 7.44

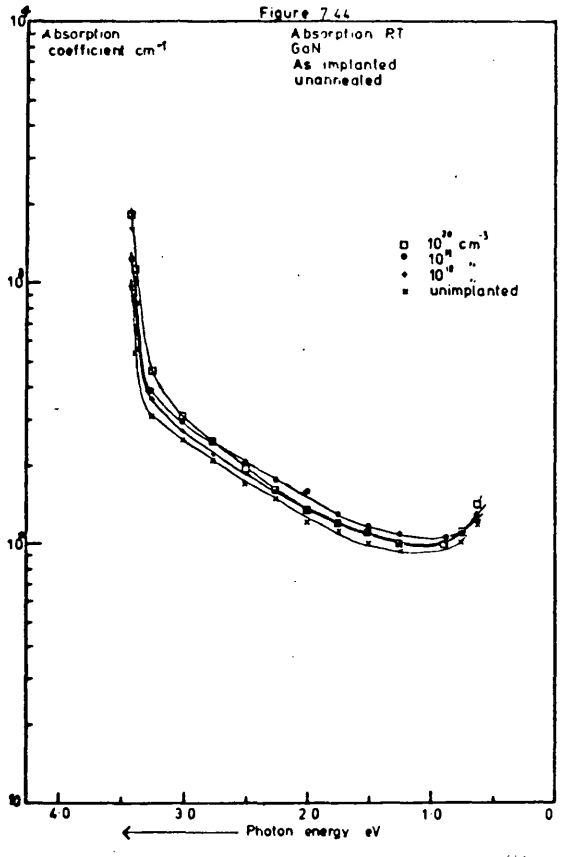

Figure 7.45

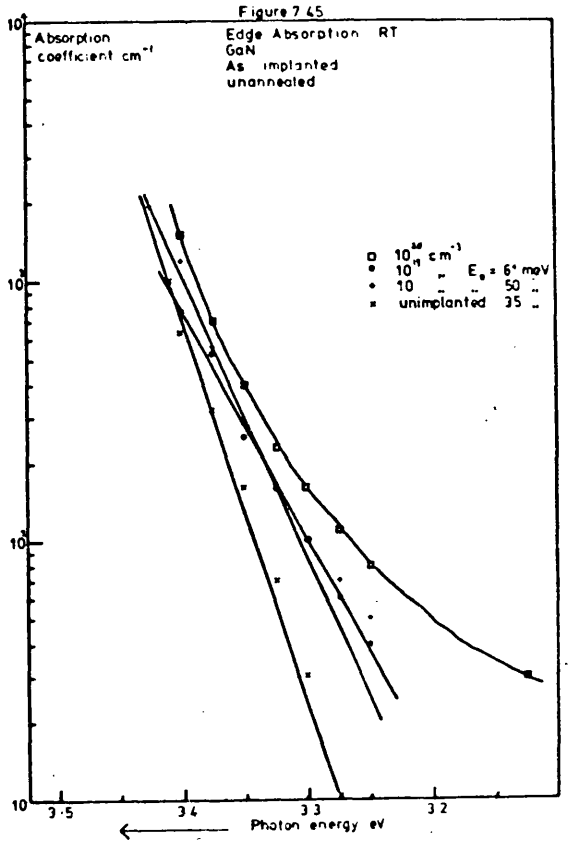

7.7 $Ga_{1-x}Al_xN$ ALLOYS

Measurements were made of absorption, of cathodoluminescence, and of photoluminescence emission and excitation on $Ga_{1-x}Al_xN$ alloy samples grown by Wickenden at HRC using chemical vapour deposition on α - Al_2O_3 substrates. The method was that described previously for GaN growth (29) with the addition of a proportion of Al to the Ga melt. A more extensive study of this alloy system has been made by Hagen (90) but these initial results are reported here where they relate to the properties of pure GaN and Al-doped GaN.

The proportion of Al included in the Ga melt covered the full range of composition. Direct determinations of x, the atom per cent of Al in the deposited alloy, were made by the Materials Characterisation Department at HRC (99) by ion probe microanalysis, and both powder and cylindrical X-ray diffraction measurements of lattice parameter were also made. The X-ray measurements showed that some oriented polycrystalline material was present and that a range of lattice parameter was present, possibly due to strain and local fluctuations in composition. Considerable discrepancies existed between the determinations of x by different methods, the electron probe method generally giving a higher value. This may be due to the presence of interstitial Al or to irregular sample thickness permitting electrons to penetrate to the α- Al_2O_3 substrate.

The optical measurements at Bath, together with CL recorded at HRC (98) give some indication of the band-gap

and by interpolation between the known values of 3.50 for GaN (9) and 5.9 for the direct gap in AlN (97) an estimate of x may be made. The variation of band-gap with composition is not usually linear. A sublinear relationship with "bowing" of the order of 5% is found in a number of systems (100). Optical estimates of gap energy from absorption edges and emission peaks are subject to errors of at least this magnitude so a linear interpolation is used. Fig 7.50 shows typical cathodoluminescence, absorption and emission spectra. All three types of spectra suggest an energy gap near to 3.6 eV, corresponding to about 4 atom per cent Al, this is much less than the 22% included in the growth melt.

Other samples do not give such clear-cut results. Fig 7.51 shows a sample in which the high energy cut-off of cathodoluminescence is near 4.8 eV indicating a composition of 50 atom per cent Al but absorption and CL spectra show numerous features and the emission spectrum of the dominant feature in photoluminescence peaks well below this value at 4.3 eV. Another part of the sample gave an absorption edge near 3.5 eV. Localised states within the gap may be responsible for these features. Such states have been reported for complexes of oxygen dipairs and Al vacancies in AlN doped with high concentrations of exygen (102). It has also been suggested that AlN has an indirect gap below the direct gap (101) and transitions at this gap may be involved.

Comparisons between optical estimates and more direct

methods do suggest that even where there is no detailed knowledge of the transitions involved in optical spectra the optical value is in fair agreement and can be used as a basis for further discussion. Table 7.1 compares a number of estimates of gap energy for $Ga_{1-x}Al_xN$ alloys. The electron probe results are extremely high in at least two cases, possibly for the reasons discussed above. Optical results, where available, are in agreement with other methods to a few percent.

Table 7.1

Atom per cent Al				
Source	47	80	46	75
Electron probe	17	66	92	93
Powder X-ray	4.5	49	-	-
Cylindrical X-ray	10,11.5	61	-	-
Absorption (RT)	7	48	-	-
CL (LNT)	4.4	45,57	27	70

There is also evidence for considerable variation in properties at different points on at least two samples. RT absorption spectra were recorded for 32 alloy samples grown with source compositions varying from 5 to 85 atom per cent Al. Of these, five showed no absorption edge, presumably because of gaps in the deposition of AlN, and thirteen

showed absorption close to the GaN absorption edge. Cathodoluminescence at RT and LNT were recorded for a selection of these samples (unfortunately insufficient time was available for a complete investigation). No emission above the absorption edge was found in any sample and no sharp line spectra like those in Al-implanted GaN were seen.

The high energy peak of cathodoluminescence was usually close to the absorption edge and in a number of samples a low energy emission was seen. Its peak photon energy was near 2.2 eV for less than 50 atom per cent Al but above this value the peak shifted to higher photon energies in most samples. In between these extremes a number of peaks were seen in the range 3.8 to 3.0 eV. In some samples peaks with phonon replicas, similar to the B-band in pure GaN, but shifted in energy were seen. Samples with a wide range of estimated concentration gave emissions close to 3.5 eV.

Excitation spectra were recorded for the emissions of samples with strong luminescence. The low energy emission gave excitation peaks within the estimated band gap, near 4.2 eV, for all concentrations above 50 atom per cent Al but typical band-edge spectra for lower concentrations.

The emissions within the estimated gap gave complex spectra with excitation peaks also within the gap suggesting the presence of a range of local recombination centres.

These results are summarised in Fig 7.52. A more detailed study of these and other $Ga_{1-x}Al_xN$ alloy samples including extensive electron microprobe analysis of sample

composition and uniformity is being carried out by Hagen. Preliminary results confirm the general patterns indicated above.

Figure 7.50

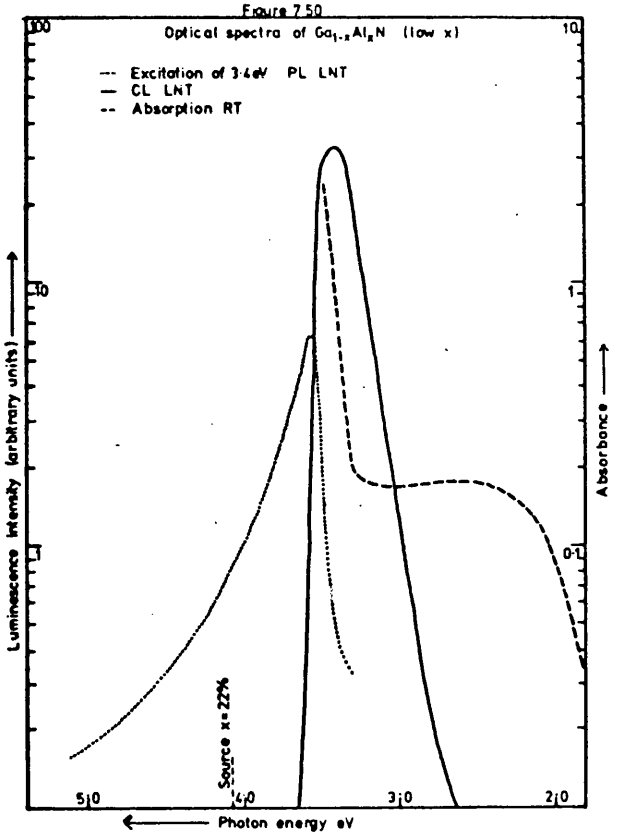

Figure 7.51

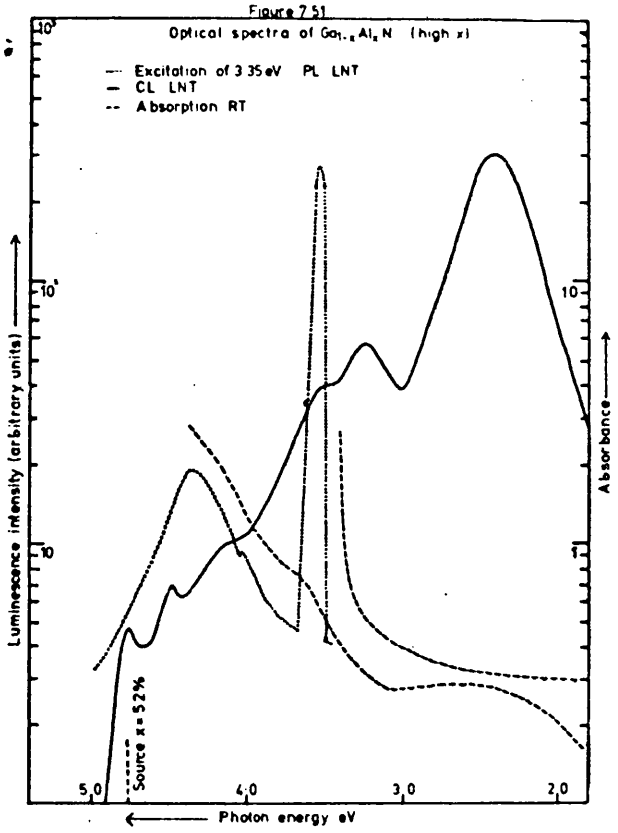

Chapter 8.

DISCUSSION AND CONCLUSIONS

8.1 SPECIFIC IMPURITIES

Before discussion of the general features found in most GaN samples the emissions clearly related to one specific implanted impurity, and the properties of $Ga_{1-x}Al_xN$ alloys are considered.

(i) Zinc Extensive studies have been made of luminescence in GaN doped with Zn during growth (16-19, 57-59, 61,62) and by implantation (63,74). A broad emission with peak photon energy near 2.9 eV is commonly seen, but under some growth conditions the peak may be as low as 1.8 eV (59). The 2.9 eV band is thought to be due to tunneling-assisted transitions from the tail of the conduction band to ionised acceptor levels associated with the valence band (59). Hole capture at the acceptor is by a fast non-radiative process. A second non-radiative process with a time constant which decreases with increasing Zn concentration is thought to provide a competing path for electron-hole recombination, quenching both the near-gap and Zn emissions. The variation of peak photon energy with temperature is considerably less than the change of the energy gap and this is explained by a variation of the quasi-Fermi level within the conduction band tail of states as temperature changes (46).

Of the Zn-implanted samples studied in this work only the 2×10^{19} cm^{-3} implant gave the typical Zn luminescence with a peak near 2.88 eV. A strong A-band and a weak yellow luminescence were also seen. The 2×10^{20} cm^{-3}

implant gave only the A-band and yellow luminescence at reduced intensity and the 2 x 10^{21} cm^{-3} implant only a very weak yellow band.

Fig 8.1 shows 8 kV cathodoluminescence emission at LNT from this 10^{19} cm^{-3} implant (curve 3) and also from another 10^{19} cm^{-3} Zn-implant (74) and growth doped Zn (Curves 2 and 1) originating from HRC. Curves 4-6 were taken from the literature and no comparison of intensity is possible among these. Curve 4 is RCA material implanted at 10^{18} cm^{-3} and curves 5 and 6 are growth doped Bell Laboratory material.

The carrier concentrations and the A and B-band spectra of these samples vary widely. The Bell Lab. material was strongly compensated with carrier concentration around 10^{17} cm^{-3}, the host material of the sample implanted at RCA had carrier concentration estimated at 3 x 10^{18} cm^{-3} and the HRC implanted material had carrier concentrations measured at 2 x 10^{19} cm^{-3} (74) and 6 x 10^{19} cm^{-3}. The carrier concentration of the HRC growth-doped material was not known, but it was not semi-insulating. All samples gave the broad emission band near 2.9 eV attributed to Zn.

Pankove and Hutchby (63) report a quenching of near-gap luminescence in all implanted samples, and a quenching of the Zn-band with increasing Zn concentration giving no detectable emission for 2 x 10^{19} cm^{-3} implanted Zn atoms. Implantation into HRC material gives near gap luminescence up to 2 x 10^{20} cm^{-3} implanted Zn ions and the Zn-band at 2 x 10^{19} cm^{-3} but not 2 x 10^{20} cm^{-3} in one sample and up to 1 x 10^{20} cm^{-3} in another (74). The implanted Zn layer is

Figure 8.1

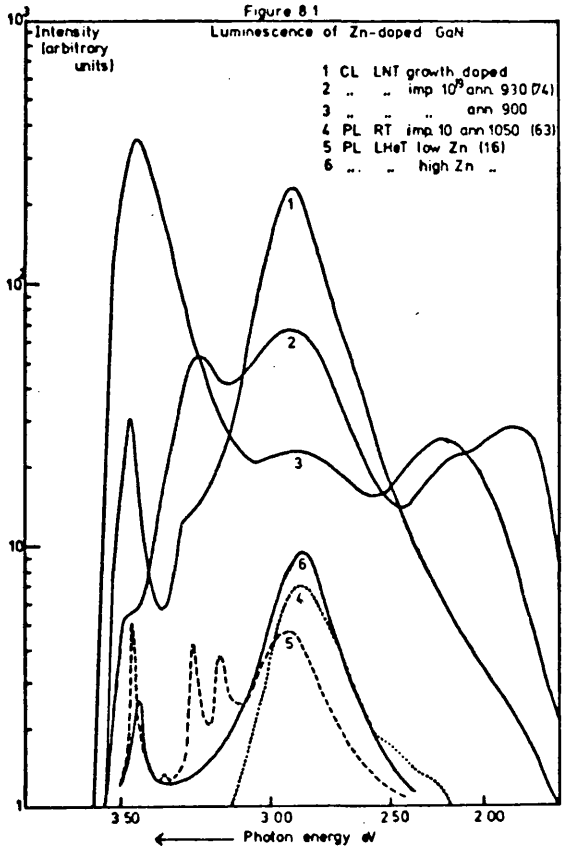
Luminescence of Zn-doped GaN
Intensity (arbitrary units)
1 CL LNT growth doped
2 " " imp 10^{19} ann 930 (74)
3 " " " ann 900
4 PL RT imp 10 ann 1050 (63)
5 PL LHeT low Zn (16)
6 " " high Zn "
10^3
10^2
10
1
3 50
3 00
2 50
2 00
Photon energy eV

rather shallower in this work than in the previous work but this is not expected to produce differences in the Zn emission. However a shallower layer will have a greater contribution to its luminescence from underlying material and a weak Zn emission could be swamped by the extensive A-band tail of the 2×10^{20} cm^{-3} implant.

The differences in quenching of HRC and RCA material may be explained by the higher carrier concentrations of the former. The time constant of tunneling-assisted processes decreases exponentially with the tunneling distance and at higher carrier concentrations, where the average separation of donors and acceptors is less, the band-to-band and Zn-band transitions will be considerably faster. The competing non-radiative process has a time constant which decreases with increasing Zn concentration (63) but it will not dominate luminescent recombination until higher ion doses if its time constant is not affected by higher carrier concentrations.

(ii) Aluminium The sharp line spectra seen in Al-implanted GaN were not seen in any other samples. Table 8.1 gives the peak photon energy after various annealing treatments. Strong peaks with half-widths less than 0.1 eV are underlined.

The sharp spectra indicate that the broadening due to the tail of states of the conduction band is not occurring. This may be because of reduction of charged impurity concentrations in the presence of a compensating acceptor or because the luminescence occurs within a localised centre.

Table 8.1

Anneal Temp.^{0}C	Sample	Luminescence type	Emission Peak Photon Energy
-	ALL	PL	3.51,3.47 eV
700	ALL	PL	3.51,3.47
750	10^{19} cm^{-3}	PL	3.49,3.33,3.24,3.13
800	10^{20} "	PL	3.43,3.36,3.32,2.44
850	10^{20} "	PL	3.49,3.36,3.32
"	10^{19} "	PL	3.43,3.36,3.32
900	ALL	CL	3.45,2.2
930	10^{20} cm^{-3}	CL	3.53,3.38,3.34
"	10^{19} "	CL	3.51,3.38,3.34

A group III impurity in a III-V compound is expected to substitute on the cation lattice. A considerable range of $Ga_{1-x}Al_xN$ alloys have been grown at GEC by a vapour deposition method similar to that used for GaN and measurements on these indicate that Al substitutes for Ga over the full range of concentrations (90). However the concentration of Al incorporated in the alloy is usually less than in the source (see above) indicating a limited solubility of Al in GaN. Isoelectronic impurities which have low solubility in the host lattice form efficient recombination centres giving sharp emission lines which have

been extensively studied in a number of compounds (91,92). Al is expected to form an isoelectronic hole trap (93) on the cation site in many III-V compounds and this type of trap has been reported for Al in InP (94). Implanted ions do tend to come to rest on substitutional sites (104) and isoelectronic traps may be the cause of the sharp spectra seen in Al implanted GaN.

At low impurity concentrations the luminescence at an isoelectronic trap involves recombination of a bound exciton, at higher concentrations lower energy transitions between pairs of traps are also seen (91). Pair recombination between a hole trapped at an isoelectronic impurity and a neutral donor have also been reported (95). Coupling to lattice vibrations is high and a large number of phonon replicas are expected. Studies of the isoelectronic traps N and Bi implanted into GaP (72,73) indicate that after annealing transitions are broadened, forbidden transitions become allowed and pair emission is concentrated at nearest neighbour pairs as a result of residual lattice damage. In epitaxial layers the thermal strains induced during annealing may augment these effects.

The sharp LNT spectra seen after the 800 and 850^{0}C anneal, and again from a limited region after the 930^{0}C anneal consist of a single line near the gap value of 3.5 eV and a pair of lines near 3.36 and 3.32 eV. The separation of 130 and 170 meV of these lines from the near-gap emission is greater than the LO phonon energy of 90 meV or the local mode phonon whose energy is expected to be (96):-

$$E_{loc} = E_{LO}.M/2\mu = 110 \text{ meV}$$

where M is the mass of the Al atom and μ the reduced mass of Ga and N.

The only emission in which phonon replicas are seen is the B-band like emission from the 10^{19} cm^{-3} sample after the 700°C anneal. The no phonon line is at 3.33 eV and may be the same as the lower energy emission of the pair mentioned above. This energy is about 60 meV higher than the DA pair emission seen in undoped GaN below 50 K and 30 meV above the free-bound transition.

The nature of the emissions seen in GaN : Al can not be determined from these results. The fine structure and phonon replicas associated with isoelectronic traps in GaP for instance are not seen, but isoelectronic traps do not necessarily give this fine structure. The emission from the hole trap Te in CdS consists of two single lines one associated with bound excitons, the other with nearest neighbour pairs (92). The presence of Al as an isoelectronic substituent in GaN is a possible explanation of the sharp spectra.

More detailed investigations of these lines was not possible because, after annealing at 900°C, the lines were no longer seen. It is unfortunate that the absence of sharp spectra coincided with the changeover from PL to CL measurements. This may have been due partly to the different depths to which PL and CL probe the sample, but the location of small parts of two samples which gave this type of luminescence shifted to higher energies, suggests

that diffusion of Al or of native defects is responsible for the absence of these sharp bands. The luminescence seen after the 930^{0}C anneal might be due to precipitation of Al in regions of high defect density. The emission was in fact seen from a small region of poor growth quality, and the shift of near-band emission to higher energies could be due to incorporation of Al at sufficient concentrations to give a band-gap shift. A shift of 0.03 eV implies 1.2 atom per cent of Al, assuming AlN to have a direct band-gap of 5.9 eV (97). This is considerably greater than the 0.2 atom per cent at the peak in the 10^{20} cm^{-3} implant. It is not clear whether diffusion leads to actual loss of Al or to an increase in the concentration of native defects due to dissociation of GaN leading to the incorporation of Al at a more complex type of centre.

The sharp line spectra are accompanied by a fall in the B-band tail and yellow band emission intensity to almost zero. Recombination at isoelectronic traps is much faster than the tunneling-assisted transitions expected in high conductivity material and this may be sufficient to explain the lack of low energy emission. Alternatively substitutional Al atoms may be occupying defect sites which are involved in these emissions in unimplanted material.

It is unfortunate that confirmatory experiments could not be carried out on other Al implanted samples. Detailed investigations of temperature dependance of emission under high resolution are needed to positively identify the nature of these sharp bands observed in GaN : Al. The mechanisms

mentioned above are based on the assumption that Al acts as an isoelectronic trap, and there is little direct proof of their nature. Strong absorption bands like those seen in N implanted GaP were not detected, but their relative strength is less in a direct-gap material.

(iii) $Ga_{1-x}Al_xN$ alloys The spectra of low Al concentration $Ga_{1-x}Al_xN$ alloys may be expected to show some of the features appearing in Al-implanted GaN. No sharp line spectra like those in the implanted samples are seen, but broader bands with subsidiary peaks at intervals of about 100 meV similar to the B-band in GaN with its no-phonon line near 3.26 eV and its phonon replicas appear in a number of samples (Fig 8.2). Two possible groups of emissions of this type have been identified, one following the band-gap variation and one with its no-phonon peak near 3.3 eV. A single peak near 3.5 eV is also often seen. The peak photon energies of these lower energy peaks vary over about 5 meV and they may have a similar cause to the sharp features seen in Al-implanted GaN. Considerable local variation of concentration is indicated and may account for the broadening. Another possibility is that the Al which is not deposited on cation sites is located in interstitial positions. However if an interstitial site is preferred for Al it is unlikely to give the sharp emission seen near the gap energy in Al implanted GaN.

The low energy band shows two components, one near 2.2 eV which dominates at low Al concentrations and another at higher energies which is usually found when x exceeds

Figure 8.2

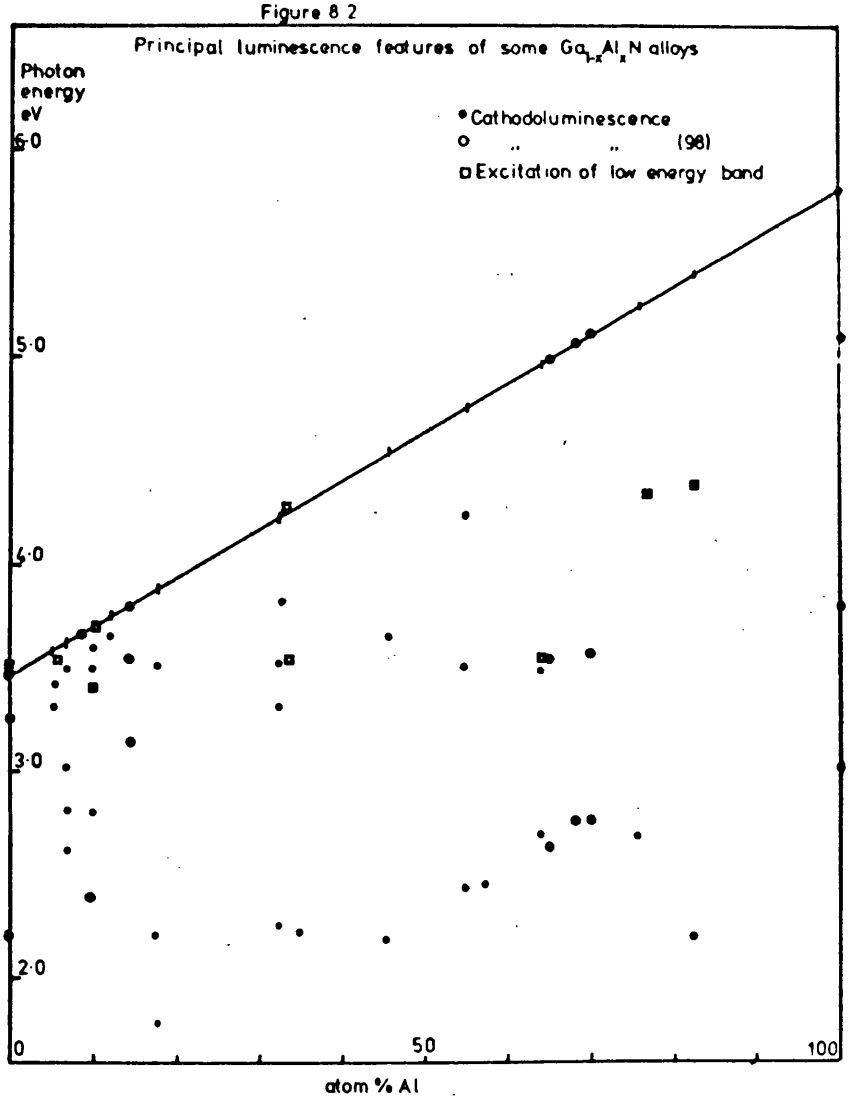
Principal luminescence features of some $Ga_{1-x}Al_xN$ alloys
Photon energy eV
• Cathodoluminescence
o .. .. (98)
□ Excitation of low energy band
6·0
5·0
4·0
3·0
2·0
0
50
100
atom % Al

50 atom per cent Al. The lower energy component may be identified with the 2.2 eV yellow emission seen in implanted and annealed GaN whilst the higher energy component is not identified. These bands show excitation peaks near 4.2 eV in high Al concentration alloys and occasionally at 3.5 eV as well as the normal band-gap excitation. A series of three levels of one impurity, the lowest near 2.2 eV another near 3.5 eV and the third near 4.2 eV at almost all alloy compositions may be indicated. Single vacancies in GaN or $Ga_{1-x}Al_xN$ are expected to be triple donors (V_N) or acceptors (V_{Ga} or V_{Al}) and could conceivably be involved. Pure AlN shows peaks at 3.0 and 3.8 eV which may be identified with this system. Alternatively luminescence due to different pair and dipair complexes like those reported for oxygen-rich GaN (102) may be involved.

A further study of luminescence of impurity levels in a complete range of $Ga_{1-x}Al_xN$ alloys may well yield a better understanding of the yellow emission with pure GaN and the sharp lines in Al-implanted GaN.

(iv) Arsenic and Phosphorus New broad-band emissions were seen in both As and P implanted GaN near 2.58 and 2.85 eV. These bands are of similar half-width and show the same lack of variation of peak photon energy with temperature as the typical Zn band near 2.90 eV. A similar tunneling-assisted transition from the conduction band tail to ionised acceptor atoms would explain this behaviour. The shape of the density of states curve would be the dominant factor in the peak photon energy value.

The reduction of A-band intensity is not out of proportion with that seen in other samples. The B-band is seen clearly resolved in the highest concentration As implant but it is not clear whether this is due to a reduction in carrier concentration or to a competing non-radiative recombination at residual defects reducing only the band-to-band recombination and not conduction band-acceptor transitions.

The P peak has a greater intensity than the As peak. This may be due to the greater mobility of P atoms in the lattice, as evinced by the lower annealing temperatures at which the P band appeared, or to the lesser amount of initial damage from P ions. P and As are both so large as to be unlikely substitutional dopants so a complex centre is expected. Strain around the larger As atom may also give extra competing non-radiative pathways reducing efficiency. Both bands fall in intensity relative to the A-band after annealing above 900^0C. The variation of CL with exciting electron energy suggests a deeper distribution of P centres than the original implanted layer after the 900^0C but the luminescent layer became shallower after the 930^0C anneal suggesting diffusion of implanted impurity is occurring. The 10^{18} cm^{-3} implant did not show the typical P-band, possibly because of incorporation of P at low concentrations in a different type of centre. The P concentration would only have to fall to this value for P luminescence to disappear.

8.2 GENERAL FEATURES

(i) The A-band Variations in the A-band luminescence may be due to the annealing process, to radiation damage, or to a contribution from the implanted impurity. A general shift occurs in the LNT peak photon energy of reference samples from the range 3.50 to 3.47 eV before annealing to 3.47 to 3.43 eV after annealing. Since carrier concentrations are high in all reference samples the A-band is thought to be due to tunneling-assisted transitions from the conduction band tail of states to the valence band or shallow acceptors. Changes in defect concentration during annealing lead to changes in the band tail density of states and are responsible for the peak shifts.

Before annealing the implanted samples show a peak shift from the 3.50 eV near-gap LHeT emission of the reference sample to 3.47 eV as ion dose increases. Luminescence near 3.47 eV has been identified with the recombination of free excitons or of excitons bound to an unidentified donor (4). This donor may be a native defect introduced by damage during implantation. After high temperature annealing the implanted samples show generally lower peak photon energies than the reference sample, the most common values being near 3.44 eV at LNT, as opposed to 3.47 eV for the reference samples. The shift of peak photon energy is probably due to a greater rate of dissociation in the GaN layers which have been damaged by ion implantation and a more rapid increase in the concentration of damage-associated centres responsible for emission near 3.47 and 3.44 eV.

The temperature variation of peak photon energy of the

A-band follows the shrinkage of the band-gap in almost all cases. The only exceptions are the Si and Ca-implants. These are samples which gave B-band luminescence of similar intensity to the A-band and the high energy wing of the B-band may be contributing to A-band emission.

The dependence of intensity on damage indicates that in a number of samples the reduction in A-band intensity follows an empirical power law relation after the 900°C anneal:-

$$I/I_o = a\, E_n^{-0.66}$$

where E_n is the energy dissipated in nuclear collisions as defined in 5.2 above. If electron-hole pairs are generated in a semiconductor at a rate G and a concentration N_c of non-radiative centres with a recombination rate r_c is introduced then the fall in intensity is

$$I/I_o = 1 - N_c r_c/G$$

The rate of recombination r_c will generally be a function of N_c. Pankove and Hutchby (63) report a luminescence efficiency in Zn implanted GaN which is proportional to the logarithm of the reciprocal of the Zn concentration. No such dependence is found in the A-band luminescence.

However the high correlation found for the reduction of intensity of the A-band of these samples permits the assumption that the reduction is due solely to damage due to the initial implantation and subsequent annealing and that native defects are responsible for the quenching of the

A-band. The samples involved are the K, B, P, As, F and Cl implants. The other samples show stronger A-band luminescence than expected. This may be due to the incorporation of the implanted impurity in a near-gap radiative centre or in an inactive complex with the defect responsible for the quenching. In two samples, the C and S implants, the A-band intensity is actually increased which suggests a near-gap emission. In the other cases, the Ca, Zn, Al and Si implants, there is some reduction in A-band intensity. Zn is known to give shallow acceptors (16) and Al implanted GaN gives sharp near-gap peaks at lower anneal temperatures so near-gap emission may again be occurring. At lower annealing tamperatures B implants also showed increased A-band luminescence but by the 900°C anneal the reduction in intensity was comparable to other samples.

The implanted ions tend to come to rest on substitutional sites (89) and the luminescence after lower temperature anneals may be due to substitutional impurities. At higher annealing temperatures defects introduced during implantation migrate and so may the implanted species. Furthermore the dissociation of GaN becomes appreciable at about 900°C and this proceeds by a self-diffusion mechanism (3). All these diffusion processes may be expected to occur at higher rates in damaged GaN. The initial damage and the consequent dissociation during annealing introduce a concentration of defects which are non-radiative recombination centres. In the absence of a contribution to the luminescence from the implanted species the A-band intensity is governed by the

amount of initial damage.

(ii) The B-band Two samples showed a resolved B-band. The shape of this band remained largely unchanged with annealing and with implantation of Si or Ca impurity.

B-band spectra also appeared in some implanted material. Two types of emission were recorded. A series of sharp features on the A-band tail were seen in F implanted GaN after implantation and up to the 750°C anneal and in the Al implanted GaN after the 750°C anneal alone. In the latter case the peaks are shifted to higher energy by about 60 meV. In both cases only the 10^{19} cm^{-3} implant shows the spectra. These sharp features may originate from comparatively narrow layers of the sample in which compensation is occurring and be almost swamped by the A-band luminescence. After annealing at around 900°C a broad B-band, rather stronger than the A-band, is seen in GaN : B (10^{18} cm^{-3}), GaN : Cl (10^{19} and 10^{20} cm^{-3}), and GaN : F (10^{19} cm^{-3}). This emission is seen only on parts of the sample and varies considerably from one annealing treatment to the next. The variation of intensity with exciting electron energy shows that the emission is not limited to the original implanted layer. It may therefore be a property of the host material, although no B-band spectra were seen on the reference samples.

The appearance of B-band luminescence in implanted GaN is limited to impurities from groups III and VII of the periodic table. The presence of the B-band is associated with low carrier concentration (52). It is identified as a DA pair emission in purer GaN at temperatures up to about

70 K and with free-bound transitions at higher temperatures or in less pure material where band tailing is appreciable (6). Its appearance therefore suggests the introduction of a shallow acceptor centre.

The defects introduced by implantation will include acceptors but these alone do not explain the appearance of the B-band in a limited number of samples. Implanted ions tend to come to rest on substitutional sites (89) but self-annealing will occur, particularly for lighter ions (69) and the ions may then migrate to interstitial centres or complex centres with defects. No single explantation can be offered of the role of group III or VII impurities in the B-band and the appearance of effects at different annealing temperatures. F present substitutionally is expected to act as a donor and the presence of B-band emission even before annealing may indicate its migration to interstitial sites, where group VII atoms act as single acceptors, or to its compensation with a native defect such as the Ga vacancy, expected to be a treble acceptor. The disappearance of the B-band in GaN : F after low temperature annealing may then be due to a reduction in defect concentration. The B-band like spectra seen in GaN : Al may be isoelectronic in nature and is discussed above.

Higher temperature annealing will tend to further reduce defect concentration due to the initial radiation damage, but this is thought to be offset by enhanced diffusion permitting dissociation of GaN and a consequent increase in defect concentrations. The role of defects is likely to be more important in luminescence after higher temperature annealing,

and compensation of group VII impurities by a native acceptor may become significant again. This may explain the reappearance of the B-band in GaN : F and GaN : Cl.

In both GaN : F and GaN : B the B-band luminescence intensity increases with increasing exciting electron energy, indicating that the implanted impurity has diffused to depths below the implanted layer at these higher temperatures.

It is of interest to note that both Al and Cl are found in the growth system, Al in the substrate material and Cl in HCl or GaCl in the cation transport stream. They are among the impurities detected in mass spectrometric analysis of GaN (12). Their concentration does not correlate with carrier concentration (12) but their influence on B-band emission is not reported. The influence of group III and group VII impurities on the luminescence of GaN, particularly of the B-band may be worth further study.

(iii) Yellow luminescence A broad band with a peak photon energy near 2.2 eV is common to almost all samples after the completion of annealing. It is normally only strong in annealed samples but small areas of some reference samples showed yellow luminescence as strong as any implanted sample. The band does not shift with increasing temperature and its half-width increases only a small amount. The intensity falls with increasing temperature in a manner similar to the Zn-band. The peak photon energy varies from sample to sample, after lower temperature annealing values as high as

2.36 eV were recorded, and in two samples, the Ca and Cl implants a peak near 2.0 eV was recorded after higher temperature annealing.

In implanted samples the variation of cathodoluminescence intensity with exciting electron energy shows that the yellow luminescence is limited to a surface layer roughly coincident with the implanted layer. This is not the case in reference samples with yellow emission or in neutron-irradiated GaN : Zn and GaN : Si after re-annealing.

The strongest yellow luminescence occurred in the Si, Ca, and C implants, the weakest in GaN : Al and GaN : B. There was no particular correlation of yellow luminescence with the energy dissipated in nuclear collisions. Yellow luminescence peaking between 2.1 and 2.3 eV has been reported from GaN doped during growth with Zn (59) Be (56,60) Li (58, 60) and Na (58). In GaN : Zn yellow or red emission is only found after low temperature growth.

Emission spectra of annealed GaN : Si (after neutron irradiation) and GaN : C show exitation peaks respectively about 25 meV below and 80 meV above the gap width at RT and LNT. This type of excitation suggests in the deep damage layers of neutron-irradiated GaN : Si a tunneling-assisted free-bound transition of the type suggested for GaN : Zn is occurring. The above-gap peak of the shallow GaN : C layer may be due to changes in absorption length with photon energy near the gap value. At values below the peak more of the exciting photons may be penetrating into the underlying layer which shows no yellow luminescence.

The role of group IV elements in the yellow luminescence is not clear. GaN : Si and GaN : C gave some of the strongest yellow peaks. Si is present as a surface contaminant and may be diffusing into the surface layers. However Si was also found in regions where yellow luminescence was not seen. The first requirement for yellow luminescence is lattice damage. This may result from ion implantation, but high temperature treatment and the accompanying dissociation of GaN is needed for strong luminescence. Native defects may be assumed to play a major part in the luminescence.

The very low level of yellow luminescence in GaN : Al when strong narrow near-gap peaks are seen may be due to the sharp line emission being a much more rapid recombination path than the yellow or B-band emissions. Or if the Al atoms are in fact isoelectronic substituents on Ga sites it may be due to a reduction of Ga vacancies. This concentration of Ga vacancies may be expected to increase again at higher temperatures where dissociation proceeds by a self-diffusion process and yellow luminescence is again seen.

The yellow luminescence may be due to a conduction band-acceptor transition like that proposed in GaN. The acceptor may be the Ga vacancy or may be a group I, II, or IV substituent on the appropriate lattice. It is suggested that in GaN : C, GaN : Si and GaN : Ca the implanted species is involved. In other samples it is a native defect alone (possibly the Ga vacancy) or an impurity from the annealing system (possibly Si).

8.3 CONCLUSIONS

Eleven different impurities from groups I to VII of the periodic table have been implanted into GaN. The properties of implanted layers have been investigated by optical means. Annealing is necessary to restore crystal order and luminescent intensity after the initial damage caused by the energetic ions. The annealing process is limited in GaN by the dissociation which occurs at elevated temperatures despite the presence of an atmosphere of ammonia. Surface damage occurs and a yellow luminescence band appears. After annealing at temperatures above 900°C a number of luminescent features fall in intensity and one disappears completely. This may be due to diffusion, or to increased defect concentration changing the nature of the luminescent centres.

(i) Zn-implanted GaN shows a luminescence band near 2.9 eV. Differences in quenching from other investigations is explained by the shorter time-constant of tunneling-assisted transitions.

(ii) Al-implanted GaN shows sharp spectra near 3.50, 3.36 and 3.32 eV after annealing up to 850°C. After higher temperature annealing these emissions are not detected over most of the sample area. Loss of Al by diffusion or migration of Al to different lattice sites are possible explanations. The sharp spectra may be due to isoelectronic centres.

(iii) $Ga_{1-x}Al_xN$ alloys show complex spectra at low Al concentrations which may include the emissions seen in Al-implanted GaN. There is some evidence for impurity levels near

3.5 and 4.2 eV in alloys with Al compositions below 50 atom per cent. These levels are associated with the 2.2 eV yellow emission.

(iv) P and As-implanted GaN show luminescence bands near 2.85 and 2.58 eV respectively. Annealing above 900°C causes loss in intensity of these bands either because of loss by diffusion, migration to inactive sites, or an increase in concentration of competing non-radiative centres.

(v) In K, B, P, As, F and Cl-implanted samples quenching of A-band luminescence is governed by the amount of initial damage. Enhanced diffusion rates lead to dissociation of GaN, and an increase in native defect concentration. Impurities giving less quenching of A-band luminescence are Ca, Zn, Al, Si and at lower anneal temperatures B. The A-band is strengthened by C and S impurities. Near-gap impurity luminescence may be present in any of these latter samples.

(vi) Sharp B-band luminescence is seen in one GaN : F sample up to 750°C anneal and in one GaN : Al sample after the 750°C anneal. The no-phonon lines are at 3.27 and 3.33 eV respectively. Broad band luminescence near 3.2 eV is seen in some GaN : B, GaN : F and GaN : Cl samples after annealing above 900°C.

(vii) A yellow luminescence near 2.2 eV appears in all implanted and some unimplanted samples after annealing. This luminescence is associated with defects generated during the dissociation of GaN during annealing at elevated temperatures. C, Si, and Ca-implanted impurities may contribute to this emission.

A recent study of photoluminescence in 35 impurities implanted into GaN, including all the above except F, has amongst its conclusions the following (103):-

(i) Impurities which give typical emission bands include Zn (2.88 eV), P (2.88 eV), As (2.58 eV), and Ca (2.50 eV).

(ii) The near-gap emission is strongest in Al and Kr implants. In all other samples the A-band intensity is a few per cent of that from the reference area.

(iii) The B implant gives an emission near 3.2 eV.

Luminescence at this peak photon energy is also introduced in some annealed unimplanted material. It may be the DA pair band or a typical band associated with B impurities.

(iv) A broad emission near 2.15 eV is identified in all implanted samples where it is not swamped by a typical emission band. It was strongest in C and Si implants.

(v) A broad emission near 1.75 eV is believed to be an artefact of the annealing process. It is stronger in implanted samples but appears on some reference areas.

These results are in agreement with this work in the identification of Zn, P and As-bands; the association of the yellow band with annealing and with C and Si implantation; the identification of a 3.2 eV band with B implantation; and the high A-band intensity in the Al implant.

Differences from this work include the absence of sharp Al spectra leading to a reduction in yellow band intensity; the absence of a strong A-band in the S implant; the absence of B-band luminescence in the F and Cl implants, the presence of a Ca-band at 2.50 eV (in this work the presence of Ca gave a strong 2.2 eV emission); and the presence of a 1.75 eV

emission after annealing.

The host material had carrier concentration about 3×10^{18} cm^{-3} and was implanted at a peak impurity concentration of 5×10^{18} cm^{-3} to a depth of 32nm. The samples were then annealed at 1050°C for 1 hour. Differences in purity of the host material leading to less diffusion of impurity and dissociation of GaN during annealing may explain a number of the discrepancies. Lower carrier concentration HRC material gives an emission at 1.8 eV after Zn implantation annealing (74). The effect of implantation with the inert gas Kr which allows the identification of quenching with implanted atoms at non-radiative centres stands in contrast with the behaviour of Ar implanted GaN (74) and the correlation between different implanted species which suggests that at lower annealing temperatures and higher carrier concentrations quenching is due to native defects in initially damaged material in which enhanced dissociation is taking place.

ACKNOWLEDGEMENTS

I would like to express my thanks to the Science Research Council for the award of a studentship, during the tenure of which the work described above was carried out. I would also like to express my appreciation to Dr. D Wickenden at the GEC Hirst Research Centre for suggesting the project and for many helpful discussions, to Dr. W.Clark for his guiding hand, to Mr. A.Todkill for the ion implantation and to all the other members of staff at HRC and Bath who gave advice and assistance.

REFERENCES

1. Bergh A.A. & Dean P.J. Proceedings of the Institute of Electrical and Electronic Engineers 60 156 (1972)

2. Moss T.S., Burrell G.J. & Ellis B. Semiconductor Opto-Electronics (Butterworth, London 1973)

3. Pankove J.I. Journal of Luminescence 7 114 (1973)

4. Pankove J.I., Bloom S. & Harbeke G RCA Review 36 163 (1975)

5. Kesmanly F.P. Soviet Physics Semiconductors 8 147 (1974)

6. Dingle R. & Ilgems M. Solid State Communications 9 175 (1971)

7. Dingle R., Sell D.D., Stokowski S.E. & Ilgems M. Physical Review B4 1211 (1971)

8. Pankove J.I., Maruska H.P. & Berkeyheiser J.E. Applied Physics Letters 17 197 (1970)

9. Lagerstadt O. & Monemar B. Journal of Applied Physics 45 2266 (1974)

10. Monemar B. Physical Review B10 676 (1974)

11. Grimmeis H.G. & Monemar B. Journal of Applied Physics 41 4054 (1970)

12. Ilgems M. & Montgomery H. Journal of Chemistry and Physics of Solids 34 885 (1973)

13. Lorenz M.R. & Binkowski B.B. Journal of the Electro-chemical Society 109 24 (1962)

14. Ban V.S. Journal of Crystal Growth 17 19 (1973)
Ban V.S. Journal of the Electrochemical Society 119 761 (1972)

15. Pankove J.I., Maruska H.P. & Berkeyheiser J.E. Journal of Luminescence 5 84 (1972)

16. Ilgems M., Dingle R. & Logan A. Journal of Applied Physics 43 3797 (1972)

17. Pankove J.I., Miller E.A., & Berkeyheiser J.E. RCA Review 32 383 (1971)

18. Pankove J.I., Miller E.A. & Berkeyheiser J.E. Journal of Luminescence 5 482 (1972)

19. Pankove J.I. & Norris P.E. RCA Review 33 377 (1972)

20. Maruska H.P., Rhines W.G. & Stevenson D.A. Materials Research Bulletin 7 777 (1972)

21. Pankove J.I. RCA Review 34 343 (1973)

22. Dingle R., Shaklee K.L., Leheney R.F. & Zetterstrom R.D. Applied Physics Letters 19 5 (1971)

23. Juza R. & Hahn H. Inorganic Chemistry 239 285 (1938)

24. Ejder E. Physica Status Solidi (a)23 K87 (1974)

25. Bloom S. Journal of Physics and Chemistry of Solids 32 2027 (1971)

26. Bourne J. & Jacobs R.L. Journal of Physics C 5 3462 (1972)

27. Jones D. & Lettington A.H. Solid State Communications 11 701 (1972)

28. Maruska H.P. & Tietjen J.J. Applied Physics Letters 15 327 (1969)

29. Wickenden D.K., Faulkner K.R., Brander R.W. & Isherwood J.J. Journal of Crystal Growth 9 158 (1971)

30. Morimoto Y., Uchicho K. & Ushio S. Journal of the Electrochemical Society 120 1783 (1973)

31. Wickenden D.K. in Crystal Growth ed. B.R.Pamplin (Pergamon, London 1973)

32. Rabenau A. in Compound Semiconductors ed. R.K.Willardson & H.C.Goering (Reinhold, New York 1962)

33. Chu T.L. Journal of the Electrochemical Society 118 1200 (1971)

34. Chu T.L., Ito K., Smeltzer R.K. & Chu S.S.C. Journal of the Electrochemical Society 121 159 (1974)

35. Hovel H.J. & Cuomo J.J. Applied Physics Letters 20 71 (1972)

36. Kosicki B.B. & Kahng D. Journal of Vacuum Science and Technology 4 593 (1972)

37. Logan R.A. & Thurmond C.D. Journal of the Electrochemical Society 119 1727 (1972)

38. Groh R., Gerey G., Bartha L. & Pankove J.I. Physica Status Solidi (a)26 353 (1974)

39. Madar R. et al. Journal of Crystal Growth 31 197 (1975)

40. Saxena A. et al. International Journal of Applied Radiation and Isotopes 26 334 (1975)

41. Pankove J.I. Optical Processes in Semiconductors (Prentice-Hall, Englewood Cliffs, New Jersey 1971)

42. Mahauti S.D. & Varma C.M. Physical Review Letters 25 1115 (1970)

43. Stern F. Journal of Applied Physics 32 2166 (1961)

44. Redfield D. Physical Review 130 914 (1963)
ibid. 130 916 (1963)

45. Burstein E. Physical Review 93 632 (1954)

46. Hayashi I. IEEE Journal of Quantum Electronics QE-4 113 (1968)

47. Kosicki B.B., Powell R.J. & Burgeil J.C. Physical Review Letters 24 1421 (1970)

48. Kurik M.V. Physica Status Solidi (a)8 9 (1971)

49. Pankove J.I. Physical Review 140 A2056 (1965)

50. Dow J.D. & Redfield D. Physical Review B1 3358 (1970)

51. Camphausen D.L. & Connell G.A.N. Journal of Applied Physics 42 4438 (1971)

52. Cunningham R.D., Brander R.W., Knee N.D. & Wickenden D.K. Journal of Luminescence 5 21 (1972)

53. Barker A.J. & Ilgems M. Physical Review B7 743 (1973)

54. Manchon D.D. Jr., Barker A.S. Jr., Dean P.J. & Zetterstrom R.D. Solid State Communications 8 1227 (1970)

55. Burns G., Dacol F., Marimace J.C., Scott B.A. & Burstein E.A. Applied Physics Letters 22 356 (1973)

56. Ilgems M. & Dingle R. Journal of Applied Physics 44 4234 (1973)

57. Grimmeis H.G. & Koelmans H. Zeitschrift fur Naturforschung 14a 264 (1959)

58. Grimmeis H.G., Groth R. & Maak J. Zeitschrift fur Naturforschung 15a 799 (1960)

59. Pankove J.I., Berkeyheiser J.E. & Miller E.A. Journal of Applied Physics 45 1280 (1974)

60. Pankove J.I., Duffy M.T., Miller E.A. & Berkeyheiser J.E. Journal of Luminescence 8 89 (1973)

61. Ejder E.J. & Grimmeis H.G. Applied Physics 5 275 (1974)

62. Matsumoto T., Sano M. & Aoki M. Japanese Journal of Applied Physics 13 373 (1974)

63. Pankove J.I. & Hutchby J.A. Applied Physics Letters 24 281 (1974)

64. Aven M. in II-VI Semiconducting Compounds ed. D.G. Thomas (Benjamin, New York 1967)

65. Henry C.H., Nassau K. & Shiever J.W. Physical Review B4 2453 (1971)

66. Williams E.W. & Bebb H.B. in Semiconductors and Semimetals Vol.8 ed. J.K.Willardson (Academic Press, New York 1972)

67. Trumbore F.A. Bell Systems Technical Journal 39 205 (1960)

68. Bruten J.W.G. MSc Thesis Lanchester Polytechnic (1971)

69. Dearnaley G. Ion Implantation (North Holland, Amsterdam 1973)

70. Degen P.L. Physica Status Solidi (a)16 9 (1973)

71. Hou S.L., Beck K. & Marley J.A. Applied Physics Letters 14 151 (1969)

72. Merz J.L., Sadowski E.A. & Rodgers J.W. Solid State Communications 9 1037 (1971)

73. Merz J.L., Feldman L.C. & Sadowski E.A. Radiation Effects 6 285 (1970)

74. Metcalfe R.D. MSc Project Report University of Bath (1971)

75. Lindhard J., Scharff M. & Schiott H.E. Mat-fys Medd. 33 14 (1963)

76. Jespersgard P. & Davies J.A. Canadian Journal of Physics 45 2983 (1967)

77. Piercey G.R., Brown F., Davies J.A. & McCargo M. Physical Review Letters 10 399 (1963)

78. Mazey D.J. & Nelson R.S. Radiation Effects 1 229 (1969)

79. Furikawa S. & Ishiwara H. Japanese Journal of Applied Physics 11 1062 (1972)

80. Degen P.L. Physica Status Solidi (a)16 9 (1973)

81. Wickenden D.K. Private communication

82. Grun A.E. Zeitschrift fur Naturforschung 12A 89 (1957)

83. Hoff P.H. & Everhardt T.E. in Record of the 10th Symposium on Electron, Ion and Laser Beam Technology ed. L. Marton (San Francisco Press 1969)

84. Wittry D.B. & Kaiser D.F. Journal of Applied Physics 38 375 (1971)

85. Klein C.A. Journal of Applied Physics 39 2029 (1968)

86. Ejder E. Physica Status Solidi (a)6 445 (1971)

87. International Critical Tables (McGraw Hill 1926)

88. Vook F.L. in Proceedings of the International Conference on Defects in Semiconductors Reading 1972 (Institute of Physics London 1972)

90. Hagen J. Private communication

91. Thomas D.G. & Hopfield J.J. Physical Review 150 680 (1966)

92. Cuthbert J.D. & Thomas D.G. Journal of Applied Physics 39 1573 (1968)

93. Kreher D. Zeitschrift fur Elektrische Inf. und Energietech. 2 182 (1972)

94. Williams E.W. et al. Journal of the Electrochemical Society 120 1741 (1973)

95. Dean P.J., Cuthbert J.D. & Lynch R.T. Physical Review 179 754 (1969)

96. Donovan B. & Angress J.F. "Lattice Vibrations" (Chapman & Hall London 1971)

97. Cox G.A., Cummins D.O., Kawabe K. & Tredgold R.H. Journal of Physics and Chemistry of Solids 28 543 (1967)

98. Mitchell R. Private communication

99. Hirst Research Centre Materials Characterisation Department Report No. 13951C

100. Van Vechten J.A. & Bergstresser T.K. Physical Review B1 3351 (1969)

101. Van Vechten J.A. Physical Review 187 3351 (1969)

102. Pastrnak J., Pacesova S. & Roscovcova L. Czechoslovakian Journal of Physics B24 1149 (1974)

103. Pankove J.I. to be published.